

isbn: 978-90-9023942-2

Imaging of Age-related Brain Changes

Meike Vernooij

Imaging of Age-related Brain Changes

A Population-based Approach

Meike Vernooij

UITNODIGING

*voor het bijwonen van
de openbare verdediging
van het proefschrift*

Imaging of Age-related Brain Changes

A Population-based Approach

Op WOENSDAG 11 MAART 2009
om 13:45 in COLLEGEZAAL 7
Faculteit der geneeskunde en
gezondheidswetenschappen.

Erasmus MC
Dr. Molewaterplein 50
Rotterdam

Receptie na afloop
van de plechtigheid in
de foyer onder de collegezaal

Meike Vernooij
Kruisplein 55a
3014DC Rotterdam
m.vernooij@erasmusmc.nl

IMAGING OF AGE-RELATED BRAIN CHANGES

A population-based approach

Meike Vernooij

ISBN: 978-90-9023942-2

Cover '*Sometimes what you see depends on what you think before you look*'

Cover photograph courtesy of Christopher Smart

Cover design: Ton Everaers & Meike Vernooij

Thesis layout: Ton Everaers

Printed by Print Partners Ipskamp

The work described in this thesis was conducted at the Department of Epidemiology in close collaboration with the Department of Radiology at the Erasmus MC University Medical Center, Rotterdam.

The Rotterdam Study is supported by the Erasmus MC University Medical Center and Erasmus University Rotterdam, the Netherlands Organization for Scientific Research (NWO), the Netherlands Organization for Health Research and Development (ZonMw), the Research Institute for Diseases in the Elderly (RIDE), the Ministry of Education, Culture and Science, the Ministry of Health, Welfare and Sports, the European Commission (DG XII) and by the Municipality of Rotterdam. The work described in this thesis was funded by the Netherlands Organization for Scientific Research (NWO) grants 948-00-010 and 918-46-615.

Financial support for the publication of this thesis was kindly provided by the Department of Radiology and the Department of Epidemiology of Erasmus MC University Medical Center Rotterdam; General Electric Healthcare, het Remmert Adriaan Laan Fonds, de J.E. Jurriaanse Stichting, de Internationale Stichting Alzheimer Onderzoek, Janssen-Cilag BV, AstraZeneca BV, Bayer Schering Pharma and Stichting Alzheimer Nederland.

Copyright © 2009 M.W. Vernooij

All rights reserved. No part of this thesis may be reproduced, distributed, stored in a retrieval system or transmitted in any form or by any means, without permission of the author, or, when appropriate, of the publishers of the publications.

IMAGING OF AGE-RELATED BRAIN CHANGES

A population-based approach

BEELDVORMING VAN AAN VEROUDERING GERELATEERDE HERSENVERANDERINGEN

Een bevolkingsonderzoek

Proefschrift

ter verkrijging van de graad van doctor aan de
Erasmus Universiteit Rotterdam
op gezag van de
rector magnificus

Prof.dr. S.W.J. Lamberts

en volgens besluit van het College voor Promoties.

**De openbare verdediging zal plaatsvinden op
Woensdag 11 maart 2009 om 13:45 uur**

door

Meike Willemijn Vernooij
geboren te Maassluis



PROMOTIECOMMISSIE

Promotores

Prof.dr. M.M.B. Breteler

Prof.dr. G.P. Krestin

Overige leden

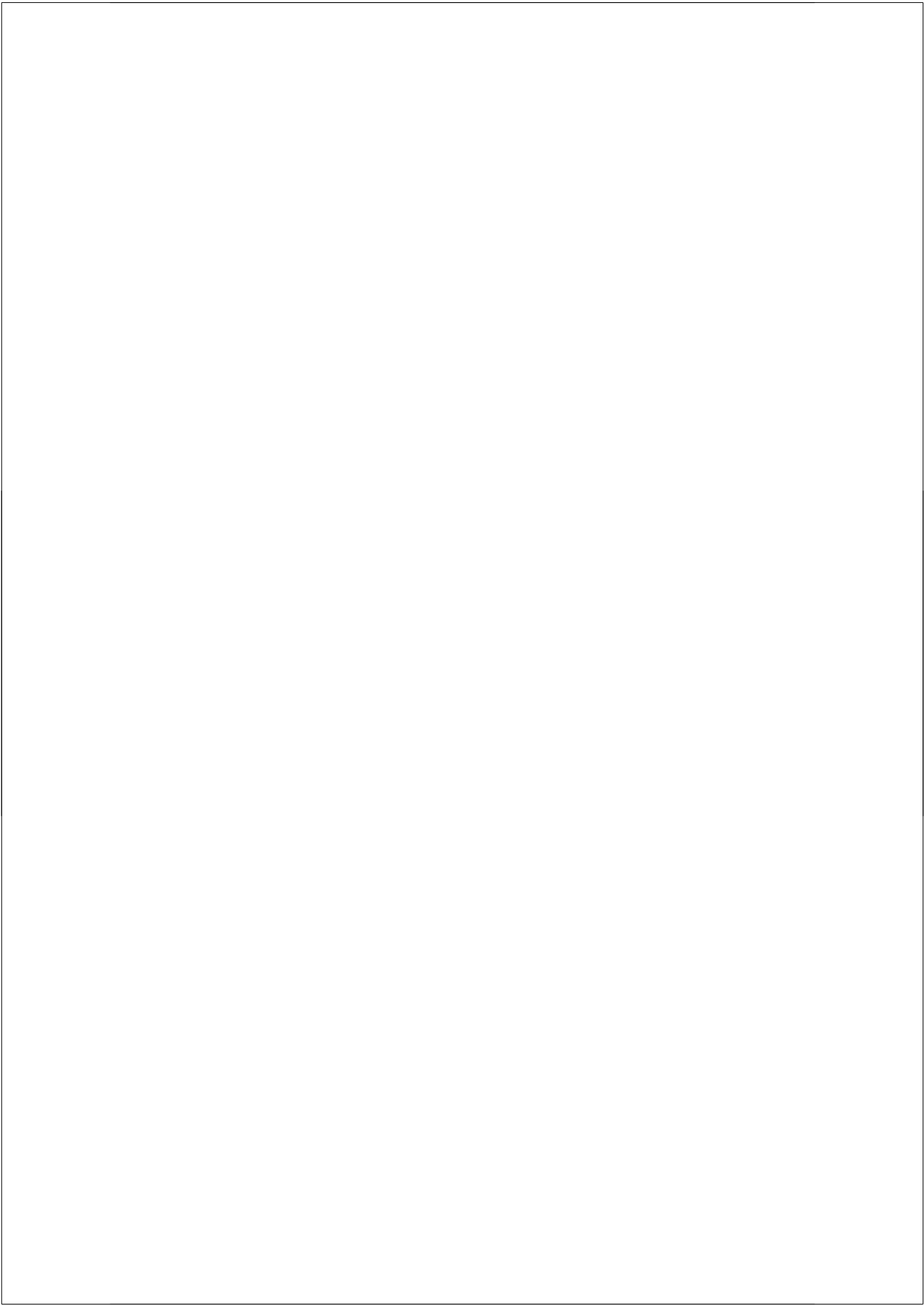
Prof.dr. M.A. van Buchem

Prof.dr. S.M. Greenberg

Prof.dr. M.G.M. Hunink

Copromotor

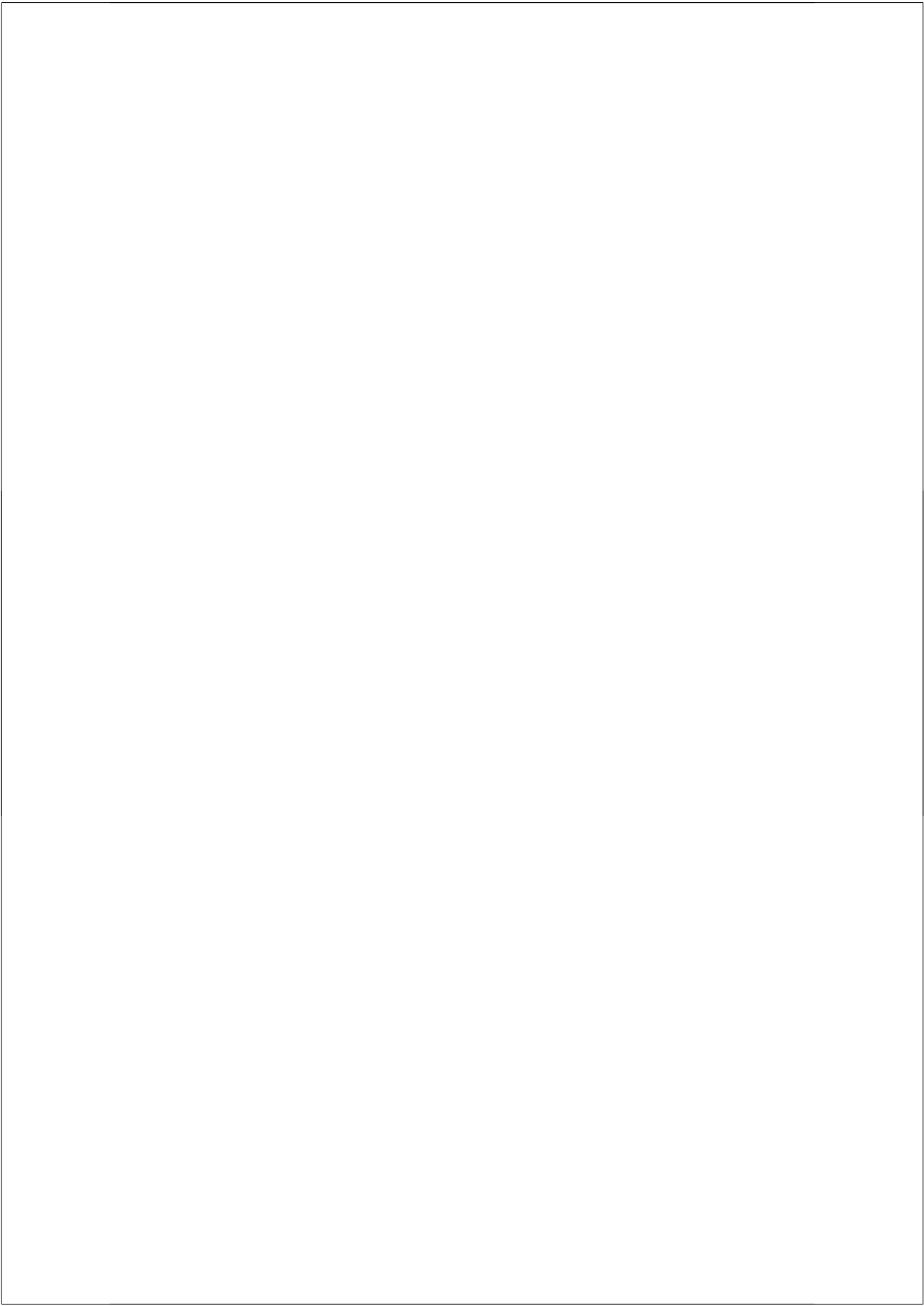
Dr. A. van der Lugt



CONTENTS

Chapter 1	General Introduction	7
Chapter 2	Methodology	13
2.1	Optimizing a 30 minute brain magnetic resonance imaging protocol for a large population-based study	15
2.2	Incidental findings on brain MRI in the general population	35
2.3	Intravestibular lipoma - An important imaging diagnosis	53
Chapter 3	Cerebral Microbleeds	61
3.1	Cerebral microbleeds: accelerated 3D T2*-weighted GRE MRI versus conventional 2D T2*-weighted GRE MRI for detection	63
3.2	Prevalence and risk factors of cerebral microbleeds	75
3.3	Use of antithrombotic drugs and presence of cerebral microbleeds	89
3.4	Cerebral microbleed preceding symptomatic intracerebral hemorrhage in a stroke-free person	103
3.5	Superficial siderosis in the general population	109
3.6	Histopathologic correlation of cerebral microbleed on T2*-weighted MRI	117
Chapter 4	Cerebral Blood Flow	123
4.1	Total cerebral blood flow and total brain perfusion in the general population	125
4.2	Total cerebral blood flow in relation to cognitive function	139

Chapter 5	<i>White Matter Microstructural Integrity</i>	147
5.1	White matter microstructural integrity and cognitive function in a general elderly population	149
5.2	White matter atrophy and lesion formation explain the loss of structural integrity of white matter in aging	171
Chapter 6	<i>General Discussion</i>	187
Chapter 7	<i>Summary / Samenvatting</i>	207
Chapter 8	<i>Dankwoord</i>	219
	<i>PhD Portfolio</i>	225
	<i>List of Publications</i>	229
	<i>About the Author</i>	233



CHAPTER 1

GENERAL INTRODUCTION

GENERAL INTRODUCTION

The function of protecting and developing health must rank even above that of restoring it when it is impaired (Hippocrates, c. 460-370 B.C.)

It is with these words that Hippocrates launched the concept of preventive medicine, nearly 2,500 years ago. Today, disease prevention is still valued as one of the highest goals in modern medicine. To be able to develop preventive measures, we have to understand what causes disease; and in order to halt disease, we need to detect pathology in an early state, before clinical symptoms become manifest.

The unprecedented increase in life expectancy over the past centuries has profound implications on the occurrence of diseases. It is estimated that by 2025 over 18% of the population in North America and 23% in Western Europe will be over the age of 65 (1). As a result of this demographic aging, the number of persons suffering from the most common and widely feared age-related brain diseases, neurodegenerative disease (dementia) and cerebrovascular disease (stroke), is expected to rise as well. In western countries, over 1 in 3 women (and 1 in 6 men) aged 55 years will develop dementia during the rest of their lives (2), whilst 1 in 5 will suffer from stroke (3). As therapeutic options after onset of disease are still limited, effective preventive strategies and methods for early diagnosis are needed. It is now widely recognized that biomarkers, defined as parameters associated with the presence or severity of specific disease states (4), may aid in early detection of disease or to identify persons that are at increased risk of development of disease (5).

In the past decades, magnetic resonance imaging (MRI) has shown to be a powerful non-invasive imaging modality to assess brain changes that may serve as biomarkers for neurodegenerative or cerebrovascular disease. Global as well as regional brain atrophy, white matter lesions and (silent) infarcts have previously been shown to be highly prevalent in a normal aging population as well as to indicate an increased risk of stroke, dementia and psychiatric disease (6-10). Recent developments in MRI hardware and acquisition techniques hold great promise to more sensitively study brain changes in aging, whilst automated post-processing algorithms facilitate the quantitative analyses of large volumes of imaging data. This opens the possibility to study the aging brain in an epidemiological context and to define new imaging biomarkers for neurodegenerative and cerebrovascular disease at the population level.

Over the past decades, evidence has been accumulating that dementia and cerebrovascular disease share many risk factors, and that these conditions often coexist, interact or may have additive effects on cognitive decline and functional disability (11). The objective of this thesis

was to study new imaging biomarkers in the aging brain that may be used to detect early signs of neurodegenerative and cerebrovascular disease, that may help to unravel their potential common pathophysiology and that may aid to identify specific risk factors for both entities. For this goal, advanced MRI techniques were applied in the Rotterdam Scan Study, a large population-based brain imaging study among middle-aged and elderly persons.

A challenge for population-based neuroimaging is to acquire high quality multimodal imaging data within the time constraints and practical setting imposed by the study design; taking into account the participants' level of discomfort. These protocol requirements and considerations are discussed in chapter 2.1. Neuroimaging in volunteers poses the risk of detecting abnormalities that are unrelated to the study purpose but may have clinical implications to the person involved (12). Chapter 2.2 describes the prevalence of such incidental brain findings in the population under study, whilst in chapter 2.3 a case of an exceptionally rare incidentally discovered abnormality is presented.

Chapters 3, 4 and 5 focus respectively on cerebral microbleeds, cerebral blood flow and microstructural integrity of white matter; MRI measures that may serve as imaging biomarkers of neurodegenerative or cerebrovascular disease.

In chapter 3.1, we present an optimized T2*-weighted MRI sequence to detect cerebral microbleeds and compare its performance with a conventional T2*-weighted sequence. Using the optimized sequence, we imaged a large elderly population and assessed the prevalence of and risk factors of microbleeds, described in chapter 3.2. The association between anti-thrombotic drug use and microbleed presence is described in chapter 3.3. In chapter 3.4, it is illustrated that a single microbleed may precede symptomatic intracerebral hemorrhage. We report on the prevalence of superficial siderosis, deposition of blood breakdown products on the brain surface, and its relation to microbleed presence, in chapter 3.5. At the end of chapter 3, we present histopathologic correlation for an MRI-detected cerebral microbleed.

Chapter 4.1 discusses the determinants of cerebral blood flow in the general population, as well as the relation between blood flow and white matter lesions on MRI. In chapter 4.2, we show how cerebral blood flow relates to cognition and investigate whether this association is influenced by brain volume.

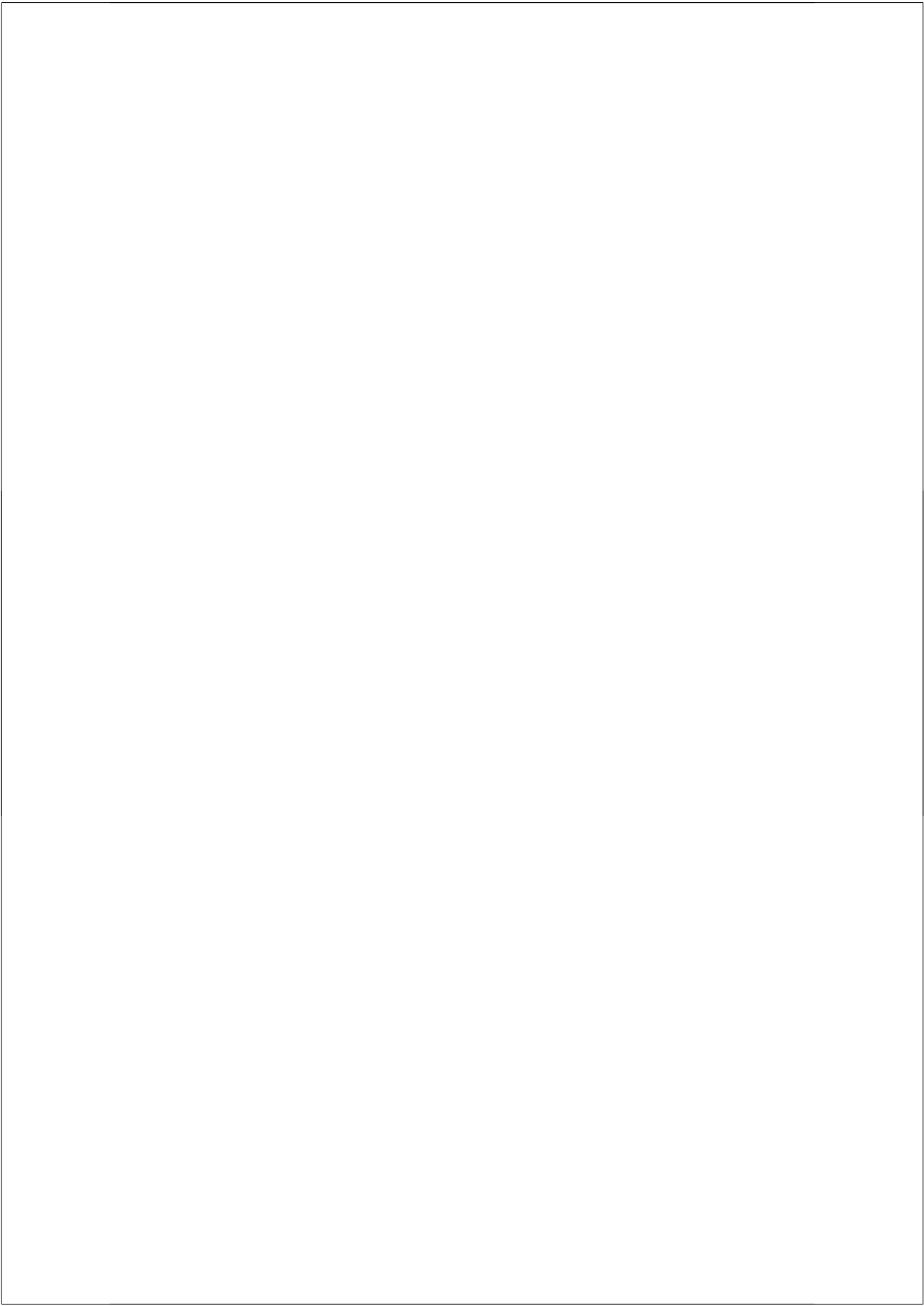
With diffusion tensor imaging (DTI), we studied in chapter 5.1 how microstructural integrity of white matter and white matter lesions relates to cognitive functioning, and whether this relation is independent of other, macrostructural, white matter changes. Microstructural integrity of white matter is known to deteriorate in aging; we investigated in which brain

regions these changes in DTI parameters primarily occur with aging and whether these are independent of white matter atrophy or lesion formation in chapter 5.2.

Finally, in chapter 6, we put our main findings in the context of current knowledge on brain changes with aging and we discuss implications and suggestions for further research.

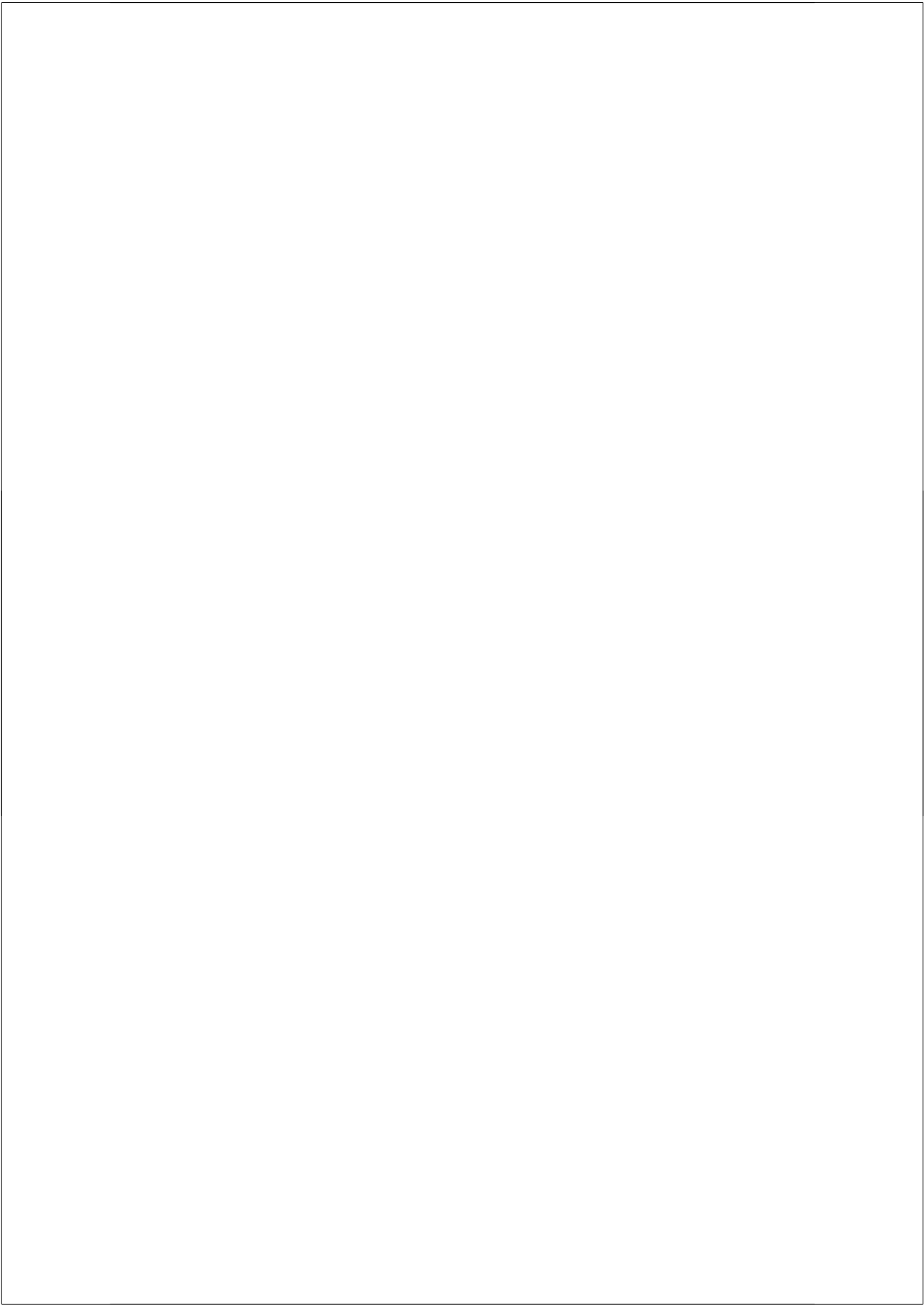
REFERENCES

1. Jeerakathil T, Wolf PA, Beiser A, et al. Cerebral microbleeds: prevalence and associations with cardiovascular risk factors in the Framingham Study. *Stroke* 2004;35:1831-1835.
2. Ott A, Breteler MM, van Harskamp F, Stijnen T, Hofman A. Incidence and risk of dementia. The Rotterdam Study. *Am J Epidemiol* 1998;147:574-580.
3. Hollander M, Koudstaal PJ, Bots ML, Grobbee DE, Hofman A, Breteler MM. Incidence, risk, and case fatality of first ever stroke in the elderly population. The Rotterdam Study. *J Neurol Neurosurg Psychiatry* 2003;74:317-321.
4. Smith JJ, Sorensen AG, Thrall JH. Biomarkers in imaging: realizing radiology's future. *Radiology* 2003;227:633-638.
5. de Leon MJ, Klunk W. Biomarkers for the early diagnosis of Alzheimer's disease. *Lancet Neurol* 2006;5:198-199.
6. Ikram MA, Vrooman HA, Vernooij MW, et al. Brain tissue volumes in relation to cognitive function and risk of dementia. *Neurobiol Aging* 2008.
7. Vermeer SE, Prins ND, den Heijer T, Hofman A, Koudstaal PJ, Breteler MM. Silent brain infarcts and the risk of dementia and cognitive decline. *N Engl J Med* 2003;348:1215-1222.
8. Vermeer SE, Hollander M, van Dijk EJ, Hofman A, Koudstaal PJ, Breteler MM. Silent brain infarcts and white matter lesions increase stroke risk in the general population: the Rotterdam Scan Study. *Stroke* 2003;34:1126-1129.
9. Steffens DC, Helms MJ, Krishnan KR, Burke GL. Cerebrovascular disease and depression symptoms in the cardiovascular health study. *Stroke* 1999;30:2159-2166.
10. de Groot JC, de Leeuw FE, Oudkerk M, Hofman A, Jolles J, Breteler MM. Cerebral white matter lesions and depressive symptoms in elderly adults. *Arch Gen Psychiatry* 2000;57:1071-1076.
11. Breteler MM. Vascular risk factors for Alzheimer's disease: an epidemiologic perspective. *Neurobiol Aging* 2000;21:153-160.
12. Illes J, Desmond JE, Huang LF, Raffin TA, Atlas SW. Ethical and practical considerations in managing incidental findings in functional magnetic resonance imaging. *Brain Cogn* 2002;50:358-365.




CHAPTER 2

METHODOLOGY



2.1

OPTIMIZING A 30 MINUTE BRAIN MAGNETIC RESONANCE IMAGING PROTOCOL FOR A LARGE POPULATION-BASED STUDY

Submitted 

*Piotr A. Wielopolski,
Meike W. Vernooij,
M. Arfan Ikram,
Marion Smits,
Henri A. Vrooman,
Gabriel P. Krestin,
Monique M.B. Breteler,
Aad van der Lugt*

2.2

INCIDENTAL FINDINGS ON BRAIN MRI IN THE GENERAL POPULATION

The New England Journal of Medicine,
2007; 357:1821-1828

*Meike W. Vernooij,
M. Arfan Ikram,
Hervé L. Tanghe,
Arnaud J.P.E. Vincent,
Albert Hofman,
Gabriel P. Krestin,
Wiro J. Niessen,
Monique M.B. Breteler,
Aad van der Lugt*

Background Magnetic resonance imaging (MRI) of the brain is increasingly used both in research and in clinical medicine, and scanner hardware and MRI sequences are continually being improved. These advances are likely to result in the detection of unexpected, asymptomatic brain abnormalities, such as brain tumors, aneurysms, and subclinical vascular pathologic changes. We conducted a study to determine the prevalence of such incidental brain findings in the general population.

Methods The subjects were 2000 persons (mean age, 63.3 years; range, 45.7 to 96.7) from the population-based Rotterdam Study in whom high-resolution, structural brain MRI (1.5 T) was performed according to a standardized protocol. Two trained reviewers recorded all brain abnormalities, including asymptomatic brain infarcts. The volume of white matter lesions was quantified in milliliters with the use of automated postprocessing techniques. Two experienced neuroradiologists reviewed all incidental findings. All diagnoses were based on MRI findings, and additional histologic confirmation was not obtained.

Results Asymptomatic brain infarcts were present in 145 persons (7.2%). Among findings other than infarcts, cerebral aneurysms (1.8%) and benign primary tumors (1.6%), mainly meningiomas, were the most frequent. The prevalence of asymptomatic brain infarcts and meningiomas increased with age, as did the volume of white matter lesions, whereas aneurysms showed no age-related increase in prevalence.

Conclusions Incidental brain findings on MRI, including subclinical vascular pathologic changes, are common in the general population. The most frequent are brain infarcts, followed by cerebral aneurysms and benign primary tumors. Information on the natural course of these lesions is needed to inform clinical management.

Magnetic resonance imaging (MRI) of the brain is increasingly used both in research and in clinical medicine, and scanner hardware and MRI sequences are improving. Performing MRI at higher resolution and field strength and with more sensitive sequences may lead to the detection of subtle or small brain abnormalities that would not have been detected previously. In combination with the increasing number of brain MRI scans obtained each year, these advances in MRI technology will probably result in more persons being confronted with incidental brain findings. Incidental findings are previously undetected abnormalities of potential clinical relevance that are unexpectedly discovered and unrelated to the purpose of the examination (1). The detection of incidental findings poses various practical and ethical issues, particularly when the participants in a research study are healthy volunteers (2). The clinical relevance and natural course of these unexpected asymptomatic findings are largely unknown and may differ markedly from those of similar symptomatic abnormalities.

Previous studies investigated incidental findings, such as brain tumors and vascular abnormalities, in healthy research volunteers or in populations of patients who underwent MRI examinations for various reasons (3-8). Katzman et al. reported a prevalence of 1.1% for clinically serious abnormalities, such as brain tumors, in a retrospective study of a heterogeneous population of volunteers, 3 to 83 years old, who were participating in a variety of research studies (9). To date, only one population-based study has reported the occurrence of incidental brain findings; this study showed a prevalence of 1.7% (10,11).

Not generally classified as incidental findings are subclinical vascular pathologic changes such as asymptomatic brain infarcts and white matter lesions, the prevalence of which is known to be high in elderly persons and to increase with age (12-17). These lesions are potentially clinically relevant because of the increased risk of adverse neurologic events associated with them (17-22). We report on the prevalence of incidental brain findings, including subclinical vascular pathologic changes, detected by high-resolution, state-of-the-art brain MRI in 2000 persons who participated in a population-based study.

METHODS

Source population

The subjects of this study were participants in the Rotterdam Study, a prospective, population-based cohort study initiated in 1990 among persons 55 years of age or older who were living in a suburb of Rotterdam, the Netherlands (23). The original cohort of the Rotterdam Study (7983 participants) was expanded in 2000 and again in 2006 to include participants who were 45 years of age or older. Every 2 to 3 years, participants are invited to the research center for interviews and extensive physical examinations. Since August 2005, all participants without contraindications to MRI have been invited to undergo MRI examination as part of the Rotterdam Scan Study, a neuroimaging study embedded in the Rotterdam Study that aims to investigate the causes and consequences of age-related brain changes.

The institutional review board at Erasmus MC University Medical Center approved the study, and all participants gave written informed consent; the consent form included a paragraph on incidental findings and the option to refuse to be informed about any unexpected abnormality. All patients who had incidental findings that required follow-up evaluation or treatment had previously agreed to be informed of such findings and were referred to appropriate specialists.

Between August 1, 2005, and February 1, 2007, 2027 of 2227 eligible subjects (91.0%) agreed to participate in the imaging study. In 27 subjects, imaging could not be performed because of physical constraints (in 21 subjects) or technical problems (in 6 subjects). Brain imaging results were thus available for 2000 participants.

Brain MRI acquisition

All scans were obtained with a 1.5-T scanner with an eight-channel head coil (GE Healthcare). Two trained technicians performed all examinations in a standardized way. The MRI protocol was identical for all participants and included four high-resolution axial sequences: a three-dimensional, T1-weighted sequence; a two-dimensional, proton density-weighted sequence; a two-dimensional, fluid-attenuated inversion recovery (FLAIR) sequence; and a three-dimensional, T2*-weighted gradient-recalled echo (GRE) sequence. The slice thickness was 1.6 mm for the T1-weighted, proton density-weighted, and T2*-weighted GRE sequences (zero-padded to 0.8 mm for the T1-weighted and T2*-weighted GRE sequences) and 2.5 mm for the FLAIR sequence; all slices were contiguous. No contrast material was administered.

Assessment of incidental findings

All scans were read for incidental findings by one of two trained reviewers. The readings were usually performed within 1 day (over 90% of all scans) and at the latest 1 week after acquisition. One reviewer was a resident in radiology, and the other a resident in neurology, with 4.5 and 2.0 years of experience in reading brain MRIs, respectively. Both reviewers were unaware of any clinical information on the subjects. The readings were performed with a digital picture archiving and communication system (PACS). Incidental findings of potential clinical relevance were defined as those requiring urgent or immediate referral, as previously described by others (9,10,24); examples include brain tumors, aneurysms, subdural fluid collections, and arachnoid cysts. The diagnoses were made on the basis of MRI findings characteristic of each lesion and were not confirmed by histologic studies. Case definitions for each incidental MRI finding are detailed in the Appendix.

In addition, the presence of brain infarcts (both lacunar and cortical) was recorded. The distinction between symptomatic and asymptomatic infarcts was verified as follows. A history of stroke is obtained from each subject on entry into the Rotterdam Study (25). Subsequently, participants are continuously monitored for incident stroke through automated linkage of the study database with files from general practitioners and hospital discharge information. All reported events are validated by an experienced neurologist (26). White matter lesion volumes (in milliliters) were quantified with a validated automated voxel classification technique, as described elsewhere (27). Brain findings that were not considered clinically relevant

and were not recorded as incidental findings included simple sinus disease and variations from the norm, such as pineal cysts, ventricular asymmetry, and enlarged Virchow–Robin spaces.

Two experienced neuroradiologists reviewed and reached a consensus on all initially reported abnormalities. To maximize sensitivity, the threshold for reporting abnormalities on initial review was kept low. To verify the sensitivity of the initial review for detecting incidental findings, an additional 230 scans (11.5% of the total of 2000) were also read by the neuroradiologists. No brain abnormalities were detected in addition to those already recorded by the initial reviewers. This result indicates that the initial review had a very high sensitivity for detection of brain abnormalities.

The management of incidental findings was defined in a protocol that was agreed on before the start of the study. Depending on the detected abnormality and after consultation with clinicians, persons with incidental findings requiring additional clinical workup or medical treatment were referred to a relevant medical specialist (a neurosurgeon, neurologist, or internist).

Statistical analysis

We calculated the prevalence of each incidental brain finding in the study population. Multiple similar findings within one participant (e.g., more than one aneurysm or multiple asymptomatic brain infarcts) were counted as a single finding. Next, we calculated the age-specific prevalence rates of the most frequent incidental findings. For white matter lesions, we calculated the age-specific median and interquartile range.

RESULTS

The mean age of the study population was 63.3 years (range, 45.7 to 96.7), and 1049 of the subjects (52.4%) were women. Table 1 shows the prevalence of each incidental finding that was recorded. Asymptomatic brain infarcts were present in 145 persons (7.2%). Among findings other than brain infarcts, aneurysms (1.8%) were the most frequent. All aneurysms except two were located in the anterior circulation, and all except three were less than 7 mm in diameter (the smallest was 2 mm). Four aneurysms had an intracavernous location. Benign tumors were also frequent (1.6%), with meningiomas being recorded most often (0.9%). The meningiomas ranged from 5 to 60 mm in diameter, and their prevalence was 1.1% in women and 0.7% in men. Pituitary macroadenoma was present in six persons (0.3%). Vestibular schwannomas had a prevalence of 0.2%. We found one possibly malignant primary brain

tumor (a low-grade glioma that was not histologically confirmed) and one case of multiple cerebral metastases in a person who in retrospect was found to have been treated for lung cancer. The finding that was medically most urgent was a large, chronic subdural hematoma in an otherwise asymptomatic person, who in retrospect was found to have had minor head trauma 4 weeks before the MRI scan. Figure 1 shows a selection of the abnormalities that were incidentally detected in this study.

None of the persons with incidental brain findings reported any symptoms, with the exception of two subjects. One person with vestibular schwannoma reported hearing loss that had been investigated 3 years earlier by computed tomography, which had not revealed any abnor-

Table 1. Incidental findings on 2000 MRI scans*

Finding	N (%)
Asymptomatic brain infarct†	145 (7.2)
Lacunar infarcts	112 (5.6)
Cortical infarcts	41 (2.0)
Primary tumors, benign	31 (1.6)
Meningioma	18 (0.9)
Vestibular schwannoma	4 (0.2)
Intracranial lipoma‡	2 (0.1)
Trigeminal schwannoma	1 (<0.1)
Pituitary adenoma	6 (0.3)
Primary tumors, malignant§	1 (<0.1)
Other findings	
Aneurysm	35 (1.8)
Cavernous angioma	7 (0.4)
Metastases	1 (<0.1)
Subdural hematoma	1 (<0.1)
Arachnoid cyst¶	22 (1.1)
Chiari I malformation	18 (0.9)
Major vessel stenosis**	9 (0.5)
Dermoid cyst of lateral orbital rim	1 (<0.1)
Fibrous dysplasia	1 (<0.1)

* The diagnoses were based on imaging only, without histologic confirmation.

† Some subjects had both lacunar and cortical infarcts.

‡ One person had quadrigeminal cistern lipoma, and one had intravestibular lipoma.

§ This finding was a possible low-grade glioma.

¶ There were 16 temporal cysts (left-to-right ratio, 3:1) and 6 infratentorial cysts.

|| Type I Chiari malformation is defined as tonsillar herniation extending more than 5 mm below the foramen magnum (28). The mean degree of herniation was 6.4 mm (range, 5.2 to 10.3).

** Major-vessel stenosis is defined as lack of flow void in the cavernous internal carotid artery (in seven subjects) or the vertebral artery (in two subjects).

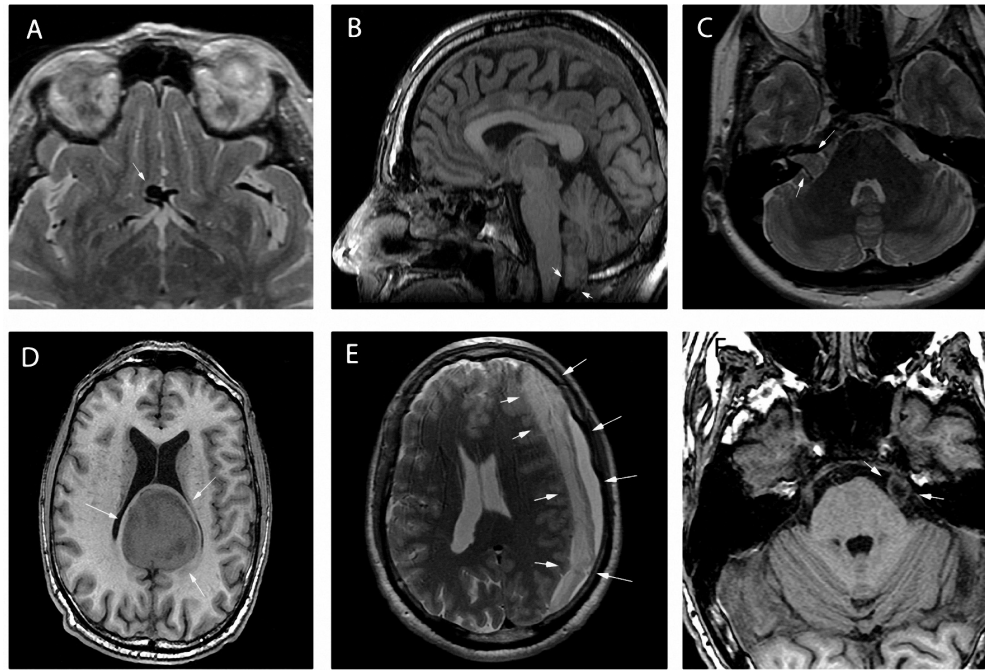


Figure 1. Incidental findings on brain MRI. Arrows indicate the abnormalities in each image. An aneurysm of the anterior communicating artery (diameter, 6 mm) is shown on the proton density-weighted axial image in Panel A. Panel B shows a tonsillar herniation (type I Chiari malformation) more than 5 mm below the level of the foramen magnum on a T1-weighted sagittal image. A typical vestibular schwannoma with extension into the right internal auditory canal is visible on the proton density-weighted axial image in Panel C. A large meningioma is shown on the T1-weighted axial image in Panel D. Panel E shows a large, chronic subdural hematoma on a proton density-weighted axial image. A trigeminal schwannoma of the left fifth cranial nerve, with cystic degeneration, is shown on the T1-weighted axial image in Panel F.

malities. The other person, who had a right-sided intravestibular lipoma, had longstanding ipsilateral hearing loss that had never been evaluated.

None of the incidental findings in Table 1 were histologically or surgically confirmed, except for those in two persons for whom operative treatment was indicated. One had subdural hematoma, and the other had a 12-mm aneurysm of the medial cerebral artery.

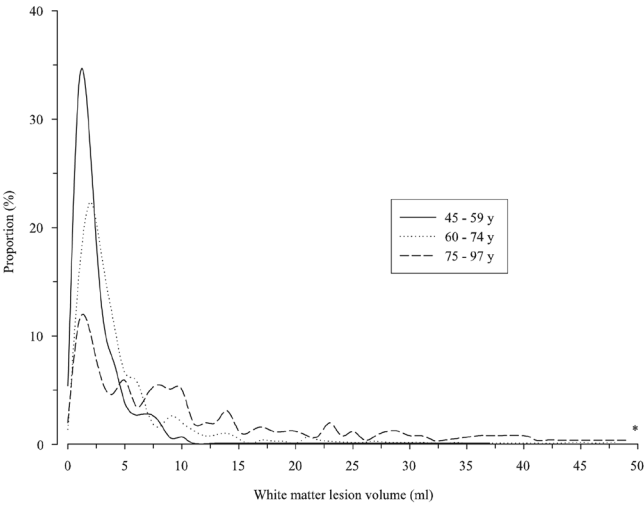
Table 2. Distribution of incidental findings according to age

Finding	45 to 59 Yr of Age (N = 750)	60 to 74 Yr of Age (N = 993)	75 to 97 Yr of Age (N = 257)
Asymptomatic brain infarct – N (%)	30 (4.0)	68 (6.8)	47 (18.3)
Meningioma – N (%)	4 (0.5)	10 (1.0)	4 (1.6)
Aneurysm – N (%)	13 (1.7)	18 (1.8)	4 (1.6)
Volume of white matter lesions - mL			
Median	1.80	3.05	7.74
Interquartile range	1.06-3.17	1.87-5.49	2.64-16.49

Table 2 shows the age-specific distribution of the most frequent incidental findings. The prevalence of asymptomatic brain infarcts increased with age. The prevalence of meningiomas increased from 0.5% in 45- to 59-year-olds to 1.6% in persons 75 years of age or older. Aneurysms showed no change in prevalence with age.

The median volume of white matter lesions increased with increased age (Table 2). The distribution of white matter lesion volumes according to age category is shown in Figure 2. The proportion of persons without any white matter lesions decreased from 5.4% in 45- to 59-year-olds to 2.0% in persons 75 years of age and older. Furthermore, with increasing age, there was a greater spread in the distribution of white matter lesion volumes (Fig. 2).

Figure 2. Age-specific distribution of white matter lesion volumes. Measured volumes of white matter lesions were rounded to the nearest milliliter before plotting. The proportion of persons with a specific volume of white matter lesions within each age category is shown on the y axis. Fourteen persons (<1%) had a white matter lesion volume of more than 50 mL. Of these persons, one was under 59 years of age, four were 60 to 74 years of age, and nine were 75 years of age or older.
*The maximum white matter lesion volume measured was 95 mL.



DISCUSSION

In the general population of persons 45 to 97 years old, we found a high prevalence of potentially clinically relevant incidental brain abnormalities, including subclinical vascular pathologic changes. The prevalence of asymptomatic brain infarcts and meningiomas increased with age, as did the volume of white matter lesions, whereas aneurysms showed no age-related increase in prevalence.

A major strength of our study is the large sample of persons 45 years of age or older. The MRI protocol was uniform for all subjects, and the reviewers were unaware of characteristics of the subjects, making detection bias unlikely. We used high-resolution, state-of-the-art imaging sequences representing the advanced imaging techniques that are increasingly used in brain research.

A potential limitation with respect to the generalizability of our study results is the fairly homogeneous composition of our geographically defined study population, which consisted mainly of white, middle-class persons (29). Our results may not be generalizable to populations that include other ethnic or socioeconomic groups. Another potential limitation of our study is that not all scans were read by neuroradiologists. However, all scans with abnormalities detected on initial review were reviewed again by two neuroradiologists. In addition, a randomly chosen subgroup of all scans was reviewed by two neuroradiologists, who did not detect any incidental findings missed on initial review. Therefore, our initial review by physicians who were not neuroradiologists had a very high sensitivity for the detection of brain abnormalities, and we do not think the results would have been different if the scans had been read primarily by neuroradiologists. The sensitivity may be lower when scans are read by professionals who are not medically qualified, as is reportedly the case in many research centers in the United States (30).

The incidental brain findings in our study were all diagnosed on the basis of imaging. Pathological confirmation of presumed brain tumors was not obtained, since none of these tumors required surgery after referral of the subject. However, the imaging characteristics of all lesions listed in Table 1 were typical and are usually considered diagnostic (see the Supplementary Appendix).

We did not use contrast-enhanced MRI. Because our study population consisted of volunteers without neurologic symptoms who were participating in a research study, the risks associated with the administration of contrast material were not considered warranted. However, the effect of the absence of contrast material, if any, would have been to leave some small lesions undetected, which would have resulted in an underestimate of the prevalence of incidental findings.

The prevalence of subclinical vascular pathologic changes in our population was high and increased with advancing age. This finding was not unexpected, since age-related changes, such as asymptomatic brain infarcts and white matter lesions, have been reported to be very frequent in the general elderly population (12,13,15-17,31). Although such changes have been shown to be associated with increased risks of stroke and cognitive decline (18,20,32), preventive therapies for patients with these MRI findings have not been evaluated in randomized trials.

The prevalence of incidental brain findings other than subclinical vascular pathologic changes in our population was much higher than that reported in previous studies (8-10,24), even when the subjects were of similar age to the patients in our study (10). We found an especially

high prevalence of small aneurysms (4,9,10,24). This difference can partly be explained by differences among study populations, since aneurysms are very infrequent in children and young adults. However, the population-based study by Yue et al. showed aneurysms in only 0.11% of persons 65 years of age or older (10). We feel that a more likely explanation for the difference is that our scanning protocol, especially the high-resolution, proton density-weighted sequence (Fig. 1A), permitted very good visualization of the circle of Willis as compared with conventional T1-weighted and T2-weighted sequences. Of course, the use of even more sensitive sequences, such as magnetic resonance angiography, might have resulted in the detection of even smaller aneurysms. However, in a systematic review of autopsy and angiographic studies, Rinkel et al. concluded that aneurysms can be found in approximately 2% of adults without risk factors for subarachnoid hemorrhage (33), a proportion very close to the 1.8% detected by MRI in our study.

Meningiomas and small aneurysms were highly prevalent in our study population of persons 45 years of age or older. The rate of growth of meningiomas is typically slow (34,35), and most meningiomas remain asymptomatic throughout life, which explains why 50% of all meningiomas are discovered at autopsy (36). The prevalence of meningiomas found at autopsy in persons over 60 years of age is 3%, and the majority of the lesions are less than 1 cm in diameter (37). Nevertheless, it is generally believed that asymptomatic meningiomas require close clinical and radiologic followup to rule out rapidly enlarging tumors (34,38). The current practice of many clinicians is to perform MRI yearly for at least 2 to 3 years to ascertain that rapid tumor growth does not occur. If this were done for all persons incidentally found to have meningiomas, many MRI examinations would be performed in otherwise healthy asymptomatic persons. In view of the resulting medical costs, as well as the psychological burden for those undergoing examination, it would be of great interest to review these guidelines on the basis of the natural course of meningiomas incidentally found on brain MRI.

Guidelines for the management of small aneurysms might also be reviewed. More than 90% of unruptured, asymptomatic aneurysms found by means of autopsy or angiography are less than 10 mm in diameter (33,39). In our study, all but three aneurysms were smaller than 7 mm, and all but two were located in the anterior circulation. The reported risk of rupture for aneurysms of this size in the anterior circulation over a period of 4 years is 0% (40). This finding was based on follow-up of a group of patients who had no history of subarachnoid hemorrhage. However, in this group there was an overrepresentation of persons with a family history of aneurysm and of persons with symptoms that had led to the detection of the unruptured aneurysm (40). The risk of rupture associated with asymptomatic aneurysms in the general population would be expected to be even lower than the reported risk in the described patient population (33). Preventive surgery or treatment of risk factors may thus not

be indicated in the general population, and the benefit of longer follow-up has not yet been proven (41). Therefore, persons in our study with aneurysms of the anterior circulation that were under 7 mm in diameter were not referred for follow-up or medical treatment.

Several large, population-based MRI studies in the elderly are ongoing (11,16,42-45), and more will be conducted because of the increasing scientific interest in age-related brain diseases such as dementia. Moreover, imaging at higher MRI field strengths and with increased resolution, as well as the use of new MRI sequences that are more sensitive to subtle structural changes, will probably increase the number of small brain abnormalities detected. Incidental findings from brain MRI in middle-aged and elderly persons will therefore become an important issue that should be considered in designing studies. The present study, as well as some previous studies (9,10), provides information on the prevalence of clinically asymptomatic brain abnormalities. This information is especially important in view of the ethical and practical issues involved in the management of incidental findings (1,2).

In conclusion, incidental findings on brain MRI in the general population are common. The most frequent findings are brain infarcts, followed by cerebral aneurysms and benign primary tumors. Such findings should be anticipated in the design of research protocols and the use of neuroimaging in clinical practice. Information on the natural course and prognosis of these lesions is needed to inform clinical management.

REFERENCES

1. Illes J, Kirschen MP, Edwards E, et al. Ethics. Incidental findings in brain imaging research. *Science* 2006; 311:783-784.
2. Illes J, Desmond JE, Huang LF, Raffin TA, Atlas SW. Ethical and practical considerations in managing incidental findings in functional magnetic resonance imaging. *Brain Cogn* 2002; 50:358-365.
3. Onizuka M, Suyama K, Shibayama A, Hiura T, Horie N, Miyazaki H. Asymptomatic brain tumor detected at brain check-up. *Neurol Med Chir (Tokyo)* 2001; 41:431-434; discussion 435.
4. Tsushima Y, Taketomi-Takahashi A, Endo K. Prevalence of abnormal findings on brain magnetic resonance (MR) examinations in adult participants of brain docking. *BMC Neurol* 2005; 5:18.
5. Moser FG, Panush D, Rubin JS, Honigsberg RM, Sprayregen S, Eising SB. Incidental paranasal sinus abnormalities on MRI of the brain. *Clin Radiol* 1991; 43:252-254.
6. Takanashi J, Tada H, Barkovich AJ, Saeki N, Kohno Y. Pituitary cysts in childhood evaluated by MR imaging. *AJNR Am J Neuroradiol* 2005; 26:2144-2147.
7. Lubman DI, Velakoulis D, McGorry PD, et al. Incidental radiological findings on brain magnetic resonance imaging in first-episode psychosis and

- chronic schizophrenia. *Acta Psychiatr Scand* 2002; 106:331-336.
8. Weber F, Knopf H. Incidental findings in magnetic resonance imaging of the brains of healthy young men. *J Neurol Sci* 2006; 240:81-84.
9. Katzman GL, Dagher AP, Patronas NJ. Incidental findings on brain magnetic resonance imaging from 1000 asymptomatic volunteers. *Jama* 1999; 282:36-39.
10. Yue NC, Longstreth WT, Jr., Elster AD, Jungreis CA, O'Leary DH, Poirier VC. Clinically serious abnormalities found incidentally at MR imaging of the brain: data from the Cardiovascular Health Study. *Radiology* 1997; 202:41-46.
11. Jack CR, Jr. MR imaging of the brain in epidemiologic research: the Cardiovascular Health Study. *Radiology* 1997; 202:17-19.
12. Vermeer SE, Koudstaal PJ, Oudkerk M, Hofman A, Breteler MM. Prevalence and risk factors of silent brain infarcts in the population-based Rotterdam Scan Study. *Stroke* 2002; 33:21-25.
13. Howard G, Wagenknecht LE, Cai J, Cooper L, Kraut MA, Toole JF. Cigarette smoking and other risk factors for silent cerebral infarction in the general population. *Stroke* 1998; 29:913-917.
14. Longstreth WT, Jr., Bernick C, Manolio TA, Bryan N, Jungreis CA, Price TR. Lacunar infarcts defined by magnetic resonance imaging of 3660 elderly people: the Cardiovascular Health Study. *Arch Neurol* 1998; 55:1217-1225.
15. de Leeuw FE, de Groot JC, Achten E, et al. Prevalence of cerebral white matter lesions in elderly people: a population based magnetic resonance imaging study. The Rotterdam Scan Study. *J Neurol Neurosurg Psychiatry* 2001; 70:9-14.
16. Liao D, Cooper L, Cai J, et al. Presence and severity of cerebral white matter lesions and hypertension, its treatment, and its control. The ARIC Study. Atherosclerosis Risk in Communities Study. *Stroke* 1996; 27:2262-2270.
17. Longstreth WT, Jr., Manolio TA, Arnold A, et al. Clinical correlates of white matter findings on cranial magnetic resonance imaging of 3301 elderly people. The Cardiovascular Health Study. *Stroke* 1996; 27:1274-1282.
18. Vermeer SE, Prins ND, den Heijer T, Hofman A, Koudstaal PJ, Breteler MM. Silent brain infarcts and the risk of dementia and cognitive decline. *N Engl J Med* 2003; 348:1215-1222.
19. Longstreth WT, Jr., Dulberg C, Manolio TA, et al. Incidence, manifestations, and predictors of brain infarcts defined by serial cranial magnetic resonance imaging in the elderly: the Cardiovascular Health Study. *Stroke* 2002; 33:2376-2382.
20. Bernick C, Kuller L, Dulberg C, et al. Silent MRI infarcts and the risk of future stroke: the cardiovascular health study. *Neurology* 2001; 57:1222-1229.
21. Prins ND, van Dijk EJ, den Heijer T, et al. Cerebral white matter lesions and the risk of dementia. *Arch Neurol* 2004; 61:1531-1534.
22. de Groot JC, de Leeuw FE, Oudkerk M, Hofman A, Jolles J, Breteler MM. Cerebral white matter lesions and depressive symptoms in elderly adults. *Arch Gen Psychiatry* 2000; 57:1071-1076.
23. Ott A, Breteler MM, van Harskamp F, Stijnen T, Hofman A. Incidence and risk of dementia. The Rotterdam Study. *Am J Epidemiol* 1998; 147:574-580.
24. Kim BS, Illes J, Kaplan RT, Reiss A, Atlas SW. Incidental findings on pediatric MR images of the brain. *AJNR Am J Neuroradiol* 2002; 23:1674-1677.
25. Hollander M, Bots ML, Del Sol AI, et al. Carotid

- plaques increase the risk of stroke and subtypes of cerebral infarction in asymptomatic elderly: the Rotterdam study. *Circulation* 2002; 105:2872-2877.
26. Bos MJ, Koudstaal PJ, Hofman A, Witteman JC, Breteler MM. Uric acid is a risk factor for myocardial infarction and stroke: the Rotterdam study. *Stroke* 2006; 37:1503-1507.
 27. Ikram MA, Vrooman HA, Vernooij MW, et al. Brain tissue volumes in the general elderly population The Rotterdam Scan Study. *Neurobiol Aging* 2007.
 28. Meadows J, Kraut M, Guarnieri M, Haroun RI, Carson BS. Asymptomatic Chiari Type I malformations identified on magnetic resonance imaging. *J Neurosurg* 2000; 92:920-926.
 29. van Rossum CT. Socioeconomic Inequalities in Cardiovascular Disease in an Ageing Population. [Thesis], 1999.
 30. Illes J, Kirschen MP, Karetsky K, et al. Discovery and disclosure of incidental findings in neuroimaging research. *J Magn Reson Imaging* 2004; 20:743-747.
 31. Price TR, Manolio TA, Kronmal RA, et al. Silent brain infarction on magnetic resonance imaging and neurological abnormalities in community-dwelling older adults. The Cardiovascular Health Study. CHS Collaborative Research Group. *Stroke* 1997; 28:1158-1164.
 32. Vermeer SE, Hollander M, van Dijk EJ, Hofman A, Koudstaal PJ, Breteler MM. Silent brain infarcts and white matter lesions increase stroke risk in the general population: the Rotterdam Scan Study. *Stroke* 2003; 34:1126-1129.
 33. Rinkel GJ, Djibuti M, Algra A, van Gijn J. Prevalence and risk of rupture of intracranial aneurysms: a systematic review. *Stroke* 1998; 29:251-256.
 34. Olivero WC, Lister JR, Elwood PW. The natural history and growth rate of asymptomatic meningiomas: a review of 60 patients. *J Neurosurg* 1995; 83:222-224.
 35. Nakamura M, Roser F, Michel J, Jacobs C, Samii M. The natural history of incidental meningiomas. *Neurosurgery* 2003; 53:62-70; discussion 70-61.
 36. Staneczek W, Janisch W. Epidemiologic data on meningiomas in East Germany 1961-1986: incidence, localization, age and sex distribution. *Clin Neuropathol* 1992; 11:135-141.
 37. Nakasu S, Hirano A, Shimura T, Llena JF. Incidental meningiomas in autopsy study. *Surg Neurol* 1987; 27:319-322.
 38. Niino M, Yatsushiro K, Nakamura K, Kawahara Y, Kuratsu J. Natural history of elderly patients with asymptomatic meningiomas. *J Neurol Neurosurg Psychiatry* 2000; 68:25-28.
 39. Inagawa T, Hirano A. Autopsy study of unruptured incidental intracranial aneurysms. *Surg Neurol* 1990; 34:361-365.
 40. Wiebers DO, Whisnant JP, Huston J, 3rd, et al. Unruptured intracranial aneurysms: natural history, clinical outcome, and risks of surgical and endovascular treatment. *Lancet* 2003; 362:103-110.
 41. White PM, Wardlaw J. Unruptured intracranial aneurysms: prospective data have arrived. *Lancet* 2003; 362:90-91.
 42. DeCarli C, Massaro J, Harvey D, et al. Measures of brain morphology and infarction in the Framingham Heart Study: establishing what is normal. *Neurobiol Aging* 2005; 26:491-510.
 43. Korf ES, White LR, Scheltens P, Launer LJ. Brain aging in very old men with type 2 diabetes: the Honolulu-Asia Aging Study. *Diabetes Care* 2006; 29:2268-2274.
 44. Schmidt R, Fazekas F, Kapeller P, Schmidt H,

Hartung HP. MRI white matter hyperintensities: three-year follow-up of the Austrian Stroke Prevention Study. *Neurology* 1999; 53:132-139.

45. Leow AD, Klunder AD, Jack CR, Jr., et al. Longitudinal stability of MRI for mapping brain change using tensor-based morphometry. *Neuroimage* 2006; 31:627-640.

APPENDIX

Imaging diagnosis	Case definition based on MRI characteristics
Asymptomatic brain infarct	
Lacunar infarct	Focal parenchymal lesion ≥ 3 mm and < 15 mm in size, with the same signal characteristics as cerebrospinal fluid on all sequences, and -when located supratentorially- with a hyperintense rim on the FLAIR images (1-3). No involvement of cortical grey matter. Commonly located in the basal ganglia, internal capsule, pons and corona radiata. Differentiation from Virchow-Robin (VR) spaces is based on signal intensity (absence of hyperintense rim on FLAIR images), shape (VR-spaces are more linear or lobulated in shape) and location (VR-spaces are often located around anterior commissure or near vertex of the brain) (4,5).
Subcortical infarct	Same MRI characteristics as lacunar infarct, but ≥ 15 mm in size.
Cortical infarct	Focal parenchymal lesion with involvement of cortical grey matter, with the same signal characteristics as cerebrospinal fluid on all sequences, and -when located supratentorially- with a hyperintense rim on the FLAIR images (1-3). Tissue loss of variable magnitude present, visible as prominent adjacent sulci and ipsilateral ventricular enlargement (6).
Primary tumors, benign	
Meningioma	Extra-axial lesion. Iso- or hypointense to grey matter on T1-weighted images, variable signal intensity on PD-weighted images. Calcifications (hypointense on T1-weighted and PD-weighted images) within lesion and/or hyperostosis of underlying bone may be present. Usually broad dural basis. When large, these lesions may cause moderate vasogenic edema in underlying brain tissue)(6).

Imaging diagnosis	Case definition based on MRI characteristics
Vestibular schwannoma	Extra-axial lesion. Iso- or hypointense to grey matter on T1-weighted images. Located in the internal auditory canal, with variable extension into the cerebellopontine angle. Often with widening of the internal auditory canal when large. Typical "ice cream cone" appearance (6). Can show cystic changes (visible as high signal intensity on PD-weighted images) (7).
Intracranial lipoma	Lesion with the same signal characteristics as subcutaneous fat on all sequences. Sometimes with intralésional vessels seen as flow voids (8,9).
Trigeminal schwannoma	Extra-axial lesion with signal characteristics similar to vestibular schwannoma except the course follows that of the 5th cranial nerve (6,10).
Pituitary macroadenoma	Intrasellar mass, extending suprasellar and/or parasellar, frequently causing deviation of the pituitary stalk. May extend upward toward the optic chiasm. The normal pituitary gland may not be identified. Signal intensity usually isointense to grey matter on all sequences, but the lesion may show cystic changes (cystic macroadenoma; high signal intensity on PD-weighted images) (6).
Primary tumors, malignant	
Low-grade glioma	Diffuse lesion with mass effect and signal changes: hypointense relative to surrounding brain on T1-weighted images, hyperintense on PD-weighted and FLAIR images. No signs of necrosis or hemorrhage (6).
Other findings	
Aneurysm	The presence of aneurysms is evaluated on PD-weighted images, on which arterial structures are visualized as flow voids (black). Aneurysms are defined as blind-ending, well delineated focal arterial out-pouchings with a saccular shape. Location usually in cavernous internal carotid artery or circle of Willis. Commonly located at vessel bifurcations (6).
Cavernous angioma	"Popcorn-like", smoothly circumscribed, well-delineated parenchymal lesion. Complex reticulated core of mixed signal intensities, representing hemorrhage in various stages of evolution. Low-signal-intensity hemosiderin rim completely surrounding the lesion on both T1-weighted and PD-weighted images. On T2* GRE imaging, paramagnetic properties of hemosiderin cause a focus of signal loss. No feeding artery or draining vein demonstrated (6).
Metastases	Multifocal parenchymal round lesions with mass effect. Generally iso- to mildly hypointense on T1-weighted images, hyperintense on PD-weighted images. Variable amount of edema surrounding each lesion. Hemorrhage may be present in some lesions (causing susceptibility artifacts on T2* GRE images) (6).

Imaging diagnosis	Case definition based on MRI characteristics
Chronic subdural hematoma	Crescent-shaped extra-axial fluid collection. Hyperintense signal intensity on PD-weighted images. Often not homogeneous in signal intensity due to presence of blood in different stages, with septae separating different blood products. The extra-axial fluid collection does not cross dural attachments, but does cross sutures (6).
Arachnoid cyst	Sharply-demarcated well-defined extra-axial cystic lesion exhibiting isointense signal to cerebrospinal fluid on all sequences (including on FLAIR images). No internal architecture. Typical locations are temporal or infratentorial (cerebellopontine angle, cisterna magna) (6).
Chiari I malformation	Tonsillar herniation extending more than 5 mm below the foramen magnum. The plane of the foramen magnum is defined on sagittal T1-weighted images by a line connecting the basion and opisthion, and degree of tonsillar herniation is measured perpendicular from this line to the most inferior aspect of the cerebellar tonsils visible on all sections (11).
Major vessel stenosis	Absence of flow void on T1-weighted and PD-weighted images in carotid or vertebral artery (12).
Extra-cranial dermoid cyst	Extra-cranial lesion usually located around bony sutures (typical near superolateral orbital rim). Well-defined lesion, usually hypointense on T1-weighted and hyperintense on PD-weighted images. May exhibit a fat-fluid level. Shows bony remodelling without destruction (13).
Fibrous dysplasia	Bony expansion with intact but thickened cortex. Low signal intensity on both T1-weighted and PD-weighted images, as well as on FLAIR images (6,14). No extension into soft tissue. Typical locations in the skull are frontal, sphenoid, maxillary, and ethmoidal bones (14).

Abbreviations: FLAIR fluid-attenuated inversion recovery; PD proton density; GRE gradient-recalled echo. Note that the PD-weighted sequence used in our MR protocol is a fast spin echo sequence with a long repetition time (12,300 ms), which results in hyperintense signal of (cerebrospinal) fluid, comparable to the tissue-fluid contrast seen in T2-weighted sequences.

APPENDIX REFERENCES

1.

Kruit MC, Launer LJ, Ferrari MD, van Buchem MA. Infarcts in the posterior circulation territory in migraine. The population-based MRI CAMERA study. Brain 2005; 128:2068-2077.

2.

Vermeer SE, Koudstaal PJ, Oudkerk M, Hofman A, Breteler MM. Prevalence and risk factors of silent

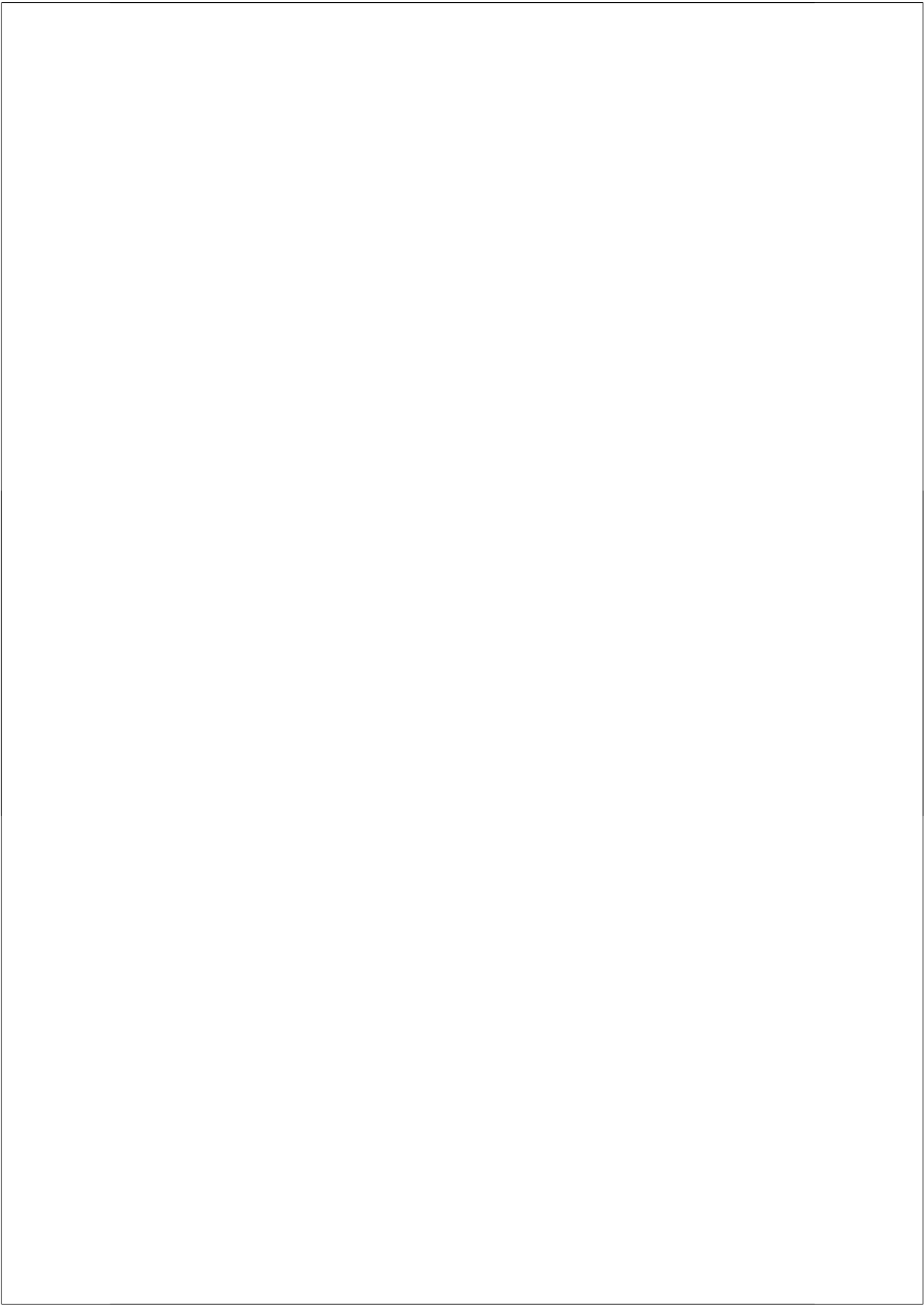
3.

brain infarcts in the population-based Rotterdam Scan Study. Stroke 2002; 33:21-25.

3.

Bryan RN, Cai J, Burke G, et al. Prevalence and anatomic characteristics of infarct-like lesions on MR images of middle-aged adults: the atherosclerosis risk in communities study. AJNR

- Am J Neuroradiol 1999; 20:1273-1280.
4. Bokura H, Kobayashi S, Yamaguchi S. Distinguishing silent lacunar infarction from enlarged Virchow-Robin spaces: a magnetic resonance imaging and pathological study. J Neurol 1998; 245:116-122.
5. Barkhof F. Enlarged Virchow-Robin spaces: do they matter? J Neurol Neurosurg Psychiatry 2004; 75:1516-1517.
6. Osborn AG. Diagnostic Neuroradiology. St. Louis: Mosby, 1994.
7. Kameyama S, Tanaka R, Kawaguchi T, Fukuda M, Oyanagi K. Cystic acoustic neurinomas: studies of 14 cases. Acta Neurochir (Wien) 1996; 138:695-699.
8. Yilmazlar S, Kocaeli H, Aksoy K. Quadrigeminal cistern lipoma. J Clin Neurosci 2005; 12:596-599.
9. Dahlen RT, Johnson CE, Harnsberger HR, et al. CT and MR imaging characteristics of intravestibular lipoma. AJNR Am J Neuroradiol 2002; 23:1413-1417.
10. Majoie CB, Hulsmans FJ, Castelijns JA, et al. Primary nerve-sheath tumours of the trigeminal nerve: clinical and MRI findings. Neuroradiology 1999; 41:100-108.
11. Meadows J, Kraut M, Guarnieri M, Haroun RI, Carson BS. Asymptomatic Chiari Type I malformations identified on magnetic resonance imaging. J Neurosurg 2000; 92:920-926.
12. Lane JI, Flanders AE, Doan HT, Bell RD. Assessment of carotid artery patency on routine spin-echo MR imaging of the brain. AJNR Am J Neuroradiol 1991; 12:819-826.
13. Mafee MF. Orbit: Embryology, Anatomy, and Pathology. In: Som PM, Curtin HD, eds. Head and Neck Imaging. St. Louis: Mosby, 2003; 563-568.
14. Amaral L, Chiurciu M, Almeida JR, Ferreira NF, Mendonca R, Lima SS. MR imaging for evaluation of lesions of the cranial vault: a pictorial essay. Arq Neuropsiquiatr 2003; 61:521-532.



2.3

INTRAVESTIBULAR LIPOMA - AN IMPORTANT IMAGING DIAGNOSIS

*Archives of Otolaryngology -
Head & Neck Surgery, 2008; 134:1225-1228*

*Meike W. Vernooij,
M. Arfan Ikram,
Arnaud J. P. E. Vincent,
Monique M. B. Breteler,
Aad van der Lugt*

Lipomas are rare intracranial tumors that are seldom located in the cerebellopontine angle or the internal auditory canal. An exceptionally rare entity is the intravestibular located lipoma, of which to date only 6 cases have been reported. We present a case of intravestibular lipoma associated with cerebellopontine angle lipoma and cystic cochleovestibular malformation (incomplete partition type I) of the inner ear. Typical MRI and CT characteristics are shown and the importance of diagnosis by imaging is stressed.

Lipomas comprise 0.1% of all intracranial tumors (1). Very rarely they are located in the cerebellopontine angle (CPA) or the internal auditory canal, and even less frequently they have been described in an intravestibular location (2-4). These lipomas should not be treated surgically because their adherence to nerves and surrounding brain structures often leads to neurological deficits when surgical removal of the lesion is attempted (1). Therefore, it is important to distinguish inner ear and CPA lipomas from more common tumors in the cerebellopontine region, such as acoustic neuromas, which are often treated surgically. Thus, noninvasive diagnosis by radiological imaging is crucial.

We report herein a case of intravestibular lipoma that is associated with CPA lipoma and cystic cochleovestibular malformation (incomplete partition type I) of the inner ear. Diagnostic magnetic resonance imaging (MRI) and computed tomographic (CT) characteristics of lipomas are discussed in detail. Furthermore, this unique combination of intravestibular lipoma with cystic cochleovestibular malformation provides more understanding of the pathophysiology of these rare tumors.

REPORT OF CASE

A 57-year-old woman was diagnosed incidentally, on participation in a research MRI study, as having a right-sided CPA lesion. For further evaluation of this lesion she was referred to a neurosurgeon (A.J.P.E.V.). She reported right-sided hearing loss of unknown origin, which had never been evaluated. Her medical history was otherwise unremarkable. No symptoms of vertigo or tinnitus were present. Other than profound sensorineural hearing loss on the right side, findings from a physical examination were unremarkable, without other cranial nerve deficits. In particular, there were no signs of nystagmus, facial weakness, or paralysis.

The MRI examination was repeated and consisted of conventional, nonenhanced, T1-weighted imaging; heavily T2-weighted imaging; fat-suppressed T1-weighted imaging; and finally T1-weighted imaging after administration of gadolinium. On nonenhanced T1-weighted imaging, the extra-axial lesion in the right cerebellopontine cistern showed marked spontaneous hyperintensity, as did a second lesion in the right vestibule (Figure 1A). Both lesions showed isointensity to slight hyperintensity relative to the cerebral cortex on T2-weighted imaging, and an anatomical connection between the 2 could not be fully excluded. On a fat-suppressed T1-weighted sequence, both lesions dropped markedly in signal intensity (Figure 1B), verifying their fatty nature. After contrast administration, no apparent enhancement was present in either lesion.

The seventh and eighth cranial nerves on the right side were surrounded by the CPA lesion and appeared smaller than those on the normal left side. Furthermore, a marked enlargement of the vestibule on the right side was seen, with the lateral semicircular canal seemingly absent, whereas the posterior and superior semicircular canals were normal. In addition, the right cochlea appeared dysplastic, and the modiolus appeared to be absent. All inner ear structures on the left side showed normal anatomy and signal intensity.

A CT-examination was performed for better visualization of the bony inner ear structures, and this confirmed the anatomical anomalies of the right vestibule and lateral semicircular canal. Also, it clearly showed an incomplete partition of the right cochlea with a normal basal turn but a common cavity where the middle and apical turn normally appear (Figure 2), in the absence of a modiolus. The vestibular aqueduct was not enlarged. The abnormalities of the vestibule, semicircular canal, and cochlea were characteristic for cystic cochleovestibular malformation, also known as incomplete partition type I (5). Both the CPA lesion and

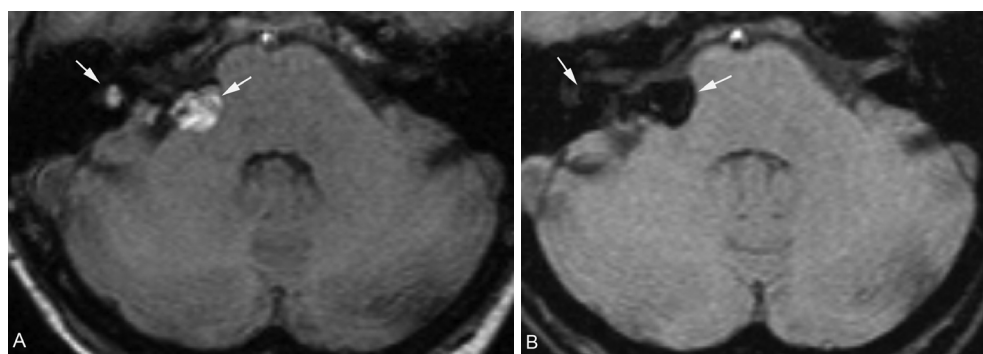


Figure 1. Magnetic resonance imaging scans of the infratentorial region. A, Axial conventional (nonenhanced) T1-weighted and (B) fat-suppressed T1-weighted scans. In the right cerebellopontine angle and the right vestibule, 2 lesions (white arrows) with marked intrinsic hyperintense signal on the nonenhanced T1-weighted image (A) are seen. The hyperintense signal on T1-weighted imaging is completely suppressed after applying a fat-suppression inversion pulse (B).

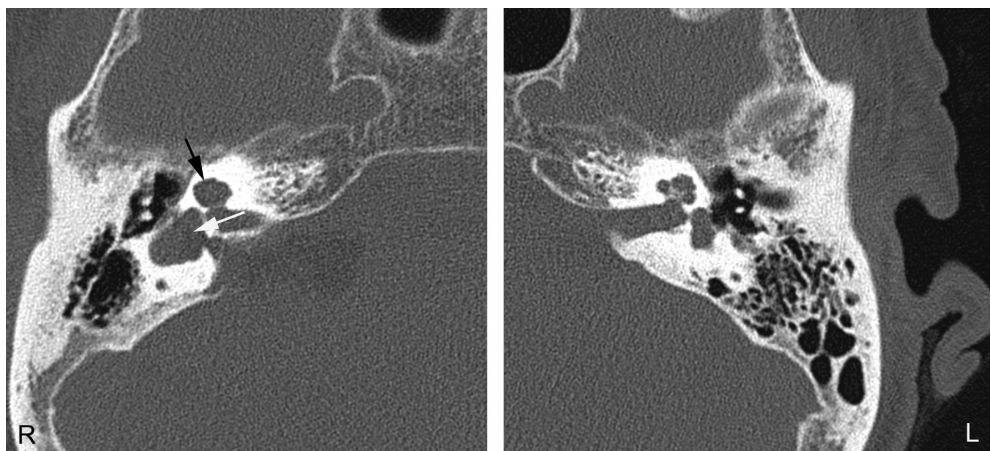


Figure 2. Axial computed tomographic image of the inner ear, bone window. In the right inner ear (R), an enlarged vestibule that incorporates the lateral semicircular canal is seen (white arrow). Also, the cochlea shows incomplete partition, with the upper turns forming a common cavity (black arrow), and there is absence of the modiolus. In comparison, in the left inner ear (L), a normal anatomy of the cochlea is seen. The findings on the right side are characteristic for cystic cochleovestibular malformation (incomplete partition type I).

the vestibular lesion were hypoattenuated, and findings from densitometry were consistent with fat (Hounsfield attenuation units [HU], -120 to -150 (Figure 3).

Based on all imaging findings, the diagnosis was made of a congenital right-sided CPA lipoma and a right-sided intravestibular lipoma in a person with cystic cochleovestibular malformation. Based on the nature of the lesions and the absence of neurological symptoms other than congenital hearing loss, no treatment was installed.

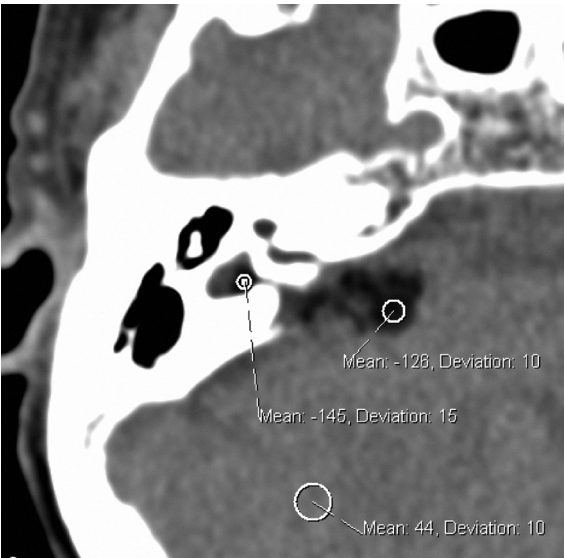


Figure 3. Axial computed tomographic image of the right inner ear, soft tissue window. Hounsfield attenuation unit (HU) measurements performed of the lesion in the vestibule and cerebellopontine angle show densities corresponding to fat (normally, -50 to -150 HU) (small, medium, and large statistics circles indicate mean [SD] measurements of -145 [15], -126 [10], and 44 [10] HU, respectively). For comparison, densitometry was performed of cerebellar brain tissue as well (large statistics circle), showing densities corresponding to brain tissue (>40 HU).

COMMENT

Intracranial lipomas in the region of the inner ear are very rare congenital lesions (4,6). To our knowledge, we report for the first time the combination of a CPA lipoma, an intravestibular lipoma, and cystic cochleovestibular malformation. Intravestibular lipomas are hypothesized to form during the fourth and fifth weeks of gestation, when the otocyst develops and incorporation of the meninx primitiva, the embryonic precursor of the subarachnoid space and meninges, may lead to an intravestibular location of a lipoma (4). Histologically, they consist of mature lipocytes (2,7). With the addition of the case presented herein, a total of 7 cases of intravestibular lipomas have been reported (3,4). Three of the previously reported intravestibular lipomas appeared in association with a CPA lipoma (4), as in our case.

To our knowledge, a cystic cochleovestibular malformation has not been described before in combination with either an intravestibular lipoma or a CPA lipoma. The well-described cystic cochleovestibular malformation is thought to result from a developmental arrest in the inner ear structures around the fifth week of gestation (5). We therefore feel that it is not a mere coincidence that an intravestibular lipoma, CPA lipoma, and cystic cochleovestibular malformation were all present in the same person, and we believe that their concurrence supports the proposed maldevelopmental origin of inner ear lipomas. The hearing loss in our patient could therefore be the result of either the congenital cochleovestibular malformation, the CPA lesion surrounding and affecting the eighth cranial nerve, or the hypothesized toxic effects on the cochlea by intramembranous spread of substances from the intravestibular lipoma (4).

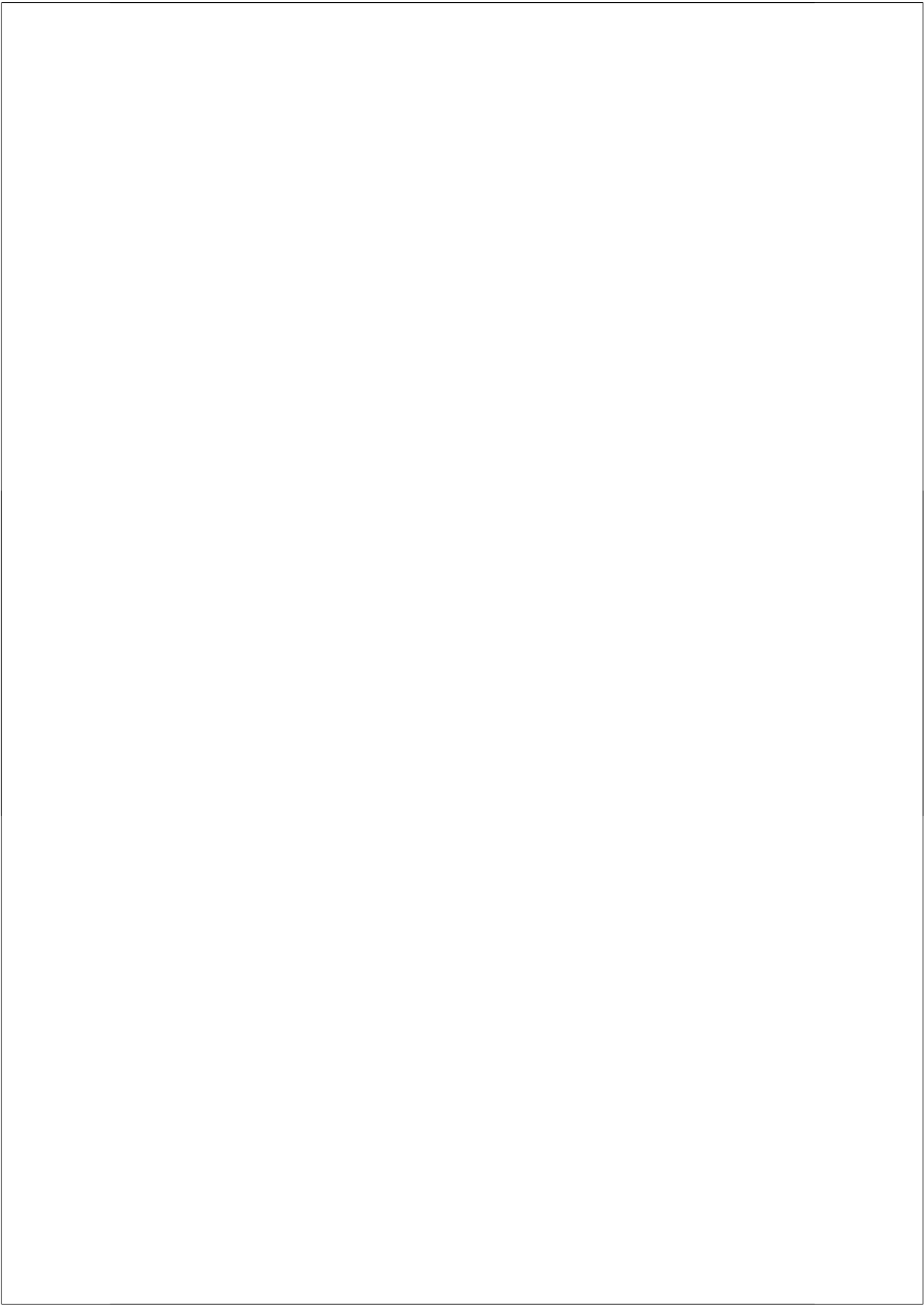
Lipomas located in the CPA or the internal auditory canal are frequently adherent to surrounding structures, most notably the seventh and eighth cranial nerves and the brainstem (1,2). The cause of the intimate relation of these lipomas to surrounding brain structures has been described as resulting from an “infiltrative” growth pattern of the lipoma (1). However, because intracranial lipomas are not thought of as neoplastic lesions but rather as developmental aberrations (7), and growth has seldom been reported, this explanation seems unlikely. Another, more likely possibility is that the apparent adhesion to other structures results from the maldifferentiation of the subarachnoid space, leading to cranial nerve fibers and lipoma to form a common structure (2). Attempts to surgically remove these lesions have therefore been followed by new cranial nerve deficits in most cases (1,2). Regarding CPA lipomas, only 18.5% of 54 surgically treated patients did not experience additional new deficits postoperatively (1). Because inner ear lipomas do not always cause congenital hearing loss but can also present with progressive unilateral sensorineural hearing loss at an older age (4), based on their clinical presentation they can be confused for acoustic neuromas, which are often treated surgically. It is therefore critical to make the diagnosis of lipoma before the pa-

tient undergoes surgery to treat a presumed acoustic neuroma or other operable lesion. Only in highly selected cases should surgery be contemplated, because the risks are high and the benefits are only marginal. Thus, there is an important role for radiological imaging to obtain a correct diagnosis by nonsurgical means.

In general, characteristics and imaging findings of intracranial lipomas on CT and MRI have been well described. On MRI, findings of a lesion with intrinsic high signal on nonenhanced T1-weighted images that shows complete suppression of the signal on fat-suppressed T1-weighted imaging (Figure 1B) and that are not enhanced after the administration of gadolinium-containing contrast agents are diagnostic for CPA lipomas. In contrast, acoustic neuromas will show low to intermediate signal intensity on nonenhanced T1-weighted MRI but will enhance after contrast-administration. Thus, on contrast-enhanced T1-weighted images; both lipomas and acoustic neuromas will be hyperintense and indistinguishable. On CT, measurement of HUs within the lesion will reveal its lipomatous nature (Figure 3) and confirm the diagnosis.

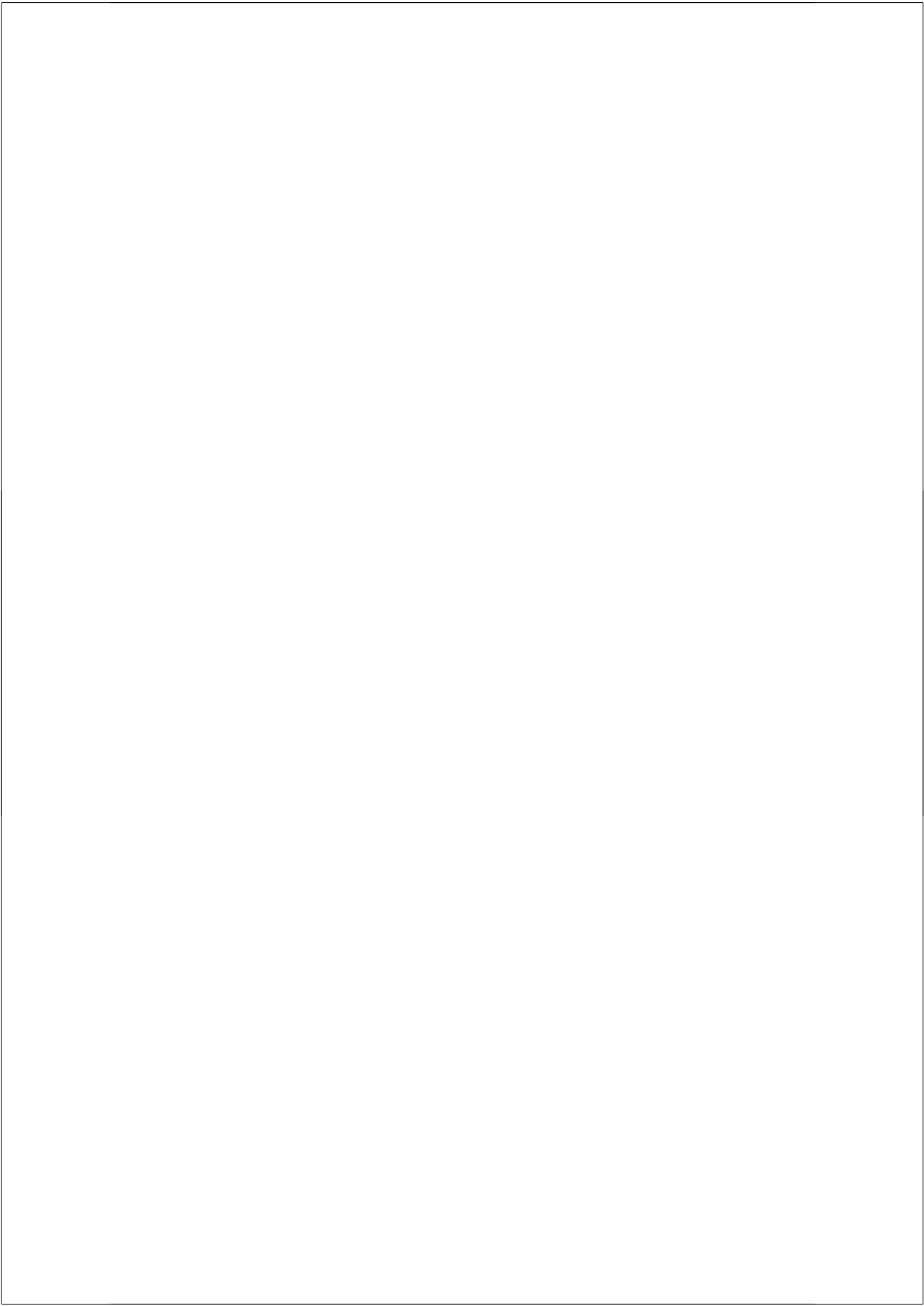
REFERENCES

1. Tankere F, Vitte E, Martin-Duverneuil N, Soudant J. Cerebellopontine angle lipomas: report of four cases and review of the literature. *Neurosurgery* 2002; 50:626-631.
2. Bigelow DC, Eisen MD, Smith PG, et al. Lipomas of the internal auditory canal and cerebellopontine angle. *Laryngoscope* 1998; 108:1459-1469.
3. Huang TS. Primary intravestibular lipoma. *Ann Otol Rhinol Laryngol* 1989; 98:393-395.
4. Dahlen RT, Johnson CE, Harnsberger HR, et al. CT and MR imaging characteristics of intravestibular lipoma. *AJNR Am J Neuroradiol* 2002; 23:1413-1417.
5. Sennaroglu L, Saatci I. A new classification for cochleovestibular malformations. *Laryngoscope* 2002; 112:2230-2241.
6. Leibrock LG, Deans WR, Bloch S, Shuman RM, Skultety FM. Cerebellopontine angle lipoma: a review. *Neurosurgery* 1983; 12:697-699.
7. Truwit CL, Barkovich AJ. Pathogenesis of intracranial lipoma: an MR study in 42 patients. *AJR Am J Roentgenol* 1990; 155:855-864; discussion 865.



CHAPTER 3

CEREBRAL MICROBLEEDS



3.1

CEREBRAL MICROBLEEDS: ACCELERATED 3D T₂*- WEIGHTED GRE MRI VERSUS CONVENTIONAL 2D T₂*-WEIGHTED GRE MRI FOR DETECTION

Radiology, 2008; 248:272-277

*Meike W. Vernooij,
M. Arfan Ikram,
Piotr A. Wielopolski,
Gabriel P. Krestin,
Monique M.B. Breteler,
Aad van der Lugt*

The purpose of this study was to prospectively compare high-spatial-resolution accelerated three-dimensional (3D) T2-weighted gradient-recalled-echo (GRE) magnetic resonance (MR) images with conventional two-dimensional (2D) T2*-weighted GRE MR images for the depiction of cerebral microbleeds.*

After obtaining institutional review board approval and informed consent, 200 elderly participants (age range, 69.7–96.7 years; 108 [54%] women) were imaged at 1.5 T by using both sequences. Presence, number, and location of microbleeds were recorded for both sequences, and differences were tested by using McNemar and signed rank tests.

Cerebral microbleeds were detected in significantly more participants on 3D T2-weighted GRE images (35.5%) than on 2D T2*-weighted GRE images (21.0%; $P < 0.001$). Furthermore, in persons with microbleeds visualized on both image sets, significantly more microbleeds ($P < 0.001$) were seen on 3D images than on 2D images. For both sequences, the proportion of participants with a microbleed in a lobar (cortical gray and subcortical white matter), deep, or infratentorial location was similar.*

In conclusion, accelerated 3D T2-weighted GRE images depict more microbleeds than do conventional 2D T2*-weighted GRE images.*

Cerebral microbleeds are hemosiderin deposits in the brain that are caused by leakage of red blood cells from small blood vessels (1). These hemosiderin deposits can be visualized by using T2*-weighted gradient-recalled-echo (GRE) magnetic resonance (MR) imaging sequences, and they appear as small foci of decreased signal intensity (1). The paramagnetic properties of hemosiderin induce local magnetic field inhomogeneities that result in phase shifts. T2*-weighted GRE sequences are very sensitive to such phase shifts, as they lack a 180° refocusing pulse (2,3).

The presence of microbleeds has been found to be related to risk of hemorrhagic transformation after ischemic stroke and to recurrence of spontaneous intracerebral bleeding (4–7). There are controversial results (8–12) suggesting that the presence of cerebral microbleeds indicates an increased risk of bleeding complications from thrombolytic treatment or the use of antiplatelet drugs. For these reasons, it is important to accurately identify those patients who have cerebral microbleeds.

Traditionally, two-dimensional (2D) T2*-weighted GRE sequences have been used for imaging of microbleeds (2,4,6,13). Haacke et al (14) presented a new method, which they refer to as susceptibility-weighted imaging, to further enhance T2*-weighted effects by using the phase information of the images collected. This susceptibility-weighted imag-

ing method was primarily designed to increase the conspicuity of deoxygenated blood for applications in venography. For the detection of microbleeds, it is not so much phase information that needs to be enhanced (as hemosiderin will cause strong phase shifts anyway), but that advances may lie more in imaging at a higher spatial resolution to minimize partial volume effects and enable the detection of smaller microbleeds. The longer acquisition time associated with imaging at small voxel sizes can be reduced through acceleration by parallel imaging.

The purpose of our study, therefore, was to prospectively compare images obtained with a high-spatial-resolution accelerated three-dimensional (3D) T2*-weighted GRE sequence with those obtained with a conventional 2D T2*-weighted GRE sequence for the depiction of cerebral microbleeds.

METHODS

Study participants

Our study was performed in participants from a larger population-based prospective cohort study, the Rotterdam Study, that aims to assess determinants of diseases in the elderly (15). For the larger study, institutional review board approval was obtained, as was informed consent from all participants. In previous years of the study, MR imaging had been performed in a randomly selected subset of participants. In 2006, all individuals who had undergone MR imaging in a previous round of the study and who were still alive and did not have contraindications to MR imaging were invited for repeat brain MR imaging with a new imaging protocol, which included sequences sensitive enough to allow detection of cerebral microbleeds, as described below.

Our institutional review board (Erasmus MC University Medical Center, Rotterdam, the Netherlands) approved the study. In total, 254 participants from the larger study were eligible for our study; 207 (81.5%) agreed to participate and gave informed consent. In four participants, imaging could not be completed due to physical problems; while in three participants, artifacts from motion or metallic dental implants prevented proper assessment. This left a total of 200 participants for analysis.

MR imaging

Imaging was performed on a 1.5-T imager (GE Healthcare, Milwaukee, Wisconsin, USA) with an eight-channel head coil. Two technologists (both with 2 years experience performing brain MR imaging) performed all MR imaging examinations according to a standard-

ized protocol. In all participants, conventional 2D T2*-weighted GRE MR imaging and accelerated 3D T2*-weighted GRE MR imaging (both spoiled GRE sequences) were performed (Table 1). Two-dimensional T2*-weighted GRE was performed with flow compensation with an echo time of 20 ms and a section thickness of 5 mm, in line with conventional settings (4,5,13,16–18). The 3D T2*-weighted GRE sequence was fully velocity compensated (with gradient moment nulling in all three orthogonal directions) and was performed with a smaller voxel size (Table 1) than the 2D T2*-weighted GRE sequence. To compensate for the decrease in dephasing associated with acquisition at a smaller voxel size, the echo time used for the 3D T2*-weighted GRE sequence was increased to 31 ms. Increasing the echo time also enabled us to lower bandwidth and thus to increase the signal-to-noise ratio on the 3D T2*-weighted GRE images.

The flip angle for the 3D T2*-weighted GRE sequence was empirically set at 13° to obtain a rather homogeneous signal intensity for gray and white matter. By using this flip angle, the signal intensity of cerebrospinal fluid appeared just slightly darker than that of gray and white matter, enabling the distinction of sulci. Because acquisition in a 3D format considerably increases acquisition time, parallel imaging with an acceleration factor of two was applied to reduce acquisition time for the 3D T2*-weighted GRE sequence to acceptable and practical limits (5 minutes 55 seconds).

Table 1. MR sequence parameters

Sequence parameter	2D T2*-weighted GRE	3D T2*-weighted GRE
Repetition time (ms)	775	45
Echo time (ms)	20	31
Flip angle (degrees)	25	13
Bandwidth (kHz)	11.90	14.71
Field of view (cm)	26 x 19.5	25 x 17.5
Matrix size	256 x 256	320 x 224
Parallel imaging	No	Yes (acceleration factor= 2)
Velocity compensation	Yes	Yes
Section thickness (mm)	5	1.6, Zero-padded to 0.8
Gap	None	None
No. of sections	26	96, Zero-padded to 192
Real voxel size (mm)	1.0 x 1.0 x 5.0	0.8 x 1.1 x 1.6
Interpolated voxel size (mm)	0.5 x 0.5 x 5.0	0.5 x 0.5 x 0.8
Acquisition time	2 min 29 s	5 min 55 s

In addition to both T2*-weighted GRE sequences, a 3D T1-weighted spoiled GRE sequence with an inversion recovery prepulse was performed (repetition time, 13.8 ms; echo time, 2.8 ms; inversion time, 400 ms; flip angle, 20°; bandwidth, 12.50 kHz; field of view, 25 cm (rectangular 0.7), matrix, 416 x 256; section thickness, 1.6 mm zero-padded to 0.8 mm), for which the number of sections and section position were matched to those of the accelerated 3D T2*-weighted GRE sequence.

The use of parallel imaging in the 3D T2*-weighted GRE sequence led to a postacquisition reconstruction time of about 5 minutes. To avoid a lag in data output and subsequent stop in imaging, the accelerated 3D T2*-weighted GRE was always performed at the end of the MR imaging protocol.

Rating of cerebral microbleeds

Acquisition date and participant identification were removed from all images. The 2D T2*-weighted GRE and 3D T2*-weighted GRE images were randomly allocated to one of two reviewers (M.W.V., M.A.I., both with 2.5 years experience reading neurologic MR images). Reviewers were blinded to the other sequence and to all clinical information. Two-dimensional T2*-weighted GRE images were read first, in random order; after a 3-week gap, the 3D T2*-weighted GRE images were read, again in random order. Fifty randomly selected 2D T2*-weighted GRE and 3D T2*-weighted GRE images were rated by both reviewers.

Reviewers independently rated the presence, location, and number of all cerebral microbleeds. Microbleeds were defined as focal areas of very low signal intensity that were smaller than 10 mm in size (13,16). In accordance with previous studies (13,16), they were categorized into one of three locations: lobar (cortical gray matter and subcortical white matter), deep (deep gray matter [basal ganglia and thalamus] and deep white matter [corpus callosum]), or infratentorial (brainstem and cerebellum). Signal voids caused by sulcal vessels, symmetric calcifications in the deep gray matter, choroid plexus calcifications, pineal calcification, and signal averaging from bone were excluded.

All studies with a potential microbleed were reviewed for confirmation by an experienced neuroradiologist (A.v.d.L., with 7 years experience reading neurologic MR images), again with a 3-week gap between the review of both sequences. At this time, the T1-weighted images additionally were used to confirm the location of microbleeds, as the inherent properties of microbleeds will cause them to appear as a focus of low signal intensity (without marked blooming) on the T1-weighted image as well. Thus, the T1-weighted image further facilitated differentiation of microbleeds from calcification in the ventricle or from sulcal vessels. After-

wards, dissimilarities between conventional 2D T2*-weighted GRE and accelerated 3D T2*-weighted GRE images were assessed in a side-by-side comparison.

Statistical analysis

For the 50 images of each sequence that were read by both reviewers, we tested the interobserver reliability for microbleed rating by using Cohen κ test. The following interpretation of the κ statistic was used: 0–0.20 = poor agreement, 0.21–0.40 = fair agreement, 0.41–0.60 = moderate agreement, 0.61–0.80 = good agreement, and 0.81–1.00 = very good agreement (19).

The prevalence and multiplicity of cerebral microbleeds were calculated for both sequences, and statistical significance of the difference was tested by using the nonparametric McNemar test for paired proportions. Furthermore, for both sequences we calculated the proportion of participants who had microbleeds in lobar, deep, or infratentorial brain locations. For those participants whose studies showed microbleeds on images obtained with both sequences, we tested whether significantly more microbleeds were visible on one image set compared with the other by using the nonparametric Wilcoxon signed rank test, as the number of microbleeds was not normally distributed. A two-tailed P value less than 0.05 was considered to indicate a statistically significant difference. All analyses were performed by using a statistical software package (SPSS, version 11.0.1 for Windows; SPSS, Chicago, Ill).

RESULTS

Microbleeds

The mean age of the 200 participants was 79.2 years (range, 69.7–96.7 years). One hundred eight (54.0%) were women. Cerebral microbleeds (Figure) were detected on the 2D T2*-weighted GRE images of 42 (21.0%) participants and on the accelerated 3D T2*-weighted GRE images of 71 (35.5%) participants (Table 2). The difference in the prevalence of cerebral microbleeds between the sequences was highly significant ($P < 0.001$).

On 2D T2*-weighted GRE images, as well as on 3D T2*-weighted GRE images, most participants who had microbleeds had these in a lobar location (Table 2). Between both sequences, the proportion of participants with a microbleed in a lobar, deep, or infratentorial location was similar (Table 2).

Side-by-side comparison

At side-by-side comparison, there were no microbleeds visualized on the 2D T2*-weighted GRE images that were not detected on the accelerated 3D T2*-weighted GRE images. Among

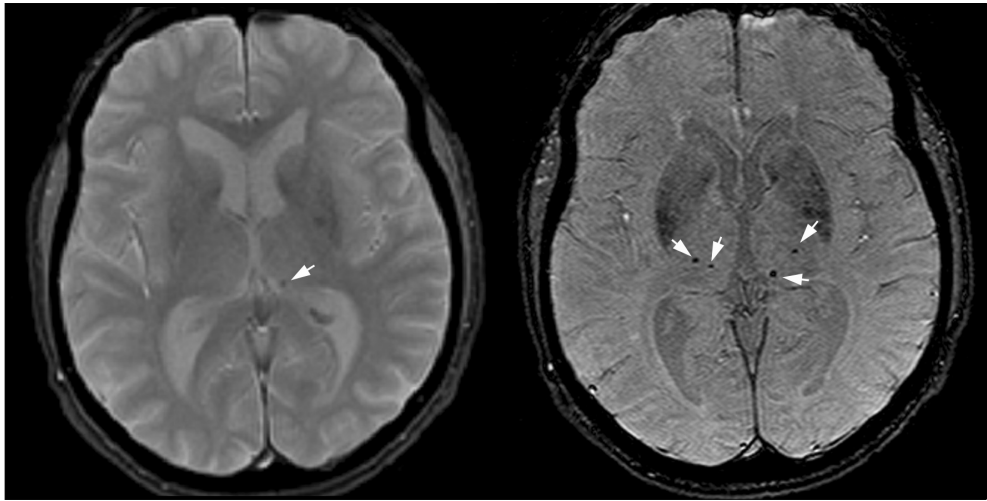


Figure. Microbleeds on 3D T2*GRE imaging compared with conventional 2D T2*GRE imaging. Axial MR images obtained with conventional 2D T2*-weighted GRE (left) (repetition time ms/echo time ms, 775/20; flip angle, 25°; section thickness, 5 mm) and accelerated 3D T2*-weighted GRE (right) (45/31; flip angle, 13°; section thickness, 1.6mm zero-padded to 0.8 mm) sequences in the same participant. More cerebral microbleeds (arrows), seen bilaterally in the thalamus region, are visible on the 3D T2*-weighted GRE image than the 2D T2*-weighted GRE image.

those persons in whom cerebral microbleeds were visible on both image sets (N = 42), significantly more microbleeds were visualized with the accelerated 3D T2*-weighted GRE sequence than with the conventional 2D T2*-weighted GRE sequence (median number of microbleeds, 2.5 vs 1.0; Wilcoxon signed rank test, P < 0.001).

Table 2. Prevalence of cerebral microbleeds on 2D and 3D GRE MR images

Prevalence	2D T2*-weighted GRE (N = 200)	3D T2*-weighted GRE (N = 200)	P value
At least one microbleed	42 (21.0)	71 (35.5)	< 0.001*
Multiple (≥ 2) microbleeds	19 (9.5)	43 (21.5)	< 0.001*
Median no. of microbleeds†	1.0 (1.0-4.0)	2.5 (1.0-9.5)	< 0.001‡
Location§			
Lobar	36 (85.7)	64 (90.1)	
Deep	7 (16.7)	11 (15.5)	
Infratentorial	14 (33.3)	25 (35.2)	

Note.—Unless otherwise specified, data are numbers of participants, with percentages in parentheses.

* McNemar test.

† Calculated in patients with microbleeds detected on both image sets (N = 42). Data in parentheses are interquartile ranges.

‡ Wilcoxon signed rank test.

§ Percentages were calculated as the proportion of participants with any microbleed on that sequence (N = 42 for 2D, N = 71 for 3D) that had a microbleed in the location. Percentages do not sum to 100% because some persons had microbleeds in more than one location.

Interobserver reliability

Interobserver reliabilities for the studies that were evaluated by both reviewers were very good when analyzed both at individual level (2D T2*-weighted GRE, $\kappa = 0.80$; 3D T2*-weighted GRE, $\kappa = 0.85$) and at microbleed level (2D T2*-weighted GRE, $\kappa = 0.90$; 3D T2*-weighted GRE, $\kappa = 0.82$).

DISCUSSION

Cerebral microbleeds were detected in more persons by using accelerated 3D T2*-weighted GRE images than by using conventional 2D T2*-weighted GRE images. Furthermore, in participants who had microbleeds detected on images from both sequences, we identified significantly more microbleeds on the 3D T2*-weighted GRE images than on the 2D T2*-weighted GRE images.

Before interpreting our data, some considerations of method and potential study limitations need to be addressed. We performed MR imaging with both sequences in a large sample of elderly persons to increase our study power. Interobserver reliability for the detection of microbleeds was very good for both sequences. We could not blind the reviewers to the sequence type, as differences between the two are readily visible. However, we tried to minimize bias by randomizing the order in which individual images were assessed and by blinding the independent reviewers to images obtained with the other sequence and to participant identification. Furthermore, the reviewers rated the two image sets with a 3-week gap between readings to eliminate recall bias.

We should also consider potential misclassification of cerebral microbleeds. Other structures in the brain (eg, deoxygenated blood in small veins, calcifications in basal ganglia or pineal gland) may resemble microbleeds on MR images. However, on the high-spatial-resolution accelerated 3D T2*-weighted GRE images, the cerebral vessels can be clearly identified as linear structures. Moreover, calcifications in the brain have a typical location and shape and, when located in the basal ganglia, are usually symmetric in distribution. We therefore believe that we did not misclassify other structures as cerebral microbleeds and thus did not overestimate the prevalence of microbleeds in either image set. On both the 2D T2*-weighted GRE and 3D T2*-weighted GRE images, we may have missed some microbleeds in the base of the brain owing to susceptibility artifacts in T2*-weighted GRE imaging caused by air and bone interfaces.

Not only on the accelerated 3D T2*-weighted GRE images, but also on the conventional 2D T2*-weighted GRE images, the prevalence of cerebral microbleeds in our study was much higher than that previously reported in population-based studies (13,16,20) that used comparable 2D T2*-weighted GRE sequences. Possible explanations for this higher prevalence are the higher mean age of our participants (79.2 years vs 60 years [13,16,20]) and the higher field strength (1.5 T vs 1.0 T in the Framingham Heart Study [13]), which causes susceptibility artifacts from hemosiderin deposits to be more pronounced. Two-dimensional T2*-weighted GRE sequences have previously been shown to better depict cerebral microbleeds than conventional spin-echo and fast spin-echo T2-weighted sequences (2, 16). By using a 3D T2*-weighted GRE sequence, we found cerebral microbleeds in even more participants than by using a 2D T2*-weighted GRE sequence. The imaging parameters chosen for our accelerated 3D T2*-weighted GRE sequence resulted in images that had a much higher spatial resolution in comparison to those obtained with a conventional 2D T2*-weighted GRE sequence (13,16) and that could be obtained within a reasonable imaging time through use of parallel imaging. Fazekas et al (1) showed with a histopathologic analysis that conventional 2D T2*-weighted GRE images do not depict small hemosiderin deposits that consist of only a few perivascular hemosiderin-laden macrophages. The much smaller voxel size in 3D T2*-weighted GRE MR imaging enables the detection of smaller microbleeds, while the combination of increased echo time and decreased bandwidth and flip angle ensures a high signal-to-noise ratio and adequate contrast between microbleeds and other brain tissue (14,21). This contrast could potentially be further intensified by using the proposed susceptibility-weighted imaging technique of Haacke et al (14), in which phase information is used to create a special phase mask that, when multiplied with the magnitude images, improves the apparent susceptibility weighting. This technique has been shown to be highly effective for venography in the brain (22). However, imaging of cerebral microbleeds is less likely to greatly benefit from this susceptibility-weighted imaging postprocessing method because hemosiderin deposits, in contrast to deoxygenated blood in veins, cause a consistent dephasing of spins. Alternatively, imaging at a higher field strength (3 T or higher) might prove beneficial for microbleed detection, as susceptibility effects caused by hemosiderin would be more pronounced (23).

The presence of cerebral microbleeds has previously been found to be associated with an increased risk of adverse neurologic events (eg, recurrence of spontaneous bleeding, hemorrhagic transformation after ischemic stroke) (4,5,7). Furthermore, although a study (9) suggested that patients with stroke who have a small number of microbleeds can be safely treated by thrombolysis, the presence of more microbleeds may indicate a diffuse hemorrhage-prone vasculopathic condition (eg, cerebral amyloid angiopathy) that warrants a more prudent approach (8,11,24–26). In clinical practice, accurate identification of those patients who have cerebral microbleeds will thus become increasingly important for clinical decision making.

In conclusion, accelerated 3D T2*-weighted GRE images depict more microbleeds than do conventional 2D T2*-weighted GRE images.

REFERENCES

1. Fazekas F, Kleinert R, Roob G, et al. Histopathologic analysis of foci of signal loss on gradient-echo T2*-weighted MR images in patients with spontaneous intracerebral hemorrhage: evidence of microangiopathy-related microbleeds. *AJNR Am J Neuroradiol* 1999;20:637-642.
2. Greenberg SM, Finklestein SP, Schaefer PW. Petechial hemorrhages accompanying lobar hemorrhage: detection by gradient-echo MRI. *Neurology* 1996;46:1751-1754.
3. Offenbacher H, Fazekas F, Schmidt R, Koch M, Fazekas G, Kapeller P. MR of cerebral abnormalities concomitant with primary intracerebral hematomas. *AJNR Am J Neuroradiol* 1996;17:573-578.
4. Nighoghossian N, Hermier M, Adeleine P, et al. Old microbleeds are a potential risk factor for cerebral bleeding after ischemic stroke: a gradient-echo T2*-weighted brain MRI study. *Stroke* 2002;33:735-742.
5. Naka H, Nomura E, Wakabayashi S, et al. Frequency of asymptomatic microbleeds on T2*-weighted MR images of patients with recurrent stroke: association with combination of stroke subtypes and leukoaraiosis. *AJNR Am J Neuroradiol* 2004;25:714-719.
6. Imaizumi T, Horita Y, Hashimoto Y, Niwa J. Dotlike hemosiderin spots on T2*-weighted magnetic resonance imaging as a predictor of stroke recurrence: a prospective study. *J Neurosurg* 2004;101:915-920.
7. Fan YH, Zhang L, Lam WW, Mok VC, Wong KS. Cerebral microbleeds as a risk factor for subsequent intracerebral hemorrhages among patients with acute ischemic stroke. *Stroke* 2003;34:2459-2462.
8. Kidwell CS, Saver JL, Villablanca JP, et al. Magnetic resonance imaging detection of microbleeds before thrombolysis: an emerging application. *Stroke* 2002;33:95-98.
9. Derex L, Nighoghossian N, Hermier M, et al. Thrombolysis for ischemic stroke in patients with old microbleeds on pretreatment MRI. *Cerebrovasc Dis* 2004;17:238-241.
10. Kakuda W, Thijs VN, Lansberg MG, et al. Clinical importance of microbleeds in patients receiving IV thrombolysis. *Neurology* 2005;65:1175-1178.
11. Leblanc R, Haddad G, Robitaille Y. Cerebral hemorrhage from amyloid angiopathy and coronary thrombolysis. *Neurosurgery* 1992;31:586-590.
12. Wong KS, Chan YL, Liu JY, Gao S, Lam WW. Asymptomatic microbleeds as a risk factor for aspirin-associated intracerebral hemorrhages. *Neurology* 2003;60:511-513.
13. Jeerakathil T, Wolf PA, Beiser A, et al. Cerebral microbleeds: prevalence and associations with cardiovascular risk factors in the Framingham Study. *Stroke* 2004;35:1831-1835.
14. Haacke EM, Xu Y, Cheng YC, Reichenbach JR. Susceptibility weighted imaging (SWI). *Magn Reson Med* 2004;52:612-618.
15. Hofman A, Breteler MM, van Duijn CM, et al. The Rotterdam Study: objectives and design update. *Eur J Epidemiol* 2007; 22: 819-829.

16. Roob G, Schmidt R, Kapeller P, Lechner A, Hartung HP, Fazekas F. MRI evidence of past cerebral microbleeds in a healthy elderly population. *Neurology* 1999;52:991-994.
17. Kinoshita T, Okudera T, Tamura H, Ogawa T, Hatazawa J. Assessment of lacunar hemorrhage associated with hypertensive stroke by echo-planar gradient-echo T2*-weighted MRI. *Stroke* 2000;31:1646-1650.
18. Alemany M, Stenborg A, Terent A, Sonninen P, Raininko R. Coexistence of microhemorrhages and acute spontaneous brain hemorrhage: correlation with signs of microangiopathy and clinical data. *Radiology* 2006;238:240-247.
19. Landis JR, Koch GG. The measurement of observer agreement for categorical data. *Biometrics* 1977;33:159-174.
20. Tsushima Y, Tanizaki Y, Aoki J, Endo K. MR detection of microhemorrhages in neurologically healthy adults. *Neuroradiology* 2002;44:31-36.
21. Edelman R. CADASIL and Microbleeds. In: *Clinical Magnetic Resonance Imaging*: Saunders, 2005: 1319-1320.
22. Rauscher A, Sedlacik J, Barth M, Haacke EM, Reichenbach JR. Noninvasive assessment of vascular architecture and function during modulated blood oxygenation using susceptibility weighted magnetic resonance imaging. *Magn Reson Med* 2005;54:87-95.
23. Kikuta K, Takagi Y, Nozaki K, et al. Asymptomatic microbleeds in moyamoya disease: T2*-weighted gradient-echo magnetic resonance imaging study. *J Neurosurg* 2005;102:470-475.
24. Chalela JA, Kang DW, Warach S. Multiple cerebral microbleeds: MRI marker of a diffuse hemorrhage-prone state. *J Neuroimaging* 2004;14:54-57.
25. McCarron MO, Nicoll JA. Cerebral amyloid angiopathy and thrombolysis-related intracerebral haemorrhage. *Lancet Neurol* 2004;3:484-492.
26. Greenberg SM. Cerebral amyloid angiopathy: prospects for clinical diagnosis and treatment. *Neurology* 1998;51:690-694.



3.2

PREVALENCE AND RISK FACTORS OF CEREBRAL MICROBLEEDS. THE ROTTERDAM SCAN STUDY

Neurology, 2008; 70:1208–1214

*Meike W. Vernooij,
Aad van der Lugt,
M. Arfan Ikram,
Piotr A. Wielopolski,
Wiro J. Niessen,
Albert Hofman,
Gabriel P. Krestin,
Monique M.B. Breteler*

Background Cerebral microbleeds are focal deposits of hemosiderin that can be visualized with MRI. Little is known on their prevalence in the general population and on their etiology. It has been suggested that, in analogy to spontaneous intracranial hemorrhage, the etiology of microbleeds differs according to their location in the brain, with lobar microbleeds being caused by cerebral amyloid angiopathy and deep or infratentorial microbleeds resulting from hypertension and atherosclerosis. We investigated the prevalence of and risk factors for microbleeds in the general population aged 60 years and older.

Methods This study is based on 1,062 persons (mean age 69.6 years) from the population-based Rotterdam Scan Study. MRI was performed at 1.5 T and included a sequence optimized to increase the conspicuity of microbleeds. We assessed the relation of APOE genotype, cardiovascular risk factors, and markers of small vessel disease to the presence and location of microbleeds with multiple logistic regression.

Results Overall prevalence of cerebral microbleeds was high and increased with age from 17.8% in persons aged 60-69 years to 38.3% in those over 80 years. APOE $\epsilon 4$ carriers had significantly more often strictly lobar microbleeds than noncarriers. In contrast, cardiovascular risk factors and presence of lacunar infarcts and white matter lesions were associated with microbleeds in a deep or infratentorial location but not in a lobar location.

Conclusion The prevalence of cerebral microbleeds is high. Our data support the hypothesis that strictly lobar microbleeds are related to cerebral amyloid angiopathy, whereas microbleeds in a deep or infratentorial location result from hypertensive or arteriolosclerotic microangiopathy.

Cerebral microbleeds are focal lesions that can be visualized on MRI (1). Histopathological analysis shows that these are hemosiderin deposits from red blood cells that presumably have leaked out of small brain vessels (2). In patients with symptomatic intracranial hemorrhage or ischemic stroke, the prevalence of cerebral microbleeds reportedly ranges from 20% to 70% (3,4). In clinical series, microbleeds were associated with an increased risk of stroke recurrence and with hemorrhagic transformation after ischemic stroke (5,6). Little is known on microbleed prevalence, risk factors, and clinical correlates in the general population. Prevalence estimates are highly dependent on the sensitivity of the MRI sequence used (7), and microbleeds may be more frequent in the general population than was thought previously. Furthermore, the exact etiology of microbleeds is still unclear. Because microbleeds often seem to accompany spontaneous intracerebral hemorrhage (ICH) (8,9), they are thought to be the asymptomatic counterpart of ICH, of which the etiologic mechanisms are better understood. Typically, ICHs that are restricted to a lobar location result from cerebral amyloid angiopathy (CAA) (10). This in contrast to ICHs in the basal ganglia, cerebellum, or pons, which are mainly attributed to hypertension (11). If this parallel between

ICH and cerebral microbleeds is indeed true, one would expect the risk factors for microbleeds to also differ according to their location in the brain. Established risk factors for lobar ICHs are the $\epsilon 2$ and $\epsilon 4$ alleles of the APOE gene (11-13), which would suggest that APOE allele status would also be primarily related to the presence of microbleeds in a lobar location. In contrast, cardiovascular risk factors and classic markers of ischemic small vessel disease, such as lacunar infarcts and white matter lesions, may preferentially relate to microbleeds in deep or infratentorial brain regions. Therefore, in the population-based Rotterdam Scan Study, we investigated the prevalence of cerebral microbleeds and studied how APOE genotype, cardiovascular risk factors, and markers of ischemic small vessel disease related to the presence of microbleeds and their location within the brain.

METHODS

Participants

The study is based on participants from the population-based Rotterdam Study (14). From August 2005 to May 2006, we randomly selected 1,073 members of the Rotterdam Study Plus cohort (14) (at that time all ≥ 60 years of age) for participation in the Rotterdam Scan Study, a prospective brain MRI study. In addition, we invited all participants who had undergone brain imaging (not including microbleed assessment) in 1995 in the context of a previous round of the Rotterdam Scan Study ($N = 302$) (15). The institutional review board approved the study. We excluded individuals who were demented ($N = 4$) or had MRI contraindications ($N = 142$). Of 1,229 eligible persons, 1,114 (91%) participated and gave written informed consent. Due to physical inabilities, imaging could not be performed in 16 individuals. Of 1,098 complete MRI examinations, 36 scans had to be excluded because of motion artifacts or susceptibility artifacts, leaving 1,062 scans to be analyzed.

Brain MRI

We performed a multisequence MRI protocol on a 1.5-T scanner (GE Healthcare). For microbleed detection, we used a custom-made accelerated three-dimensional T2*-weighted gradient-recalled echo (three-dimensional T2* GRE) sequence with high spatial resolution and long echo time (7), which was previously shown to detect microbleeds nearly twice as often as conventional 2D T2* GRE imaging (7). The other sequences in the imaging protocol consisted of three high-resolution axial scans, i.e., a T1-weighted sequence, a proton density-weighted sequence, and a fluid-attenuated inversion recovery (FLAIR) sequence (16). Slice position of the T1-weighted and three-dimensional T2* GRE scans was matched.

Rating of cerebral microbleeds

All three-dimensional T2* GRE scans were reviewed by one of two trained raters (M.W.V., M.A.I.; both 2.5 years of experience in microbleed rating) who recorded the presence, number, and location of cerebral microbleeds. Both raters were blinded to the other MRI sequences and to clinical data, and the three-dimensional T2* GRE scan did not reveal the presence of infarcts and white matter lesions. Microbleeds were defined as focal areas of very low signal intensity, smaller than 10 mm in size (17,18). They were categorized into one of three locations: lobar (cortical gray and subcortical or periventricular white matter), deep (deep gray matter: basal ganglia and thalamus, and the white matter of the corpus callosum, internal, external, and extreme capsule), and infratentorial (brainstem and cerebellum) (17,18). Signal voids caused by sulcal vessels, symmetric calcifications in the basal ganglia, choroid plexus, and pineal calcifications, and signal averaging from bone were excluded. All scans that were rated positive in the initial rating, mixed with a random selection of scans that had been rated negative, were reviewed by an experienced neuroradiologist (A.v.d.L.). The neuroradiologist did not confirm 2% of the initial positive ratings, and no additional microbleeds were detected on the scans that had been rated negative. The neuroradiologist additionally used the T1-weighted scan to confirm the location of the microbleed and to differentiate from ventricular calcification or from sulcal vessels. Intraobserver (N = 500, one rater) and interobserver (N = 300) reliabilities were $\kappa = 0.87$ and $\kappa = 0.85$, which corresponds to very good agreement.

Ischemic small vessel disease on MRI

Infarcts were rated on FLAIR, proton density-weighted, and T1-weighted sequences by the two raters who had scored cerebral microbleeds, after an interval of at least two weeks. Both raters were blinded to all clinical data and to the presence of cerebral microbleeds. Lacunar infarcts were defined as focal lesions ≥ 3 mm and < 15 mm in size with the same signal characteristics as CSF on all sequences, and (when located supratentorially) with a hyperintense rim on the FLAIR sequence (19). Lesions ≥ 15 mm in size, but otherwise similar, were rated as subcortical infarcts. Infarcts showing involvement of cortical gray matter were classified as cortical infarcts. All infarcts were reviewed in a consensus meeting with an experienced neuroradiologist (A.v.d.L.). White matter lesion volume was quantified with a validated tissue classification technique (20). Manual editing of classification results was necessary in 86 scans (8%), mainly because of motion artifacts. In two persons, excessive motion necessitated exclusion from analysis. One other person was excluded because of a large meningioma, which complicated white matter lesion classification. White matter lesion volumes (milliliters) were calculated by summing all voxels of the white matter lesion-class across the whole brain.

Apolipoprotein E genotyping

APOE genotyping was performed on coded genomic DNA samples (21) and was available in 1,000 participants. The distributions of APOE genotype and allele frequencies in this population were in Hardy-Weinberg equilibrium.

Cardiovascular risk factors

Cardiovascular risk factors were examined by interview and laboratory and physical examination at the preceding regular visit of study participants to the research center. Sitting blood pressure was measured twice on the right arm with a random-zero sphygmomanometer. We used the average of these two measurements. We calculated pulse pressure by subtracting diastolic blood pressure from systolic blood pressure. We defined two categories of severity of hypertension according to WHO criteria (22). First, persons who had a systolic blood pressure ≥ 140 mm Hg and < 160 mm Hg or a diastolic blood pressure ≥ 90 mm Hg and < 100 mm Hg, or used blood pressure-lowering medication, were classified as mild hypertensive (grade 1 of 2003 WHO criteria (22)). Second, individuals with a systolic blood pressure ≥ 160 mm Hg or a diastolic blood pressure ≥ 100 mm Hg regardless of the use of blood pressure-lowering medication were classified as severe hypertensive (grades 2 and 3 of 2003 WHO criteria (22)). Smoking habits were classified as “ever” or “never” smoking. Alcohol use was categorized as “never,” “former,” or “current” use (intake of alcohol within the past 12 months). Current alcohol use was further categorized into “light” (less than one drink per day), “moderate” (one or more than one drink per day but less than four drinks per day), and “heavy” (four or more drinks per day). Diabetes was considered present when a person used oral antidiabetic drugs or insulin, or when fasting blood glucose was ≥ 7.0 mmol/L. Serum total cholesterol and high-density lipoprotein (HDL-cholesterol) were determined using an automated enzymatic procedure (Hitachi analyzer, Roche Diagnostics). The use of lipid-lowering drugs and blood pressure-lowering medication was assessed by interview and house visits during which medication use was registered.

Data analysis

We calculated the prevalence of cerebral microbleeds for three age categories (60–69, 70–79, and 80–97 years). To test our hypothesis that lobar microbleeds have a different etiology, and hence different risk factors, than deep or infratentorial microbleeds, we categorized persons based on microbleed location. According to the Boston criteria (23) for CAA, persons aged ≥ 55 years with primary ICH restricted to lobar regions can be diagnosed as having “possible” (one hemorrhage) or “probable” (more than one hemorrhage) CAA-related hemorrhage. Accordingly, we made a separate category (“strictly lobar microbleeds”) of persons who had one or more microbleeds restricted to a lobar location. Persons with microbleeds in a deep or infratentorial location, with or without one or more lobar microbleeds, were assigned to the

category “deep or infratentorial microbleeds.” We additionally analyzed this group excluding persons with lobar microbleeds to investigate whether results were different for persons with “strictly” deep or infratentorial microbleeds. We analyzed the relation of APOE allele status and cardiovascular risk factors to the presence and location of microbleeds using multiple logistic regressions, adjusted for age and, when appropriate, sex. We additionally adjusted analyses of APOE genotype and microbleeds for serum levels of cholesterol. Also, we dichotomized serum total cholesterol at the 10th percentile (4.42 mmol/L) and analyzed the association of very low cholesterol level with presence of microbleeds at different locations. We used multiple logistic regression models, adjusting for age and sex and additionally for cardiovascular risk factors (blood pressure, smoking, alcohol use, diabetes, total serum cholesterol and HDL-cholesterol), to analyze whether cerebral microbleeds were more frequent in persons with brain infarcts or white matter lesions. Because the distribution of white matter lesion volume was skewed leftward, we used the natural log-transformed variable. Finally, we repeated all analyses after exclusion of persons with cortical infarcts on MRI. All analyses were performed using the statistical software package SPSS (version 11.0.1).

RESULTS

Table 1 shows the characteristics of the study population. Mean age was 69.6 years, and 543 (51%) were women. The prevalence of microbleeds was high and increased strongly with age, as did the proportion of participants with multiple microbleeds (Table 2). Of those with microbleeds ($n=250$), 146 (58.4%) had microbleeds in a strictly lobar location. Of these, 44 had multiple strictly lobar microbleeds. There were 104 (41.6%) persons who had microbleeds located in a deep or infratentorial brain region. Of these, 58 persons also had one or more lobar microbleeds.

The prevalence of microbleeds increased with age for all locations and did not differ between men and women (Table 3). Carriers of the APOE $\epsilon 4$ allele had cerebral microbleeds significantly more often in a strictly lobar location when compared with persons with the $\epsilon 3/\epsilon 3$ genotype [age-adjusted OR = 1.87, 95% CI (1.25–2.81) (Table 3)]. This was even more pronounced for persons with multiple strictly lobar microbleeds: OR = 2.68, 95% CI (1.37–5.27). We did not find an association between APOE $\epsilon 2$ allele carriership and presence of microbleeds in either location. However, although based on very few cases, we did find an association for the $\epsilon 2/\epsilon 2$ genotype with strictly lobar microbleeds [OR = 10.70, 95% CI (2.29 –50.11)]. When we analyzed persons with deep or infratentorial microbleeds excluding those with additional lobar microbleeds, results did not markedly change, yet the association with APOE $\epsilon 4$ allele carriership attenuated further

Table 1. Characteristics of the study population (N = 1062)

Age, y, mean \pm SD	69.6 \pm 7.2
Women, N (%)	543 (51.1)
Systolic blood pressure, mean \pm SD	144.4 \pm 18.7
Diastolic blood pressure, mean \pm SD	80.2 \pm 10.3
Mild hypertension, N (%)	541 (51.5)
Severe hypertension, N (%)	214 (20.4)
Smoking (ever), N (%)	755 (72.2)
Alcohol use, N (%)	
Former	65 (6.2)
Current light (< 1 drink/day)	417 (39.9)
Current moderate (\geq 1 drink/day, < 4 drinks/day)	446 (42.6)
Current heavy (\geq 4 drinks/day)	60 (5.7)
Diabetes, N (%)	95 (9.2)
Serum total cholesterol, mean \pm SD	5.67 \pm 0.96
Serum HDL cholesterol, mean \pm SD	1.44 \pm 0.38
APOE ϵ 2 allele carrier, N (%)	155 (15.5)
APOE ϵ 4 allele carrier, N (%)	273 (27.3)
Cortical infarct on MRI, N (%)	37 (3.5)
Lacunar infarct on MRI, N (%)	93 (8.8)
Subcortical infarct on MRI, N (%)	2 (0.2)
White matter lesions on MRI, mL, median (interquartile range)	3.4 (2.0-7.3)

Data are missing for blood pressure/ hypertension (N = 11), smoking (N = 17), alcohol use (N = 16), diabetes (N = 24), serum cholesterol N = 17), APOE genotype (N = 62), white matter lesions (N = 3).

Table 2. Age-specific prevalence of cerebral microbleeds

Age range	No. of persons	Cerebral microbleeds % (N)	Multiple cerebral microbleeds % (N)
60-69 y	670	17.8 (119)	5.4 (36)
70-79 y	272	31.3 (85)	16.5 (45)
80-97 y	120	38.3 (46)	23.3 (28)

[OR = 0.61, 95% CI (0.26 – 1.42)]. Additional adjustment for serum cholesterol did not change any of these associations.

High systolic blood pressure, high pulse pressure, and smoking were associated with presence of microbleeds in a deep or infratentorial brain location (Table 4). Associations of blood

Table 3. APOE allele status and the presence of cerebral microbleeds

	Any microbleed (N =250)	Strictly lobar microbleeds (N =146)	Deep or infratentorial microbleeds‡ (N =104)
Age, per year*	1.06 (1.04 - 1.08)	1.05 (1.03 - 1.08)	1.07 (1.04 - 1.10)
Women, versus men†	1.01 (0.76 - 1.35)	1.14 (0.80 - 1.63)	0.83 (0.55 - 1.26)
APOE ε4, versus ε3/ε3†	1.53 (1.09 - 2.14)	1.87 (1.25 - 2.81)	1.17 (0.70 - 1.93)
APOE ε2, versus ε3/ε3†	1.31 (0.86 - 1.99)	1.40 (0.83 - 2.35)	1.19 (0.65 - 2.16)

* Adjusted for sex; † adjusted for age; ‡ With or without lobar microbleeds

Table 4. Cardiovascular determinants and the presence of cerebral microbleeds

	All microbleeds (N =250)	Strictly lobar microbleeds (N =146)	Deep or infratentorial microbleeds‡ (N=104)
Systolic BP* per SD increase	1.16 (1.00 - 1.35)	1.08 (0.91 - 1.29)	1.29 (1.05 - 1.58)
Diastolic BP* per SD increase	1.15 (0.99 - 1.35)	1.19 (0.98 - 1.44)	1.12 (0.90 - 1.40)
Pulse pressure* per SD increase	1.10 (0.95 - 1.29)	0.99 (0.82 - 1.20)	1.28 (1.03 - 1.59)
Hypertension,			
Mild, versus none	1.07 (0.75 - 1.52)	0.97 (0.63 - 1.49)	1.24 (0.73 - 2.10)
Severe, versus none	1.33 (0.87 - 2.02)	1.15 (0.69 - 1.92)	1.66 (0.91 - 3.05)
Smoking, ever versus never	1.45 (1.02 - 2.07)	1.29 (0.84 - 1.98)	1.70 (0.98 - 2.93)
Alcohol use,			
Former, versus never	0.94 (0.43 - 2.07)	1.06 (0.41 - 2.76)	0.75 (0.25 - 2.26)
Current light, versus never	0.61 (0.33 - 1.14)	0.75 (0.35 - 1.61)	0.43 (0.18 - 1.03)
Current moderate, versus never	0.81 (0.44 - 1.51)	0.83 (0.39 - 1.77)	0.73 (0.31 - 1.69)
Current heavy, versus never	0.66 (0.27 - 1.58)	0.51 (0.16 - 1.68)	0.76 (0.24 - 2.39)
Diabetes, yes versus no	0.88 (0.53 - 1.48)	0.87 (0.46 - 1.65)	0.91 (0.44 - 1.90)
Serum total cholesterol† per SD increase	0.85 (0.72 - 1.00)	0.87 (0.71 - 1.07)	0.83 (0.65 - 1.05)
Serum HDL cholesterol† per SD increase	0.91 (0.78 - 1.07)	0.85 (0.70 - 1.04)	1.01 (0.80 - 1.27)
Serum total cholesterol† <4.42 mmol/L versus higher	2.01 (1.24 - 3.26)	2.28 (1.28 - 4.06)	1.67 (0.85 - 3.31)

All values are age and sex-adjusted.

*Additionally adjusted for the use of blood pressure-lowering medication.

† Additionally adjusted for the use of lipid-lowering drugs.

‡ With or without lobar microbleeds.

BP = blood pressure, HDL = high-density lipoprotein

pressure with deep or infratentorial microbleeds were stronger after exclusion of persons who also had lobar microbleeds [age- and sex-adjusted OR for systolic blood pressure (per SD increase) = 1.65, 95% CI (1.24 –2.19) and for pulse pressure OR =1.77, 95% CI (1.29 –2.43)]. With increasing serum total cholesterol, the prevalence of microbleeds decreased (Table 4).

Table 5. Cerebral vascular disease and the presence of cerebral microbleeds

	All microbleeds (N =250)	Strictly lobar microbleeds (N =146)	Deep or infratentorial microbleeds† (N =104)
Cortical infarcts, versus no infarct	1.03 (0.48 - 2.21)	1.36 (0.59 - 3.12)	0.56 (0.13 - 2.42)
Lacunar infarcts, versus no infarct	2.58 (1.60 - 4.17)	1.25 (0.61 - 2.55)	4.75 (2.71 - 8.34)
White matter lesion volume* per SD increase	1.32 (1.13 - 1.53)	1.12 (0.93 - 1.35)	1.67 (1.34 - 2.08)

All values are age and sex-adjusted.

* ln-transformed. † With or without lobar microbleeds

When we subsequently analyzed serum cholesterol as a variable dichotomized at the 10th percentile (<4.42 mmol/L versus higher values), we found a strong association of very low serum cholesterol level with the presence of strictly lobar microbleeds (Table 4).

Cortical infarcts on MRI were not related to the presence of cerebral microbleeds; however, both lacunar infarcts and white matter lesion volume were strongly associated with microbleeds in a deep or infratentorial location but not with those in a lobar location (Table 5). Additional adjustment for cardiovascular risk factors did not change these results. Finally, exclusion of persons with cortical infarcts on MRI (N = 37) did not change any of the above-described results.

DISCUSSION

We found in a general population of persons aged 60 years and older a high prevalence of cerebral microbleeds, which increased with age. Determinants of the presence of cerebral microbleeds differed according to microbleed location in the brain, suggesting different etiologies for microbleeds in different locations.

Major strengths of our study are its population-based design and large sample size of elderly persons. We used an MRI sequence that was optimized for the detection of cerebral microbleeds (7). Despite our very high response rate among eligible Rotterdam Study participants, there is a possibility of selection bias. Persons who refuse to participate or those with MRI contra-indications are generally older than participants (24). However, this will likely have led us to underestimate the actual prevalence of cerebral microbleeds. We should consider potential misclassification of cerebral microbleeds. Deoxygenated blood in small veins and cerebral calcifications may resemble microbleeds on MRI. However, on our high-resolution

MR images, vessels can be identified clearly as linear structures and will never present as a single dot. Moreover, cerebral calcifications have a typical location and shape, and when located in the basal ganglia are usually symmetric in distribution. We therefore believe that we did not misclassify other structures as cerebral microbleeds and thus did not overestimate the prevalence of microbleeds.

We found a three- to fourfold higher overall prevalence of cerebral microbleeds as compared with other population-based studies (17,18,25). A factor that potentially contributes to this difference in prevalence is the higher mean age of our participants compared with previous studies (17,18,25). Furthermore, the magnetic field strength that we used (1.5 T) was higher than in the Framingham Study (18). However, the most important explanation for this difference is that we used a custom-made accelerated three-dimensional T2* GRE sequence that has shown a higher sensitivity in detecting cerebral microbleeds when compared with conventional 2D T2*GRE sequences (7), because of its higher spatial resolution and longer echo time (17,18).

We found the APOE $\epsilon 4$ allele to be strongly associated with the presence of (multiple) strictly lobar microbleeds. As in Alzheimer disease, the APOE $\epsilon 4$ allele is a known risk factor for lobar ICH and CAA (11,12,26). The APOE $\epsilon 4$ allele was previously found to be more frequent in patients with CAA when compared with controls (12) and was furthermore associated with an increased risk of recurrent hemorrhage in CAA patients (26). Although the exact molecular mechanism is not clear, APOE $\epsilon 4$ carriership is presumed to lead to hemorrhage by increased vascular deposition of β -amyloid (26,27). Our data also seem to indicate an association of the $\epsilon 2/\epsilon 2$ genotype and lobar microbleeds. This is again in line with data from CAA patients (13,26,28) and with a single other study that took into account microbleed location non-CAA patients (29). It is thought that APOE $\epsilon 2$ accelerates the development of vasculopathic changes leading to hemorrhage of amyloid-laden vessels in CAA (13,28). The associations we found between APOE genotype and presence of strictly lobar microbleeds, especially for persons with multiple lobar microbleeds, are thus in line with clinical studies in CAA patients and further support that strictly lobar microbleeds in the general population may be an indicator of CAA.

APOE genotype was not related to deep or infratentorial microbleeds. Rather, microbleeds in these locations were associated with cardiovascular factors such as high systolic blood pressure, pulse pressure, and smoking. The lack of a clear association with hypertension is in contrast to some studies that analyzed the overall prevalence of microbleeds regardless of their location (17,30) but is in line with others (18,31). Yet, deep and infratentorial microbleeds were furthermore strongly related to lacunar infarcts and white matter lesions, both classic markers

of ischemic cerebral small vessel disease. These findings suggest that microbleeds in deep or infratentorial locations are etiologically different from those that are strictly lobar in location, and that they are rather attributable to hypertensive or arteriolosclerotic microangiopathy.

In our study, serum total cholesterol levels were inversely related to the presence of cerebral microbleeds. There has been a single other study that found similar results (32). Our results also fit previous reports of a higher risk of spontaneous hemorrhagic stroke in persons with low cholesterol levels or who use high-dose statins (33-35). Although it seems possible that serum cholesterol might play a role in vessel wall integrity, the underlying mechanism of this association is still unknown.

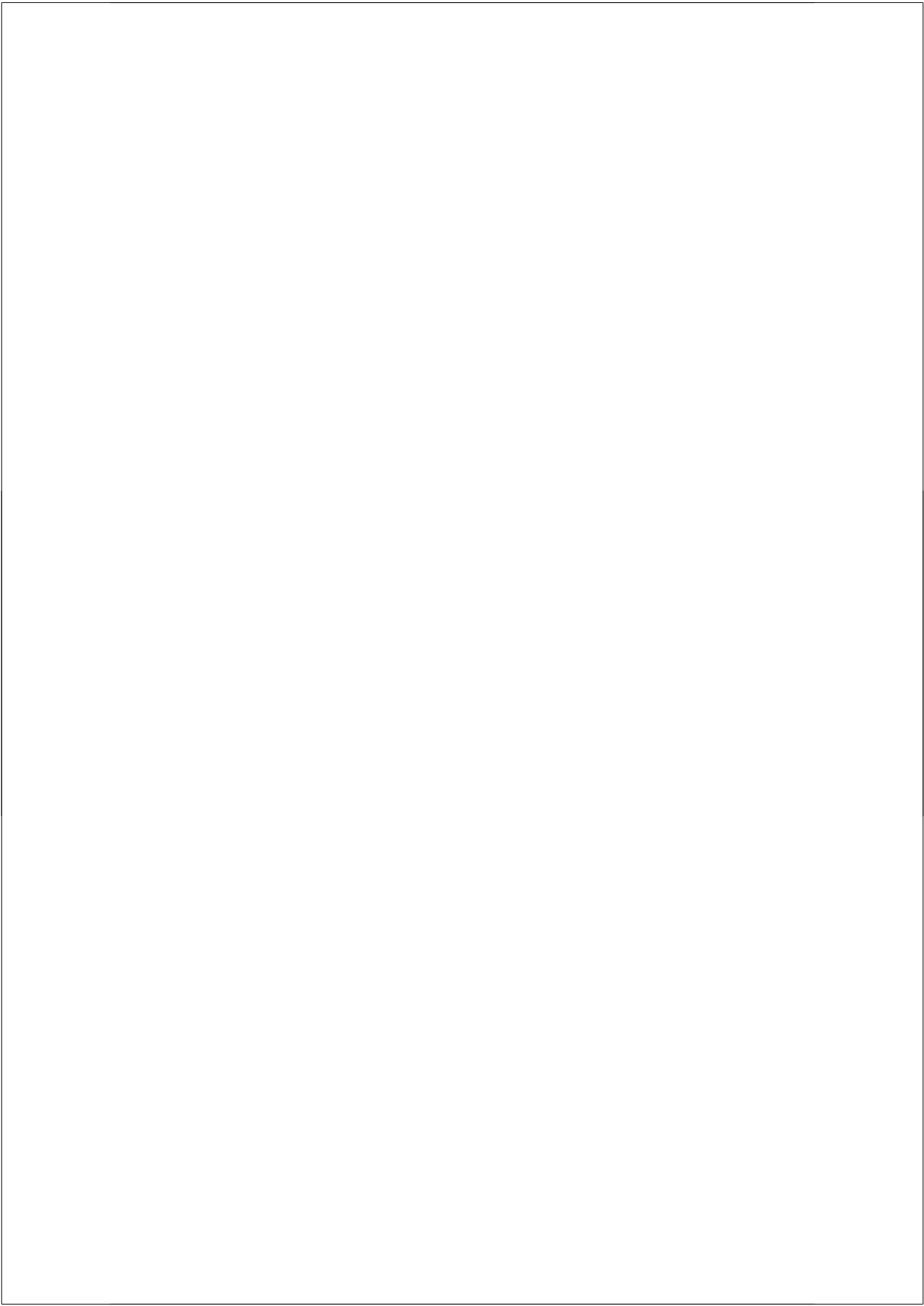
The high prevalence of cerebral microbleeds in our study as well as the finding that risk factors vary according to microbleed location has major importance in view of previous reports from small clinical series suggesting that microbleeds may reflect an increased risk of recurrence of stroke and hemorrhagic transformation of ischemic stroke (5,6). Although the relationship between microbleeds and therapy-induced bleeding complications has not been uniformly confirmed in all clinical series (36,37), it is important to further investigate whether the choice for thrombolytic treatment in persons with ischemic vascular disease or the installment of antiplatelet therapy as primary prevention in asymptomatic persons should depend on the coexistence of cerebral microbleeds in certain locations (38). In addition, a potential relation of microbleeds with impaired cognition (39) or with severity of small vessel disease (40) suggests a clinical relevance of these lesions. As such, our study offers new insights into risk factors for microbleeds and warrants further investigation into the prognosis of microbleeds in the general population, focusing on strictly lobar and deep or infratentorial microbleeds separately.

REFERENCES

1. Offenbacher H, Fazekas F, Schmidt R, Koch M, Fazekas G, Kapeller P. MR of cerebral abnormalities concomitant with primary intracerebral hematomas. *AJNR Am J Neuroradiol* 1996; 17:573-578.
2. Fazekas F, Kleinert R, Roob G, et al. Histopathologic analysis of foci of signal loss on gradient-echo T2*-weighted MR images in patients with spontaneous intracerebral hemorrhage: evidence of microangiopathy-related microbleeds. *AJNR Am J Neuroradiol* 1999; 20:637-642.
3. Koennecke HC. Cerebral microbleeds on MRI: prevalence, associations, and potential clinical implications. *Neurology* 2006; 66:165-171.
4. Viswanathan A, Chabriot H. Cerebral microhemorrhage. *Stroke* 2006; 37:550-555.
5. Nighoghossian N, Hermier M, Adeleine P, et al. Old microbleeds are a potential risk factor for

- cerebral bleeding after ischemic stroke: a gradient-echo T2*-weighted brain MRI study. *Stroke* 2002; 33:735-742.
6. Imaizumi T, Horita Y, Hashimoto Y, Niwa J. Dotlike hemosiderin spots on T2*-weighted magnetic resonance imaging as a predictor of stroke recurrence: a prospective study. *J Neurosurg* 2004; 101:915-920.
7. Vernooij MW, Ikram MA, Wielopolski PA, Krestin GP, Breteler MMB, van der Lugt A. Comparison of accelerated 3D T2* GRE imaging and conventional 2D T2* GRE imaging for the detection of cerebral microbleeds. *Radiology* 2008; 248:272-277.
8. Imaizumi T, Honma T, Horita Y, et al. Dotlike hemosiderin spots are associated with past hemorrhagic strokes in patients with lacunar infarcts. *J Neuroimaging* 2005; 15:157-163.
9. Lee SH, Bae HJ, Kwon SJ, et al. Cerebral microbleeds are regionally associated with intracerebral hemorrhage. *Neurology* 2004; 62:72-76.
10. Greenberg SM. Cerebral amyloid angiopathy: prospects for clinical diagnosis and treatment. *Neurology* 1998; 51:690-694.
11. Woo D, Sauerbeck LR, Kissela BM, et al. Genetic and environmental risk factors for intracerebral hemorrhage: preliminary results of a population-based study. *Stroke* 2002; 33:1190-1195.
12. Greenberg SM, Rebeck GW, Vonsattel JP, Gomez-Isla T, Hyman BT. Apolipoprotein E epsilon 4 and cerebral hemorrhage associated with amyloid angiopathy. *Ann Neurol* 1995; 38:254-259.
13. Greenberg SM, Vonsattel JP, Segal AZ, et al. Association of apolipoprotein E epsilon2 and vasculopathy in cerebral amyloid angiopathy. *Neurology* 1998; 50:961-965.
14. Hofman A, Breteler MM, van Duijn CM, et al. Rotterdam Study: design update. *Eur J Epidemiol* 2007; 22:819-829.
15. de Groot JC, de Leeuw FE, Oudkerk M, Hofman A, Jolles J, Breteler MM. Cerebral white matter lesions and subjective cognitive dysfunction: the Rotterdam Scan Study. *Neurology* 2001; 56:1539-1545.
16. Vernooij MW, van der Lugt A, Ikram MA, et al. Total cerebral blood flow and total brain perfusion in the general population: The Rotterdam Scan Study. *J Cereb Blood Flow Metab* 2008; 28:412-419.
17. Roob G, Schmidt R, Kapeller P, Lechner A, Hartung HP, Fazekas F. MRI evidence of past cerebral microbleeds in a healthy elderly population. *Neurology* 1999; 52:991-994.
18. Jeerakathil T, Wolf PA, Beiser A, et al. Cerebral microbleeds: prevalence and associations with cardiovascular risk factors in the Framingham Study. *Stroke* 2004; 35:1831-1835.
19. Kruit MC, Launer LJ, Ferrari MD, van Buchem MA. Infarcts in the posterior circulation territory in migraine. The population-based MRI CAMERA study. *Brain* 2005; 128:2068-2077.
20. Ikram MA, Vrooman HA, Vernooij MW, et al. Brain tissue volumes in the general elderly population. *Neurobiology of Aging* 2008; 29:882-890.
21. Wenham PR, Price WH, Blandell G. Apolipoprotein E genotyping by one-stage PCR. *Lancet* 1991; 337:1158-1159.
22. Whitworth JA. 2003 World Health Organization (WHO)/International Society of Hypertension (ISH) statement on management of hypertension. *J Hypertens* 2003; 21:1983-1992.
23. Knudsen KA, Rosand J, Karluk D, Greenberg SM. Clinical diagnosis of cerebral amyloid angiopathy: validation of the Boston criteria. *Neurology* 2001; 56:537-539.

24. de Leeuw FE, de Groot JC, Achten E, et al. Prevalence of cerebral white matter lesions in elderly people: a population based magnetic resonance imaging study. The Rotterdam Scan Study. *J Neurol Neurosurg Psychiatry* 2001; 70:9-14.
25. Tsushima Y, Tanizaki Y, Aoki J, Endo K. MR detection of microhemorrhages in neurologically healthy adults. *Neuroradiology* 2002; 44:31-36.
26. O'Donnell HC, Rosand J, Knudsen KA, et al. Apolipoprotein E genotype and the risk of recurrent lobar intracerebral hemorrhage. *N Engl J Med* 2000; 342:240-245.
27. Premkumar DR, Cohen DL, Hedera P, Friedland RP, Kalaria RN. Apolipoprotein E-epsilon4 alleles in cerebral amyloid angiopathy and cerebrovascular pathology associated with Alzheimer's disease. *Am J Pathol* 1996; 148:2083-2095.
28. Nicoll JA, Burnett C, Love S, et al. High frequency of apolipoprotein E epsilon 2 allele in hemorrhage due to cerebral amyloid angiopathy. *Ann Neurol* 1997; 41:716-721.
29. Kim M, Bae HJ, Lee J, et al. APOE epsilon2/epsilon4 polymorphism and cerebral microbleeds on gradient-echo MRI. *Neurology* 2005; 65:1474-1475.
30. Roob G, Lechner A, Schmidt R, Flooh E, Hartung HP, Fazekas F. Frequency and location of microbleeds in patients with primary intracerebral hemorrhage. *Stroke* 2000; 31:2665-2669.
31. Cordonnier C, van der Flier WM, Sluimer JD, Leys D, Barkhof F, Scheltens P. Prevalence and severity of microbleeds in a memory clinic setting. *Neurology* 2006; 66:1356-1360.
32. Lee SH, Bae HJ, Yoon BW, Kim H, Kim DE, Roh JK. Low concentration of serum total cholesterol is associated with multifocal signal loss lesions on gradient-echo magnetic resonance imaging: analysis of risk factors for multifocal signal loss lesions. *Stroke* 2002; 33:2845-2849.
33. Reed DM. The paradox of high risk of stroke in populations with low risk of coronary heart disease. *Am J Epidemiol* 1990; 131:579-588.
34. Segal AZ, Chiu RI, Eggleston-Sexton PM, Beiser A, Greenberg SM. Low cholesterol as a risk factor for primary intracerebral hemorrhage: A case-control study. *Neuroepidemiology* 1999; 18:185-193.
35. Amarenco P, Bogousslavsky J, Callahan A, 3rd, et al. High-dose atorvastatin after stroke or transient ischemic attack. *N Engl J Med* 2006; 355:549-559.
36. Derex L, Nighoghossian N, Hermier M, et al. Thrombolysis for ischemic stroke in patients with old microbleeds on pretreatment MRI. *Cerebrovasc Dis* 2004; 17:238-241.
37. Wong KS, Chan YL, Liu JY, Gao S, Lam WW. Asymptomatic microbleeds as a risk factor for aspirin-associated intracerebral hemorrhages. *Neurology* 2003; 60:511-513.
38. McCarron MO, Nicoll JA. Cerebral amyloid angiopathy and thrombolysis-related intracerebral haemorrhage. *Lancet Neurol* 2004; 3:484-492.
39. Werring DJ, Frazer DW, Coward LJ, et al. Cognitive dysfunction in patients with cerebral microbleeds on T2*-weighted gradient-echo MRI. *Brain* 2004; 127:2265-2275.
40. Werring DJ, Coward LJ, Losseff NA, Jager HR, Brown MM. Cerebral microbleeds are common in ischemic stroke but rare in TIA. *Neurology* 2005; 65:1914-1918.



3.3

USE OF ANTITHROMBOTIC DRUGS AND PRESENCE OF CEREBRAL MICROBLEEDS. THE ROTTERDAM SCAN STUDY

Archives of Neurology, in press



Meike W. Vernooij,
Mendel D.M. Haag*,
Aad van der Lugt,
Albert Hofman,
Gabriel P. Krestin,
Bruno H. Stricker,
Monique M.B. Breteler.*

** Both authors contributed
equally to this work.*

3.4

CEREBRAL MICROBLEED PRECEDING SYMPTOMATIC INTRACEREBRAL HEMORRHAGE IN A STROKE-FREE PERSON


Neurology, in press



*Meike W. Vernooij,
Jan Heeringa,
Gert Jan de Jong,
Aad van der Lugt,
Monique M.B. Breteler*

3.5

**SUPERFICIAL SIDEROSIS IN
THE GENERAL POPULATION**

Submitted 

*Meike W. Vernooij,
M. Arfan Ikram,
Albert Hofman,
Gabriel P. Krestin,
Monique M.B. Breteler,
Aad van der Lugt*

3.6

HISTOPATHOLOGIC CORRELATION OF CEREBRAL MICROBLEED ON T₂*- WEIGHTED GRE MRI

Work in progress



*Meike W. Vernooij,
Piotr A. Wielopolski,
Monique M.B. Breteler,
Johan M. Kros,
Aad van der Lugt*

CHAPTER 4

CEREBRAL BLOOD FLOW

4.1

TOTAL CEREBRAL BLOOD FLOW AND TOTAL BRAIN PERFUSION IN THE GENERAL POPULATION. THE ROTTERDAM SCAN STUDY

Journal of Cerebral Blood Flow & Metabolism,
2008; 28:412–419

*Meike W. Vernooij,
Aad van der Lugt,
M. Arfan Ikram,
Piotr A. Wielopolski,
Henri A. Vrooman,
Albert Hofman,
Gabriel P. Krestin,
Monique M.B. Breteler*

Background *Reduced cerebral perfusion may contribute to the development of cerebrovascular and neurodegenerative diseases. Little is known on cerebral perfusion in the general population, as most measurement techniques are too invasive for application in large groups of healthy individuals. Total cerebral blood flow (tCBF) can be noninvasively measured by magnetic resonance imaging (MRI) but is highly correlated with brain volume.*

Methods *We calculated total brain perfusion by dividing tCBF by brain volume, and we investigated determinants of total brain perfusion in comparison with tCBF. Secondly, we studied whether persons with a low tCBF or low total brain perfusion have a larger volume of white matter lesions (WML). This study is based on 892 persons aged 60 to 91 years from the Rotterdam Study, a population-based cohort study. We performed two-dimensional (2D) phase-contrast MRI for tCBF measurement. Brain volume and WML volume were quantitatively assessed. Cardiovascular determinants were assessed by interview and physical examination. We assessed associations between cardiovascular determinants and flow measures with linear regression models, adjusted for age and sex. Associations between tCBF or total brain perfusion and WML volume were assessed using general linear models.*

Results *We found that determinants of tCBF and total brain perfusion differed largely due to the large influence of brain volume on tCBF values. Persons with low total brain perfusion had a significantly larger WML volume compared with those with high total brain perfusion.*

Conclusion *Prospective studies are required to unravel whether hypoperfusion contributes to WML formation or that tissue damage, manifested by WML, leads to brain hypoperfusion.*

Cerebral perfusion and its regulation are of great importance for the constant supply of oxygen and nutrients to the brain, which are needed to maintain normal brain function and structural integrity (1). Reductions in cerebral perfusion have been reported in patients with transient ischemic attack, ischemic stroke and Alzheimer's disease (2-4). Also, perfusion was found to be reduced in the white matter of patients with white matter lesions (WML) (5, 6). This might imply that impaired cerebral perfusion contributes to the development of cerebrovascular and neurodegenerative brain disease.

Cerebral perfusion and its correlates have hardly been investigated in the general population. This is mainly related to the invasiveness and complexity of most measurement techniques, such as positron emission tomography and xenon computed tomography (7, 8). In the past decade, a non-invasive magnetic resonance imaging (MRI) technique, two-dimensional (2D) phase-contrast MRI, has been developed for fast and accurate measurement of total cerebral blood flow (tCBF) by summing blood flow in the internal carotid and basilar arteries (9, 10). This MRI technique has shown to be applicable in large populations of healthy subjects (9,

11, 12) and was recently used to study determinants of tCBF in patients with symptomatic vascular disease (9, 11, 12). However, a complicating factor is that tCBF strongly depends on the amount of brain tissue, as it is closely coupled to the cerebral oxidative metabolism (13). To account for this we introduce total brain perfusion, calculated by dividing tCBF by brain volume. In the general population, we investigated how cardiovascular determinants relate to total brain perfusion in comparison with tCBF. Furthermore, we studied how total brain perfusion and tCBF each relate to WML volume.

METHODS

Participants

This study is embedded within the Rotterdam Study, a large population-based cohort study in the Netherlands that started in 1990 (14) and is aimed at investigating determinants of various chronic diseases among elderly participants. The original study population consisted of 7,983 participants aged 55 years and older within the Ommoord area, a suburb of Rotterdam. In 2000, the cohort was extended with 3,011 persons (≥ 55 years) who were living in the study area and had not been included before. Participants are invited at regular time intervals (approximately once every 3 years) to the research center for follow-up examinations (interview and physical examination). From August 2005 to May 2006, we randomly selected 1,073 members of this extended cohort for the current MRI study, the Rotterdam Scan Study. We excluded individuals who were demented (assessed by a previously described three-step protocol (14)) or had MRI contraindications (including claustrophobia). The Institutional Review Board approved the study. A total of 975 persons were eligible, of whom 907 participated and gave written informed consent (response 93%). This population consisted of more than 95% of persons of Caucasian descent. Owing to physical disabilities (e.g., back pain), imaging could not be performed or completed in 12 individuals (1.3%). A total of 895 complete MRI examinations were performed.

Magnetic resonance imaging scan protocol

Magnetic resonance imaging of the brain was performed on a 1.5-T MRI scanner (Signa Excite II, General Electric Healthcare, Milwaukee, WI, USA). An eight-channel head coil was used for reception of the signal. For flow measurement, 2D phase-contrast imaging was performed similar to techniques described previously (11, 15). First, a sagittal 2D phase-contrast MRI angiographic scout image was performed (repetition time (TR) = 24 ms, echo time (TE) = 9 ms, field of view (FOV) = 32x32 cm², matrix = 256x160, flip angle = 10°, number of signals averaged (NEX) = 1, bandwidth (BW) = 8.06 kHz, velocity encoding = 60 cm/sec, slice thickness = 60 mm). Acquisition time was 12 secs. On this scout image, a transverse imaging

plane perpendicular both to the precavernous portion of the internal carotid arteries and to the middle part of the basilar artery was chosen (Figure 1A) for a 2D gradient-echo phase-contrast sequence (TR = 20 ms, TE = 4 ms, FOV = 19x19 cm², matrix = 256x160, flip angle = 80, NEX = 8, BW = 22.73 kHz, velocity encoding = 120 cm/sec, slice thickness = 5 mm). Acquisition time was 51 secs, and no cardiac gating was performed (9).

We further performed three high-resolution axial MRI sequences, that is a T1-weighted three-dimensional fast radio frequency spoiled gradient recalled acquisition in steady state with an inversion recovery pre-pulse (FASTSPGR-IR) sequence (TR = 13.8 ms, TE = 2.8 ms, inversion time (TI) = 400 ms, FOV = 25 cm (rectangular), matrix = 416x256, flip angle = 200, NEX = 1, BW = 12.50 kHz, 96 slices with slice thickness 1.6 mm zero-padded to 0.8 mm), a proton density-weighted sequence (TR = 12,300 ms, TE = 17.3 ms, FOV = 25 cm (rectangular), matrix = 416x256, NEX = 1, BW = 17.86 kHz, 90 slices with slice thickness 1.6 mm), and a fluid attenuated inversion recovery sequence (TR = 8000 ms, TE = 120 ms, TI = 2,000 ms, FOV = 25X25 cm, matrix = 320x224, NEX = 1, BW = 31.25 kHz, 64 slices with slice thickness 2.5 mm). All slices were contiguous.

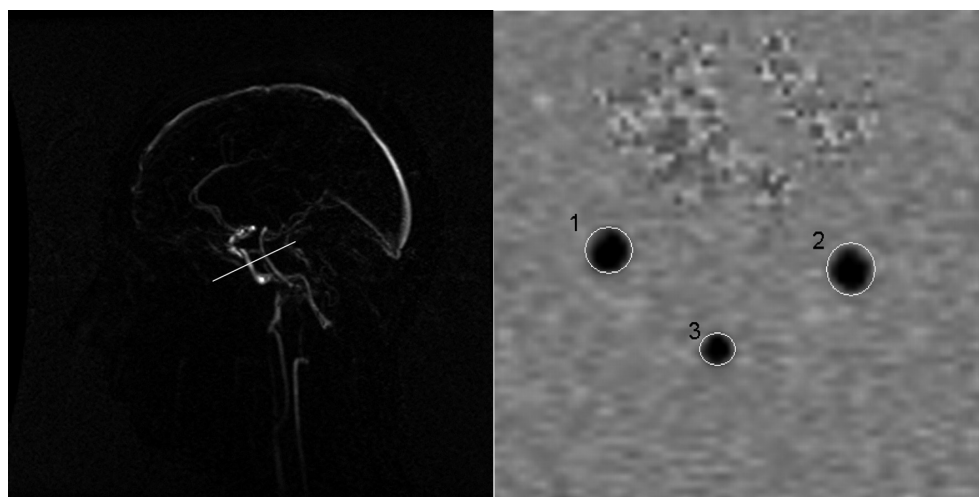


Figure 1. Two-dimensional (2D) phase-contrast MRI flow measurement. (A) Sagittal 2D phase-contrast MRI angiographic scout image for localization of the phase-contrast imaging plane (white line) perpendicular to the carotid and basilar arteries. (B) Two-dimensional phase-contrast MR image (orientation as indicated by the white line in (A)) depicting the carotid arteries (1=right and 2=left) and the basilar artery (3) in black. Manually placed ROIs outline the vessels in white. Note that for improved visualization of vessel boundaries, the contrast between the arteries of interest and the background in (B) is inverted compared with (A).

Total cerebral blood flow and total brain perfusion

Flow was calculated from the phase-contrast images using interactive data language-based custom software (Cinetool version 4, General Electric Healthcare, Milwaukee, WI, USA). Circular to elliptical regions of interest (ROIs) were drawn manually around both carotids and the basilar artery on the phase-contrast images (Figure 1B). These ROIs encompassed the entire lumen of the vessel. The value of mean signal intensity in each ROI reflected the flow velocity in the vessel (cm/sec). Flow (in mL/sec) was calculated by multiplying the average velocity with the cross-sectional area of the vessel. To calculate tCBF (in mL/min), flow rates for the carotid arteries and the basilar artery were summed and multiplied by 60 secs/min. This method is similar to flow measurement methods described previously (11, 15).

Two independent experienced technicians performed all manual ROI drawing and subsequent flow measurements. Double rating was performed in 533 scans, yielding inter rater correlations > 0.94 for all vessels, indicating excellent agreement. In three persons, tCBF could not be measured due to incorrect positioning of the phase contrast imaging plane, leaving a total of 892 persons in our analysis. We calculated total brain perfusion (in mL/min per 100 mL) by dividing tCBF (mL/min) by each individual's brain volume (mL) and multiplying the obtained result by 100.

Assessment of brain volume and white matter lesion volume

For the assessment of brain volume and WML volume, the structural MRI scans (T1-weighted, proton density-weighted, and fluid attenuated inversion recovery) were transferred offline to a Linux workstation. Preprocessing steps and the classification algorithm have been described elsewhere (16). In summary, preprocessing included co-registration, non-uniformity correction and variance scaling. We used the k-nearest neighbor classifier (17) to classify scans into brain tissue and cerebrospinal fluid. White matter lesions were classified as a separate tissue class using the same method. All segmentation results were visually inspected and if needed manually corrected. Manual editing of WML was necessary in 67 scans (7.6%), owing to WML segmentation problems, which were mainly caused by motion artifacts. In 12 persons, metallic dental implants caused severe artifacts, which necessitated exclusion from analysis. To remove non-cerebral tissue, for example, eyes, skull, and cerebellum, we applied non-rigid registration (18) to register to each brain a template scan in which these tissues were manually masked. Brain volume and WML volume were calculated by summing all voxels of the corresponding tissue class across the whole brain, to yield volumes in mL.

Assessment of infarcts

Two physicians (MWV and MAI) who were masked to all clinical information rated infarcts on T1-weighted, proton density-weighted and fluid attenuated inversion recovery sequences.

Infarcts were defined as lesions ≥ 3 mm in size exhibiting the same signal characteristics as cerebrospinal fluid on all sequences, and, if located supratentorially, with a hyperintense rim on the fluid attenuated inversion recovery sequence. Cortical infarcts were those infarcts showing involvement of cortical gray matter. All infarcts were confirmed by an experienced neuroradiologist (AvdL).

Cardiovascular determinants

We obtained information on cardiovascular determinants from interview and physical examination performed at the participants' regular visit to the research center preceding the MRI examination (average time interval between preceding visit and MRI was 1.2 years, and standard deviation (SD) of 0.5). Blood pressure was measured twice on the right arm with a random-zero sphygmomanometer. We used the average of these two measurements. We calculated pulse pressure by subtracting diastolic blood pressure from systolic blood pressure. Hypertension was defined in two ways. First, we defined hypertension according to grades 2 and 3 of 2003 WHO criteria (19), as a systolic blood pressure ≥ 160 mm Hg and/or a diastolic blood pressure ≥ 100 mm Hg, and/or the use of blood pressure-lowering medication. Secondly, we applied less stringent criteria and also classified persons as hypertensive according to grade 1 of WHO criteria (systolic blood pressure ≥ 140 mm Hg and/or a diastolic blood pressure ≥ 90 mm Hg, and/or the use of blood pressure-lowering medication). We considered diabetes mellitus present if a person was taking oral antidiabetics or insulin, or if fasting plasma glucose was ≥ 7 mmol/L (≥ 126 mg/dL). A physician assessed participants' smoking habits, and smoking status was further classified as current, former, or never. Body mass index (BMI) was calculated by dividing weight (kg) by the square of height (m^2). Assessment of significant carotid stenosis ($> 50\%$) was performed using 5-MHz pulsed Doppler ultrasonography through interpretation of velocity profiles according to standard criteria (20).

Data analysis

We assessed the association of cardiovascular determinants with tCBF and total brain perfusion using multiple linear regression models. Because the distribution of WML volume was skewed leftward, we used the natural log transformed (\ln) variable for analysis as a continuous variable. To calculate the WML volume for quartiles of tCBF and total brain perfusion, we used analysis of covariance (ANCOVA). Next, we used linear regression models, to assess the linear relation between both flow measures (per SD) and WML volume. As it is known that hypertension influences autoregulatory functions in the brain (21, 22), we also investigated this relation for persons with and without hypertension separately and assessed the presence of any interaction. All linear regression analyses were adjusted, when appropriate, for age and sex. Furthermore, the analyses with WML volume as outcome measure were additionally

adjusted for blood pressure, smoking status, diabetes and BMI. All analyses were performed using the statistical software package SPSS (Chicago, IL, USA), version 11.0.1 for Windows.

RESULTS

Table 1 presents the characteristics of the study population. Mean age of the population at time of MRI was 67.5 years (SD = 5.5; age range = 60.7 to 91.7 years), with 451 (50.6%) women. Mean tCBF was 497.4 mL/min (SD 86.2) and mean total brain perfusion was 51.2 mL/min per 100 mL (SD 8.8).

In Table 2, results for tCBF and total brain perfusion are presented for men and women separately. Women had a significantly lower basilar blood flow than men ($P < 0.001$), whereas flow in the carotid arteries did not differ between sexes (Table 2). As expected, persons with a larger brain volume had a higher tCBF (36.00 mL/min increase in tCBF per SD increase in brain volume; 95% confidence interval (CI): 30.00; 42.10).

Table 1. Characteristics of the study population (N = 892)

Age, mean (SD)	67.5 (5.5)
Women, N (%)	451 (50.6)
Systolic blood pressure, mmHg, mean (SD)	143.8 (18.5)
Diastolic blood pressure, mmHg, mean (SD)	81.0 (10.2)
Pulse pressure, mmHg, mean (SD)	62.8 (15.8)
Hypertension; according to WHO grades 2 and 3*, N (%)	417 (46.9)
Hypertension; according to WHO grades 1-3*, N (%)	628 (70.6)
Body mass index, kg/m ² , mean (SD)	27.6 (3.7)
Current smoking, N (%)	267 (29.9)
Former smoking, N (%)	361 (40.5)
Diabetes, N (%)	85 (9.6)
Stenosis > 50% on ultrasound, N (%)†	33 (3.7)
MRI findings	
Any infarct on MRI, N (%)	81 (9.1)
Cortical infarct on MRI, N (%)	21 (2.4)
Volume of white matter lesions, mL, median (interquartile range ‡)	3.4 (2.0-6.3)
Brain volume, mL, mean (SD)	976.8 (114)

* (19).

† Data not available in 61 persons.

‡ Data not available in 12 persons.

Table 2. Total cerebral blood flow and total brain perfusion

	Men	Women
Total blood flow left carotid artery, mL/min	197.3 (46.6)	200.7 (48.9)
Total blood flow right carotid artery, mL/min	201.5 (51.8)	198.2 (44.4)
Total blood flow basilar artery, mL/min	103.8 (33.7)	93.4 (35.7)
Total cerebral blood flow, mL/min	502.6 (85.4)	492.3 (86.7)
Total brain perfusion, mL/min per 100 mL	49.2 (8.4)	53.2 (8.7)

Values are means (standard deviation).

Table 3. Cardiovascular determinants, total cerebral blood flow and total brain perfusion

	Total cerebral blood flow (mL/min)	Total brain perfusion (mL/min per 100 mL)
Age*, per year increase	-2.93 (-3.95; -1.91)	0.02 (-0.09; 0.12)
Sex†, women versus men	-10.77 (-21.92; 0.37)	4.02 (2.90; 5.15)
Systolic blood pressure‡, per SD increase	-2.26 (-7.95; 3.42)	0.55 (-0.03; 1.12)
Diastolic blood pressure‡, per SD increase	-6.06 (-11.82; -0.30)	0.09 (-0.49; 0.67)
Pulse pressure‡, per SD increase	1.26 (-4.71; 7.23)	0.64 (0.04; 1.24)
Hypertension; WHO grade 2 & 3‡§, yes versus no	-18.97 (-30.14; -7.80)	-0.02 (-1.15; 1.12)
Hypertension; WHO grade 1, 2, 3‡§, yes versus no	-15.96 (-28.21; -3.71)	0.25 (-0.99; 1.49)
Body mass index‡, per SD increase	-6.75 (-12.31; -1.19)	0.59 (0.03; 1.15)
Smoking‡, current versus never	11.00 (-4.58; 26.58)	2.19 (0.62; 3.76)
Smoking‡, former versus never	-13.87 (-27.59; -0.15)	-0.24 (-1.62; 1.15)
Diabetes‡, yes versus no	-18.69 (-37.70; 0.33)	0.75 (-1.17; 2.67)
Stenosis > 50% on ultrasound‡, yes versus no	-33.69 (-63.13; -4.25)	-2.69 (-5.59; 0.21)
Any infarct on MRI‡, yes versus no	-6.37 (-26.29; 13.54)	0.87 (-1.13; 2.88)
Cortical infarct on MRI‡, yes versus no	-34.10 (-70.94; 2.79)	-3.18 (-6.89; -0.54)

MRI, magnetic resonance imaging; WHO, World Health Organization.

Values are adjusted mean differences (95% confidence interval) in total brain perfusion or total cerebral blood flow for unit increase or presence of each determinant.

* Adjusted for age; † Adjusted for sex; ‡ Adjusted for age and sex; § (19).

We found that tCBF decreased with increasing age and was lower for women than men (Table 3). Presence of hypertension, a higher BMI, former smoking, and presence of carotid stenosis were all associated with lower tCBF. In contrast, total brain perfusion did not change with increasing age (Table 3). Moreover, women had on average 4 mL/min per 100 mL higher total brain perfusion than men. Furthermore, increased pulse pressure, increased BMI, and current smoking were all associated with higher total brain perfusion.

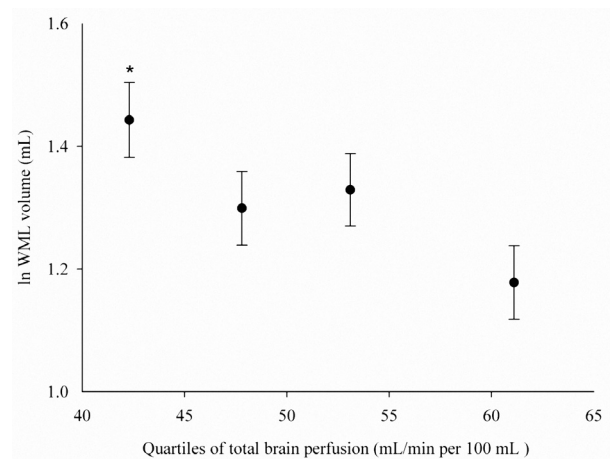


Figure 2. Quartiles of total brain perfusion and white matter lesion volume. Age- and sex-adjusted mean white matter lesion volume for each quartile of total brain perfusion (plotted at the median of each quartile). Error bars represent standard errors of the mean. *P value <0.01 when compared with fourth quartile (=highest total brain perfusion). P trend=0.007. WML, white matter lesion.

Both as a continuous variable and when analyzed in quartiles, tCBF was not related to WML volume (per SD increase of tCBF, difference in

lnWML volume 0.03 (95% CI: -0.03; 0.09); data for analysis of tCBF in quartiles not shown). In contrast, persons in the lowest quartile of total brain perfusion had a significantly larger total volume of WML than persons in the highest quartile (Figure 2). Per SD decrease in total brain perfusion, the difference in lnWML volume was 0.07 (95% CI: 0.02; 0.14). Adjustment for systolic and diastolic blood pressure, smoking status, diabetes, and BMI did not attenuate this association.

The association between total brain perfusion and amount of WML seemed more pronounced in persons with hypertension, although the interaction was not significant (per SD increase in total brain perfusion, difference in lnWML volume for those with hypertension (WHO grades 2 and 3) was -0.11 (95% CI: -0.20; -0.02) and -0.04 (95% CI -0.11; 0.04) for persons without hypertension; P interaction= 0.21). Using a definition of hypertension that comprised WHO grade 1 and higher (19) did not yield different results. Also, excluding persons with carotid stenosis (N = 33) and/or cortical infarcts on MRI (N = 21) did not change any of the above-mentioned results.

DISCUSSION

In the general population, we investigated tCBF and total brain perfusion using 2D phase-contrast MRI. We found that determinants of tCBF and total brain perfusion differed largely, which can be explained by the large influence of brain volume on tCBF values. We further found that persons with lower total brain perfusion had significantly more WML compared to persons with high total brain perfusion.

A major strength of our study is the population-based design, with a large sample size of elderly subjects. Other strengths of our study are the quantification of brain volume and WML volume. The 2D phase-contrast MRI technique as used in our study is non-invasive and fast. Superior imaging techniques are available that can assess perfusion at the brain tissue level, including positron emission tomography, xenon computed tomography, perfusion computed tomography, and perfusion MRI (7, 8). However, disadvantages such as limited availability, exposure to radiation and invasiveness of the procedure render all of these techniques inadequate for application in a population-based study (7, 8).

To our knowledge, we are the first to use the 2D phase-contrast MRI technique to indirectly estimate total brain perfusion by taking into account brain volume. We found a mean total brain perfusion of 51.2 mL/min per 100 mL. When divided by brain tissue density (1.034 g/mL) (23), this yields a mean total brain perfusion of 49.5 mL/min per 100 g brain tissue, which is in accordance with normal values of cerebral perfusion as assessed by other imaging techniques (1). Of note is that we measured blood flow in the basilar artery at the level before the superior cerebellar arteries arise, which supply the dorsal cerebellum, midbrain, and pons. These structures were not included in the measured brain volume that we used to calculate total brain perfusion. However, the resulting underestimation of each individual's brain volume is expected to be proportional to the measured brain volume and will therefore not have influenced the distribution of total brain perfusion in our population. Taking into account this slight overestimation in total brain perfusion, the mean total brain perfusion we assessed with this method is also very much in concordance with early work by Kety and Schmidt (1948) who established normal values of cerebral perfusion using the nitrous oxide method (24), a technique which can be regarded as the reference method for measurement of global average cerebral blood flow. They report a total brain perfusion (referred to in their report as mean cerebral blood flow) of 54 mL/min per 100 g. However, later studies proposed that this value should be corrected for a slight overestimation because diffusion equilibrium for inert gas tracer between the brain and its venous blood was not reached (25), leading to a corrected flow value using the Kety and Schmidt method of 46 mL/min per 100 g (25, 26).

The association we found between increasing age and lower tCBF is comparable to previous reports, taking age differences between populations into account (11, 12, 27). Furthermore, the estimates we found for associations of BMI, previous cerebrovascular disease (in our data defined as cortical infarct on MRI) and presence of diabetes mellitus with tCBF, are very concordant with results presented recently (12). Like other studies, we found that men had a higher tCBF than women (11, 12). However, we found that total brain perfusion was higher in women than in men. A higher cerebral perfusion in women compared with men was described in 1988 by Rodriguez et al., using 133-xenon inhalation (28). Also in contrast

to tCBF, total brain perfusion was not associated with age. Moreover, other cardiovascular determinants, including blood pressure and BMI, showed opposite associations to total brain perfusion when compared with tCBF (Table 3). All of this can be explained by the fact that both tCBF and the cardiovascular determinants studied are strongly related to brain volume (16, 29, 30). This signifies the importance of taking into account brain atrophy when analyzing global blood flow to the brain.

Current smoking was associated with a higher total brain perfusion compared with never smoking and former smoking. This is in line with known effects of nicotine on blood flow in animal studies as well as in healthy volunteers (31-33). Most probably, nicotine reduces vascular resistance in cerebral arteries via activation of nicotine receptors, causing an increase in cerebral perfusion (31, 33). Furthermore, inhalation of carbon monoxide results into formation of carboxyhemoglobin through its binding to hemoglobin. Carboxyhemoglobin has a decreased oxygen carrying capacity, which promotes tissue hypoxia and as such causes release of mediators of hypoxic vasodilatation and a subsequent increase in cerebral perfusion (34, 35).

The association we found between a lower total brain perfusion and a higher volume of WML is in accordance with small clinical studies showing that a low tissue perfusion in white matter is associated with the presence of WML (5, 6, 36). Using 2D phase-contrast MRI, Bisschops et al. showed a significant association between high tCBF and a lower WML load (37). With transcranial Doppler, it has been shown that cerebral blood flow velocity and vasomotor reactivity are strongly associated to qualitatively graded amount of WML (38, 39). We did not directly measure tissue perfusion in the white matter, but reasoned that total brain perfusion provides a reflection of perfusion within the white matter. The association between total brain perfusion and WML volume seemed somewhat stronger for persons with hypertension compared with persons without hypertension. It is known that hypertension induces alterations in both large and small arteries and causes both limits of autoregulatory range to shift towards higher pressure limits (21, 40). It could therefore be hypothesized that persons with hypertension are more vulnerable to relatively small decreases in total brain perfusion, resulting in relative tissue hypoperfusion and subsequent WML formation.

Our study was cross-sectional, which limits drawing conclusions regarding cause and effect. For example, the relation we found between lower total brain perfusion and a higher volume of WML could signify that tissue hypoperfusion contributes to WML pathogenesis (41, 42). However, it may also be that tissue damage and loss of white matter integrity, manifested by WML, lead to brain hypoperfusion. The same holds true for the relation between cardiovascular determinants and total brain perfusion. We cannot exclude that the association we

found between cardiovascular determinants and total brain perfusion is not causal but actually results from cardiovascular determinants leading to tissue damage and other processes, such as brain atrophy (16, 29, 30), which in turn affect total brain perfusion. By accounting for brain volume in the assessment of total brain perfusion we tried to eliminate this influence. However, longitudinal studies would be better able to disentangle the causal pathways.

In conclusion, this study underlines the importance of taking into account brain volume when studying total blood flow to the brain. We show that in the general population, persons with a low total brain perfusion have higher WML volumes. Our results suggest that tissue hypoperfusion contributes to WML pathogenesis, although we cannot exclude that tissue damage due to decreasing demand contributes to brain hypoperfusion. This remains to be further elucidated by longitudinal research.

Acknowledgement

We wish to thank Mr. Gavin C. Houston, PhD, for his technical support concerning the blood flow measurements.

REFERENCES

1. Kirkness CJ. Cerebral blood flow monitoring in clinical practice. *AACN Clin Issues* 2005;16:476-487.
2. Matsuda H. Cerebral blood flow and metabolic abnormalities in Alzheimer's disease. *Ann Nucl Med* 2001;15:85-92.
3. Yao H, Fujishima M. Cerebral blood flow and metabolism in silent brain infarction and related cerebrovascular disorders. *Ann Med* 2001;33:98-102.
4. Vorstrup S, Hemmingsen R, Henriksen L, Lindewald H, Engell HC, Lassen NA. Regional cerebral blood flow in patients with transient ischemic attacks studied by Xenon-133 inhalation and emission tomography. *Stroke* 1983;14:903-910.
5. O'Sullivan M, Lythgoe DJ, Pereira AC, et al. Patterns of cerebral blood flow reduction in patients with ischemic leukoaraiosis. *Neurology* 2002;59:321-326.
6. Markus HS, Lythgoe DJ, Ostegaard L, O'Sullivan M, Williams SC. Reduced cerebral blood flow in white matter in ischaemic leukoaraiosis demonstrated using quantitative exogenous contrast based perfusion MRI. *J Neurol Neurosurg Psychiatry* 2000;69:48-53.
7. Hoeffner EG. Cerebral perfusion imaging. *J Neuroophthalmol* 2005;25:313-320.
8. Wintermark M, Sesay M, Barbier E, et al. Comparative overview of brain perfusion imaging techniques. *J Neuroradiol* 2005;32:294-314.
9. Spilt A, Box FM, van der Geest RJ, et al. Reproducibility of total cerebral blood flow measurements using phase contrast magnetic resonance imaging. *J Magn Reson Imaging* 2002;16:1-5.

10. Marks MP, Pelc NJ, Ross MR, Enzmann DR. Determination of cerebral blood flow with a phase-contrast cine MR imaging technique: evaluation of normal subjects and patients with arteriovenous malformations. *Radiology* 1992;182:467-476.
11. Buijs PC, Krabbe-Hartkamp MJ, Bakker CJ, et al. Effect of age on cerebral blood flow: measurement with ungated two-dimensional phase-contrast MR angiography in 250 adults. *Radiology* 1998;209:667-674.
12. van Raamt AF, Appelman AP, Mali WP, van der Graaf Y. Arterial blood flow to the brain in patients with vascular disease: the SMART Study. *Radiology* 2006;240:515-521.
13. Strandgaard S. Cerebral blood flow in the elderly: impact of hypertension and antihypertensive treatment. *Cardiovasc Drugs Ther* 1991;4:1217-1221.
14. Ott A, Breteler MM, van Harskamp F, Stijnen T, Hofman A. Incidence and risk of dementia. The Rotterdam Study. *Am J Epidemiol* 1998;147:574-580.
15. Spilt A, Van den Boom R, Kamper AM, Blauw GJ, Bollen EL, van Buchem MA. MR assessment of cerebral vascular response: a comparison of two methods. *J Magn Reson Imaging* 2002;16:610-616.
16. Ikram MA, Vrooman HA, Vernooij MW, et al. Brain tissue volumes in the general elderly population. The Rotterdam Scan Study. *Neurobiology of Aging* 2008;29: 882-890.
17. Anbeek P, Vincken KL, van Bochove GS, van Osch MJ, van der Grond J. Probabilistic segmentation of brain tissue in MR imaging. *Neuroimage* 2005;27:795-804.
18. Rueckert D, Sonoda LI, Hayes C, Hill DL, Leach MO, Hawkes DJ. Nonrigid registration using free-form deformations: application to breast MR images. *IEEE Trans Med Imaging* 1999;18:712-721.
19. Whitworth JA. 2003 World Health Organization (WHO)/International Society of Hypertension (ISH) statement on management of hypertension. *J Hypertens* 2003;21:1983-1992.
20. Taylor DC, Strandness DE, Jr. Carotid artery duplex scanning. *J Clin Ultrasound* 1987;15:635-644.
21. Paulson OB, Strandgaard S, Edvinsson L. Cerebral autoregulation. *Cerebrovasc Brain Metab Rev* 1990;2:161-192.
22. Barry DI. Cerebral blood flow in hypertension. *J Cardiovasc Pharmacol* 1985;7 Suppl 2:S94-98.
23. Lescot T, Bonnet MP, Zouaoui A, et al. A quantitative computed tomography assessment of brain weight, volume, and specific gravity in severe head trauma. *Intensive Care Med* 2005;31:1042-1050.
24. Kety SS, Schmidt CF. The Nitrous Oxide Method for the Quantitative Determination of Cerebral Blood Flow in Man: Theory, Procedure and Normal Values. *J Clin Invest* 1948;27:476-483.
25. Madsen PL, Holm S, Herning M, Lassen NA. Average blood flow and oxygen uptake in the human brain during resting wakefulness: a critical appraisal of the Kety-Schmidt technique. *J Cereb Blood Flow Metab* 1993;13:646-655.
26. Lassen NA, Lane MH. Validity of internal jugular blood for study of cerebral blood flow and metabolism. *J Appl Physiol* 1961;16:313-320.
27. Spilt A, Weverling-Rijnsburger AW, Middelkoop HA, et al. Late-onset dementia: structural brain damage and total cerebral blood flow. *Radiology* 2005;236:990-995.
28. Rodriguez G, Warkentin S, Risberg J, Rosadini G. Sex differences in regional cerebral blood flow. *J Cereb Blood Flow Metab* 1988;8:783-789.

29. Knopman DS, Mosley TH, Catellier DJ, Sharrett AR. Cardiovascular risk factors and cerebral atrophy in a middle-aged cohort. *Neurology* 2005;65:876-881.
30. Salerno JA, Murphy DG, Horwitz B, et al. Brain atrophy in hypertension. A volumetric magnetic resonance imaging study. *Hypertension* 1992;20:340-348.
31. Shiba K, Machida T, Uchida S, Hotta H. Effects of nicotine on regional blood flow in the olfactory bulb in rats. *Eur J Pharmacol* 2006;546:148-151.
32. Kodaira K, Fujishiro K, Wada T, et al. A study on cerebral nicotine receptor distribution, blood flow, oxygen consumption, and other metabolic activities--a study on the effects of smoking on carotid and cerebral artery blood flow. *Yakubutsu Seishin Kodo* 1993;13:157-165.
33. Gong CL, Chiu YT, Lin NN, et al. Regulation of the common carotid arterial blood flow by nicotinic receptors in the medulla of cats. *Br J Pharmacol* 2006;149:206-214.
34. Paulson OB, Parving HH, Olesen J, Skinhoj E. Influence of carbon monoxide and of hemodilution on cerebral blood flow and blood gases in man. *J Appl Physiol* 1973;35:111-116.
35. Koehler RC, Traystman RJ. Cerebrovascular effects of carbon monoxide. *Antioxid Redox Signal* 2002;4:279-290.
36. Hatazawa J, Shimosegawa E, Satoh T, Toyoshima H, Okudera T. Subcortical hypoperfusion associated with asymptomatic white matter lesions on magnetic resonance imaging. *Stroke* 1997;28:1944-1947.
37. Bisschops RH, van der Graaf Y, Mali WP, van der Grond J. High total cerebral blood flow is associated with a decrease of white matter lesions. *J Neurol* 2004;251:1481-1485.
38. Tzourio C, Levy C, Dufouil C, Touboul PJ, Ducimetiere P, Alperovitch A. Low cerebral blood flow velocity and risk of white matter hyperintensities. *Ann Neurol* 2001;49:411-414.
39. Bakker SL, de Leeuw FE, de Groot JC, Hofman A, Koudstaal PJ, Breteler MM. Cerebral vasomotor reactivity and cerebral white matter lesions in the elderly. *Neurology* 1999;52:578-583.
40. Novak V, Chowdhary A, Farrar B, et al. Altered cerebral vasoregulation in hypertension and stroke. *Neurology* 2003;60:1657-1663.
41. Fazekas F, Kleinert R, Offenbacher H, et al. Pathologic correlates of incidental MRI white matter signal hyperintensities. *Neurology* 1993;43:1683-1689.
42. Pantoni L, Garcia JH. Pathogenesis of leukoaraiosis: a review. *Stroke* 1997;28:652-659.

4.2

TOTAL CEREBRAL BLOOD FLOW IN RELATION TO COGNITIVE FUNCTION. THE ROTTERDAM SCAN STUDY

Journal of Cerebral Blood Flow & Metabolism,
2008; 28:1652-1655

*Mariëlle M.F. Poels,
M. Arfan Ikram,
Meike W. Vernooij,
Gabriel P. Krestin,
Albert Hofman,
Wiro J. Niessen,
Aad van der Lugt,
Monique M.B. Breteler*

Cerebral hypoperfusion has been associated with worse cognitive function. We investigated the association between cerebral blood flow and cognition and whether this association is independent of brain volume. In 892 participants, aged 60 to 91 years of the population-based Rotterdam Scan Study, we measured total cerebral blood flow (tCBF) and brain volume using magnetic resonance imaging. Lower tCBF was associated with worse information processing speed, executive function and global cognition. However, after correcting tCBF for brain volume, these associations disappeared. The association between tCBF and cognition may be mediated or confounded by brain atrophy. Future studies on tCBF should take into account brain atrophy.

Elderly persons often suffer from deterioration of cognitive function. Vascular risk factors may contribute to cognitive impairment by affecting blood flow to the brain (1). Moreover, it has been suggested that cerebral hypoperfusion precedes and possibly contributes to the onset of clinical dementia (2).

To assess perfusion at the brain tissue level is difficult as most measurement techniques are invasive and complex. Phase-contrast magnetic resonance imaging (MRI) enables fast and accurate measurement of total cerebral blood flow (tCBF) and has shown to be applicable in population-based studies (3). Previous studies showed that lower tCBF assessed with phase-contrast MRI was related to poorer cognition, in particular information processing speed, and dementia (4, 5). However, these studies did not assess whether this association was independent of brain atrophy. It can be hypothesized that smaller brain volume leads to decreased cerebral metabolic demand, and as such confounds the association between tCBF and cognitive function. Thus, the aim of our study was to investigate whether diminished tCBF is associated with specific domains of cognitive function independent of brain volume.

METHODS

Participants

This study is embedded within the Rotterdam Study, a large population-based cohort study in the Netherlands (6). The original study population consisted of 7,983 participants aged 55 years and older from the Ommoord area, a suburb of Rotterdam. In the year 2000, the cohort was expanded with the addition of 3,011 persons (≥ 55 years) (6). From August 2005 to May 2006, we randomly selected 1,073 members of this cohort expansion for participation in the Rotterdam Scan Study, a population-based brain imaging study. After exclusion of individuals who were demented or had MRI contraindications, 975 persons were found to be eligible,

of whom 907 participated and gave written informed consent. Because of physical inabilities (for example, back pain), imaging could not be performed or completed in 12 individuals. Therefore, a total of 895 complete MR examinations were performed. The institutional review board approved the study.

Magnetic resonance imaging scan protocol

Magnetic resonance imaging of the brain was performed on a 1.5T MRI scanner (General Electric Healthcare, Milwaukee, WI, USA), using an 8-channel head coil. For flow measurement, 2D phase-contrast imaging was performed as described previously (7). In brief, a sagittal 2D phase-contrast MRI angiographic scout image was performed. On this scout image, a transverse imaging plane perpendicular to both the precavernous portion of the internal carotid arteries and to the middle part of the basilar artery was chosen for a 2D gradient-echo phase-contrast sequence (repetition time = 20ms, echo time = 4 ms, field of view = 19x19 cm², matrix = 256x160, flip angle = 8°, number of excitations = 8, bandwidth = 22.73 kHz, velocity encoding = 120 cm/sec, slice thickness = 5 mm). For an example, see (7). Acquisition time was 51 secs, and no cardiac gating was performed (3). We further performed three high-resolution axial MRI sequences, that is, a T1-weighted sequence, a proton density-weighted sequence, and a fluid attenuated inversion recovery (FLAIR) sequence (7).

Measurement of total cerebral blood flow and total brain perfusion

Flow was calculated from the phase-contrast images using interactive data language-based custom software (Cinetool version 4, General Electric Healthcare, Milwaukee, WI, USA) (7). Two independent, experienced technicians drew all the manual regions of interest (ROI) and performed subsequent flow measurements (inter rater correlations (N = 533) > 0.94 for all vessels) (7). In three persons, tCBF could not be measured because of incorrect positioning of the phase-contrast imaging plane, leaving a total of 892 persons in our analysis. We calculated total brain perfusion (in mL/min per 100 mL) by dividing tCBF (mL/min) by each individual's brain volume (mL) and multiplying the obtained result by 100 (7).

Assessment of brain volume

For the assessment of brain volume, the structural MRI scans (T1-weighted, proton density-weighted, and fluid attenuated inversion recovery) were transferred to a Linux workstation. Preprocessing steps and the classification algorithm have been described elsewhere (8). In summary, preprocessing included coregistration, nonuniformity correction and variance scaling. We used the k-nearest-neighbor classifier (9) to classify scans into brain tissue and cerebrospinal fluid using the multispectral MR intensities. All segmentation results were visually inspected and if needed manually corrected. To remove non-cerebral tissue, for example, eyes, skull, and cerebellum, we applied nonrigid registration (10) to register to each brain a

template scan in which these tissues were manually masked. Brain volume was calculated by summing up all the voxels across the whole brain, to yield volumes in milliliters.

Cognitive function

Cognitive function was assessed with a neuropsychological test battery comprising the MMSE (mini-mental state examination), the Stroop test, the LDST (letter-digit substitution task; number of correct digits in 1 min), the WFT (word fluency test; animal categories), and a 15-WLT (15-word verbal learning test; based on Rey’s recall of words) (11). For each participant Z-scores were calculated for each test separately (individual test score minus mean test score divided by the standard deviation), except for MMSE. To obtain more robust measures, we constructed compound scores for information-processing speed, executive function, memory and global cognitive function. The compound score for information processing speed was the average of the Z-scores for the Stroop reading and Stroop color-naming subtask and the LDST. Executive function included the Z-scores of the Stroop interference subtask, the LDST and the WFT (number of animals in 1 min). The compound score for memory was the average of the Z-scores for the immediate and delayed recall of the 15-WLT. For global cognitive function, we used the average of the Z-scores of the Stroop test (average of the reading, color-naming and interference subtask), the LDST, the WFT, and the immediate and delayed recall of the 15-WLT (11).

Covariates

We assessed the level of education and current smoking by interview. Systolic and diastolic blood pressures were measured twice on the right arm with a random-zero sphygmomanometer. The mean of the two readings was used in the analyses. Diabetes mellitus was defined as the use of blood glucose-lowering medication or fasting serum glucose level ≥ 7.0 mmol/L. Carotid plaque score was assessed by Doppler ultrasound (12).

Data analysis

We evaluated the association of both tCBF (mL/min) and total brain perfusion (mL/min per 100 mL brain

Table 1. Characteristics of the study population (N = 892)

Characteristics	
Men, N (%)	441 (49.4)
Age, years (SD)	67.5 (5.5)
Primary education, N (%)	38 (4.4)
Systolic Blood Pressure, mmHg (SD)	143.8 (18.5)
Diastolic Blood Pressure, mmHg (SD)	81.0 (10.2)
Diabetes Mellitus, N (%)	85 (9.6)
Current Smokers, N (%)	267 (29.9)
Plaques in Carotid Artery, range: 0-12*	3.0 (1.0-5.0)
Mini Mental State Examination, score (SD)	27.9 (1.8)
Brain Volume, mL (SD)	976.8 (114)
Total Cerebral Blood Flow, mL/min (SD)	497.4 (86.2)
Total Brain Perfusion, mL/min per 100mL brain tissue (SD)	51.2 (8.8)

Values are means (SD) or numbers (percentages)
* Median, interquartile range

tissue) per standard deviation (SD) increase with cognitive function using multiple linear regression models. All analyses were adjusted for age, sex and education. To examine whether associations were independent of vascular risk factors, we additionally adjusted for current smoking, systolic and diastolic blood pressure, diabetes mellitus and carotid plaque score.

RESULTS

Characteristics of the study population are shown in Table 1. Lower tCBF was associated with worse performance on tests of information-processing speed, executive function and global cognition, but not with the MMSE score and memory performance (Table 2).

Total brain volume was a strong determinant of tCBF (per SD increase in brain volume 36.00 mL/min increase in tCBF; 95% confidence interval 30.00; 42.10). The associations of tCBF with cognition disappeared upon correcting for brain volume (Table 2). Adjustments for vascular risk factors did not change any of these associations (Table 2).

Table 2. Association of tCBF and total brain perfusion with cognitive function (Z-scores), using linear regression models (N=892)

	Difference in test scores (95% CI) per SD increase in flow measure.				
	MMSE	Z-score information processing speed	Z-score executive function	Z-score memory	Z-score global cognition
tCBF					
Model 1	0.08 (-0.04;0.19)	0.08 (0.03;0.14)	0.07 (0.02;0.12)	0.00 (-0.07;0.06)	0.05 (0.01;0.10)
Model 2	0.09 (-0.03;0.20)	0.07 (0.02;0.13)	0.06 (0.01;0.11)	0.00 (-0.07;0.06)	0.05 (0.01;0.10)
Total Brain Perfusion					
Model 1	0.07 (-0.05;0.19)	0.04 (-0.02;0.09)	0.00 (-0.05;0.05)	0.03 (-0.04;0.09)	0.02 (-0.02;0.07)
Model 2	0.08 (-0.04;0.20)	0.04 (-0.02;0.09)	0.00 (-0.05;0.05)	0.03 (-0.03;0.09)	0.02 (-0.02;0.07)

CI, confidence interval; MMSE, mini-mental state examination; tCBF, total cerebral blood flow.
Model 1 = adjusted for age, sex and level of education
Model 2 = additionally adjusted for systolic blood pressure, diastolic blood pressure, current smoking, diabetes mellitus and plaque score

DISCUSSION

We found that persons with low tCBF performed significantly worse on tasks assessing information-processing speed, executive function, and global cognitive function compared with persons with higher tCBF. However, total brain perfusion, indicating the flow in mL per 100

mL of brain tissue volume, was not associated with cognitive function. Adjustments for vascular risk factors did not change the results.

Before interpreting the results, some methodological issues need to be addressed. The strengths of our study are its population-based setting, the high response rate and the large sample size. A limitation is the cross-sectional design, which restricts our interpretation of the data with respect to cause and consequence. Furthermore, we only assessed average brain perfusion. Hence, we cannot exclude that brain perfusion in distinct brain regions may relate differently to cognitive performance. Finally, we could not measure blood flow into the cerebellum as we measured blood flow in the basilar artery at the level after the anterior and posterior inferior cerebellar arteries arise.

It can be hypothesized that cerebral hypoperfusion causes brain atrophy that subsequently leads to cognitive decline (1, 13). Conversely, it may also be that because of a diminished demand, brain atrophy itself affects CBF. Thus, the association between tCBF and cognitive function may be mediated or confounded by brain atrophy.

In the past, blood flow velocity measured by transcranial Doppler ultrasonography has been used as a proxy measure for CBF. Several studies using CBF velocity reported that subjects with greater CBF velocity were less likely to have dementia (2). Furthermore, a greater CBF velocity was found to be related with larger hippocampal and amygdalar volumes (2). More recently, associations of tCBF with speed, executive function (4), and dementia (5) were found using phase-contrast MRI. Our data are in line with these studies, as we also found the strongest associations for cognitive domains of speed and executive function (4, 5). However, none of those previous studies assessed whether the associations between tCBF and cognitive function were independent of brain volume. We went a step further by correcting for brain volume, and found no associations between total brain perfusion and cognitive function. Thus far, only a few small studies reported that regional patterns of hypoperfusion in the brain may relate to cognitive decline or dementia independent of global differences (14, 15). As mentioned, we could not evaluate this in our study. Further studies are needed to investigate this.

In conclusion, our findings show that the relation between tCBF and worse performance on several domains of cognitive function is dependent on brain volume. Our study emphasizes that future studies on tCBF should take into account brain atrophy.

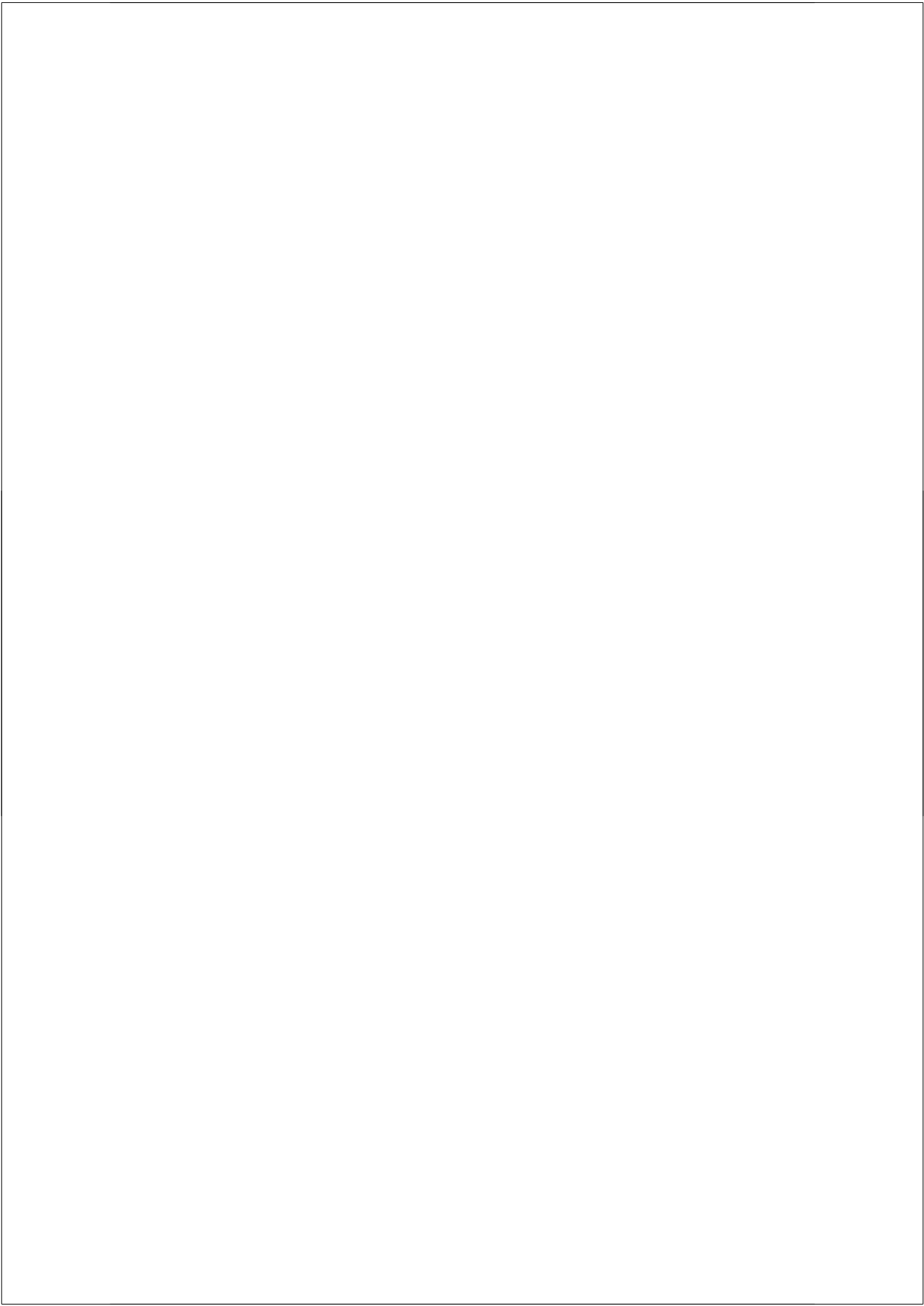
REFERENCES

1. Meyer JS, Rogers RL, Judd BW, Mortel KF, Sims P. Cognition and cerebral blood flow fluctuate together in multi-infarct dementia. *Stroke* 1988;19:163-169.
2. Ruitenberg A, den Heijer T, Bakker SL, et al. Cerebral hypoperfusion and clinical onset of dementia: the Rotterdam Study. *Ann Neurol* 2005;57:789-794.
3. Spilt A, Box FM, van der Geest RJ, et al. Reproducibility of total cerebral blood flow measurements using phase contrast magnetic resonance imaging. *J Magn Reson Imaging* 2002;16:1-5.
4. Rabbitt P, Scott M, Thacker N, et al. Losses in gross brain volume and cerebral blood flow account for age-related differences in speed but not in fluid intelligence. *Neuropsychology* 2006;20:549-557.
5. Spilt A, Weverling-Rijnsburger AW, Middelkoop HA, et al. Late-onset dementia: structural brain damage and total cerebral blood flow. *Radiology* 2005;236:990-995.
6. Hofman A, Breteler MM, van Duijn CM, et al. The Rotterdam Study: objectives and design update. *Eur J Epidemiol* 2007;22:819-829.
7. Vernooij MW, van der Lugt A, Ikram MA, et al. Total cerebral blood flow and total brain perfusion in the general population: the Rotterdam Scan Study. *J Cereb Blood Flow Metab* 2008;28:412-419.
8. Vrooman HA, Cocosco CA, van der Lijn F, et al. Multi-spectral brain tissue segmentation using automatically trained k-Nearest-Neighbor classification. *Neuroimage* 2007;37:71-81.
9. Anbeek P, Vincken KL, van Bochove GS, van Osch MJ, van der Grond J. Probabilistic segmentation of brain tissue in MR imaging. *Neuroimage* 2005;27:795-804.
10. Rueckert D, Sonoda LI, Hayes C, Hill DL, Leach MO, Hawkes DJ. Nonrigid registration using free-form deformations: application to breast MR images. *IEEE Trans Med Imaging* 1999;18:712-721.
11. Prins ND, van Dijk EJ, den Heijer T, et al. Cerebral small-vessel disease and decline in information processing speed, executive function and memory. *Brain* 2005;128:2034-2041.
12. van Popele NM, Grobbee DE, Bots ML, et al. Association between arterial stiffness and atherosclerosis: the Rotterdam Study. *Stroke* 2001;32:454-460.
13. de la Torre JC. Critical threshold cerebral hypoperfusion causes Alzheimer's disease? *Acta Neuropathol* 1999;98:1-8.
14. Johnson NA, Jahng GH, Weiner MW, et al. Pattern of cerebral hypoperfusion in Alzheimer disease and mild cognitive impairment measured with arterial spin-labeling MR imaging: initial experience. *Radiology* 2005;234:851-859.
15. Kogure D, Matsuda H, Ohnishi T, et al. Longitudinal evaluation of early Alzheimer's disease using brain perfusion SPECT. *J Nucl Med* 2000;41:1155-1162.



CHAPTER 5

WHITE MATTER MICROSTRUCTURAL INTEGRITY



5.1

WHITE MATTER MICROSTRUCTURAL INTEGRITY AND COGNITIVE FUNCTION IN A GENERAL ELDERLY POPULATION

Archives of General Psychiatry, in press



*Meike W. Vernooij,
M. Arfan Ikram,
Henri A. Vrooman,
Piotr A. Wielopolski,
Gabriel P. Krestin,
Albert Hofman,
Wiro J. Niessen,
Aad van der Lugt,
Monique M.B. Breteler*

5.2

WHITE MATTER ATROPHY AND LESION FORMATION EXPLAIN THE LOSS OF STRUCTURAL INTEGRITY OF WHITE MATTER IN AGING

NeuroImage, 2008; 43:470-477

Meike W. Vernooij,
Marius de Groot*,
Aad van der Lugt,
M. Arfan Ikram,
Gabriel P. Krestin,
Albert Hofman,
Wiro J. Niessen,
Monique M.B. Breteler*

**Both authors contributed
equally to this study.*

Background The importance of macrostructural white matter changes, including white matter lesions and atrophy, in intact brain functioning is increasingly being recognized. Diffusion tensor imaging (DTI) enables measurement of the microstructural integrity of white matter. Loss of white matter integrity in aging has been reported, but whether this is inherent to the aging process itself or results from specific white matter pathology is unknown.

Methods In 832 persons aged 60 years and older from the population-based Rotterdam Study, we measured fractional anisotropy (FA) and directional diffusivities in normal-appearing white matter using DTI. All subjects' DTI measures were projected onto a common white matter skeleton to enable robust voxelwise comparison.

Results With increasing age, multiple regions showed significant decreases in FA or increases in axial or radial diffusivity in normal-appearing white matter. However, nearly all of these regional changes were explained by either white matter atrophy or by white matter lesions; each of which related to changes in distinct brain regions.

Conclusion These results indicate that loss of white matter integrity in aging is primarily explained by atrophy and lesion formation and not by the aging process itself. Furthermore, white matter atrophy and white matter lesion formation relate to loss of integrity in distinct brain regions, indicating the two processes are pathophysiologically different.

Intact white matter connections in the brain are important for the processing and integration of information generated by neural networks. Loss of integrity of these white matter pathways is thought to cause loss of “connectivity” and subsequent age-related cognitive decline (1). There are two distinct macroscopic processes affecting the white matter that are commonly seen in aging and which are readily recognized in both radiologic and pathologic examinations. Firstly, atrophy of white matter dominates brain tissue loss in aging, rather than does loss of grey matter neurons (2). Secondly, over 90% of elderly persons demonstrate on brain magnetic resonance imaging (MRI) so-called ‘white matter lesions’ (3), which pathologically represent signs of ischemic injury (4). Although white matter atrophy and white matter lesion formation often coincide and have shared determinants (5), it is still not understood whether these are part of the same pathophysiologic spectrum or whether these are independent processes. Furthermore, it is unknown whether and how these two macroscopic processes are related to loss of microstructural integrity of normal-appearing white matter.

Diffusion tensor imaging (DTI) (6) enables non-invasive quantification of the microstructural integrity of white matter using MRI (7). DTI measures the amount and directional dependence of microscopic diffusion of water molecules in the brain. In white matter, diffusion is hindered by the high degree of structural organization, resulting in anisotropic movement

of water molecules predominantly parallel to the orientation of the fiber tracts. A lower fractional anisotropy (FA) as measured by DTI signifies less anisotropic diffusion and thus lower microstructural integrity (6). Furthermore, from animal studies, it has been suggested that analysis of directional diffusivities - axial (λ_{ax}) and radial (λ_{rad}) diffusivity - may provide additional information on the underlying mechanisms of loss of white matter integrity. Myelin breakdown has been associated with increased diffusivity perpendicular to the white matter tract (λ_{rad}), whilst axonal damage is reflected in diffusivity changes parallel (λ_{ax}) to the primary fiber orientation (8-10).

So far, FA in white matter has been shown to decrease with age (11), but it is unknown to what extent this represents concurrent macroscopic changes in white matter, or whether aging itself causes white matter microstructural changes. Furthermore, analysis of regional patterns in FA changes has so far been limited to manually placed regions-of-interest (11) or to voxelwise measurement methods, both of which are prone to methodological constraints hindering interpretation and analysis of FA data (12, 13). Tract-based spatial statistics (TBSS) is a new technique for aligning FA images from multiple subjects and constructing a common skeleton of the white matter tracts, enabling robust voxelwise analysis of the microstructural integrity of white matter across subjects (13). Using TBSS, we investigated in 832 persons aged 60 years and older from the general population whether white matter atrophy and white matter lesions relate to integrity of normal-appearing white matter independent from aging, and if so, in which brain regions these associations are strongest.

MATERIALS & METHODS

Participants

This study is embedded within the Rotterdam Study, a large population-based cohort study in The Netherlands that started in 1990-1993 and is aimed at investigating determinants of various chronic diseases among elderly participants (14). The original study population consisted of 7983 participants aged 55 years and older within the Ommoord area, a suburb of Rotterdam. In 2000, the cohort was expanded with 3011 persons (≥ 55 years) who were living in the study area and had not been included before (14). From August 2005 to May 2006, we randomly selected 1,073 members of this cohort expansion for the current MRI study, the Rotterdam Scan Study. We excluded individuals who were demented or had MRI contraindications (including claustrophobia). The institutional review board approved the study. A total of 975 persons were eligible, of whom 907 participated and gave written informed consent (response 93%). Due to physical inabilities (e.g. back pain), imaging could not be performed

or completed in 12 individuals. A total of 895 MRI examinations were performed. Image quality was substandard due to motion artifacts or DTI artifacts in 63 scans, leaving a total of 832 scans in this analysis.

Image acquisition

We performed a multi-sequence MRI protocol on a 1.5-Tesla MRI scanner (General Electric Healthcare, Milwaukee, WI, USA). For DTI, we performed a single shot, diffusion-weighted spin echo echo-planar imaging sequence (repetition time (TR)= 8000 ms, echo time (TE)= 68.7 ms, field-of-view (FOV)= 21x21 cm², matrix= 96x64, interpolated to 256x256) slice thickness= 3.5 mm, 36 contiguous slices, applying parallel imaging (array spatial sensitivity encoding technique) with acceleration factor= 2). Maximum b-value was 1000 s/mm² in 25 non-collinear directions (number of excitations (NEX)= 1), and one volume was acquired without diffusion weighting (b-value= 0 s/mm²). Acquisition time was 3:44 min.

We further performed three high-resolution axial MRI sequences, i.e. a T1-weighted 3D Fast RF Spoiled Gradient Recalled Acquisition in Steady State with an inversion recovery prepulse (FASTSPGR-IR) sequence (TR= 13.8 ms, TE= 2.8 ms, inversion time (TI)= 400 ms, FOV= 25x17.5 cm², matrix= 416x256 (interpolated to 512x512), flip angle= 20°, NEX= 1, bandwidth (BW)= 12.50 kHz, 96 slices with slice thickness 1.6 mm zero-padded in the frequency domain to 0.8 mm), a proton density-weighted sequence (TR= 12,300 ms, TE= 17.3 ms, FOV= 25x17.5 cm², matrix= 416x256, NEX= 1, BW= 17.86 kHz, 90 slices with slice thickness 1.6 mm), and a fluid-attenuated inversion recovery (FLAIR) sequence (TR= 8000 ms, TE= 120 ms, TI= 2,000 ms, FOV= 25x25 cm², matrix= 320x224, NEX= 1, BW= 31.25 kHz, 64 slices with slice thickness 2.5 mm). All slices were contiguous.

Normal-appearing white matter and white matter lesion segmentation

For the assessment of volumes of normal-appearing white matter and white matter lesions, the structural MRI scans (T1-weighted, proton density-weighted, FLAIR) were transferred offline to a Linux workstation. Preprocessing steps and the classification algorithm have been described elsewhere (15). In summary, preprocessing included co-registration, non-uniformity correction and variance scaling. We used a k-nearest neighbour classifier based on multispectral MRI intensities to label voxels into cerebrospinal fluid, grey matter, normal-appearing white matter and white matter lesions (16). The feature space for the automated classification was created from manually segmented datasets, as described elsewhere (5, 15). In a postprocessing step, normal-appearing white matter was dilated with one voxel to assess overlap between voxels classified as white matter and those labelled as white matter lesion in order to remove voxels that were incorrectly classified as white matter lesion (e.g. in cortical grey matter). All segmentation results were visually inspected and, if needed, manually cor-

rected. To remove non-cerebral tissue, e.g. eyes, skull, and cerebellum, we applied non-rigid registration (17) to register to each brain a template scan in which these tissues were manually masked.

Global normal-appearing white matter and white matter lesion volumes were calculated by summing all voxels of the corresponding tissue class across the whole brain, to yield volumes in mL. To normalize for head size, these tissue volumes were expressed as percentage of total intracranial volume (which is the summation of all tissue classes, i.e. cerebrospinal fluid, grey matter, normal-appearing white matter and white matter lesions). As normal-appearing white matter volume was highly correlated with total white matter volume (i.e. the sum of normal-appearing white matter and white matter lesions) (Pearson's $r = 0.991$), we used relative normal-appearing white matter volume as a measure of white matter atrophy.

Global normal-appearing white matter volume was further subdivided into lobar volumes (frontal, occipital, parietal, temporal lobes and deep region) using a previously described protocol (18), in which a template brain with labels for the various lobes was non-rigidly registered to all scans. Lobar white matter atrophy was defined as normal-appearing white matter volume in the specific region relative to the total lobe volume (the summation of all tissue classes in the specific lobe).

Processing of raw DTI data

Processing of DTI data was performed with FSL (19) (<http://www.fmrib.ox.ac.uk/fsl/>). Eddy current and head-motion correction were performed by means of an affine registration to the reference (b0) volume. The corrected data was skull-stripped by applying FSL's Brain Extraction Tool (BET) on both the b0 and the diffusion-weighted images (20). Next, a tensor model was fitted to the diffusion data using FMRIB's Diffusion Toolbox (FDT) (19) to yield FA and both axial (λ_1) and radial [$(\lambda_2 + \lambda_3)/2$] diffusivities.

Tract-based spatial statistics processing

Voxelwise statistical analysis of the DTI data was carried out using Tract-Based Spatial Statistics (TBSS 1.1) (13), part of FSL (19). As the mean age of our study population differed greatly from the FMRIB cohort from which the TBSS template brain was derived (13), we used the anatomically most representative subject from our dataset as study specific template brain. For computational reasons, a two-stage hierarchical search strategy was used to find this target. All 832 FA images were randomly split into 26 subgroups of 32 subjects each. Cross-wise nonlinear registration using the Image Registration Toolkit (IRTK) (17) was performed on the Erasmus Computing Grid (Rotterdam, The Netherlands). The 26 candidate targets from each subset identified by the lowest summed transformation cost were subsequently cross-

wise registered to identify the subject closest to the group mean anatomy. In accordance with the standard TBSS pipeline, the remaining 831 subjects were then transformed to this study specific template subject in a stereotactic coordinate system (MNI space) using the ICBM152 template (21).

Subsequently, all FA images were averaged to produce a group mean FA image. Next, the mean FA image was thinned to create a mean FA skeleton, which represents the centres of all white matter tracts common to the group. This skeleton was thresholded at an FA value of 0.20 (13), to include the major white matter pathways but exclude pathways with large inter-subject variability. Each subject's aligned FA data was then projected onto this skeleton by searching perpendicular to the skeleton to find local maxima in FA. This step locally corrects for residual misalignment and lines up the centres of individual tracts. Next, values of λ_{ax} and λ_{rad} were mapped onto the skeleton by using the projection vectors from each individual's FA-to-skeleton transformation (13). Voxelwise analysis of FA and directional diffusivity data across the group of subjects was performed only on the data projected onto the skeleton template.

Removal of white matter lesions

White matter lesion maps (automatically classified as described above) were resampled to the DTI image space and fed into the pipeline for non-FA data provided by TBSS (13). By applying the FA-to-skeleton transformation on this lesion map, as was also done for the directional diffusivities, we created a lesion mask in skeleton space. This mask was used to identify voxels on the skeletons that originated in lesions (Fig. 1). These voxels were then removed from the skeleton to obtain in each individual a skeleton of the normal appearing white matter.

Voxelwise statistical analysis

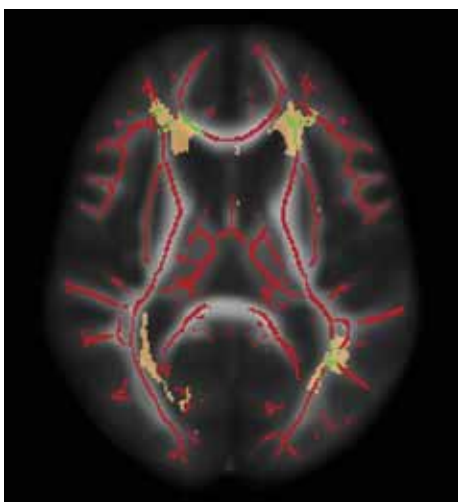
Skeletonized FA images created by TBSS were analyzed using a generalized linear model implementation in Matlab's Statistical Toolbox (Version 6.1, Release 2007b, The MathWorks, Natick, MA, USA). In a voxelwise manner, a multiple linear regression model was fitted to identify those voxels on the white matter skeleton that showed significant decrease in FA associated with age, relative global normal-appearing white matter volume and relative white matter lesion volume. Because of skewness of the untransformed measure, relative white matter lesion volume was natural log-transformed. All analyses were adjusted for sex and furthermore, if appropriate, for each of the other variables in the model (age and relative volumes of global normal-appearing white matter and white matter lesions). We subsequently analyzed the relation between lobar white matter volumes and FA, for each lobe separately, adjusted for age, sex and white matter lesion volume. Finally, we investigated changes in λ_{ax} and λ_{rad} associated with age, relative global normal-appearing white matter volume and rela-

tive white matter lesion volume. For all analyses, the null distributions of the t-values were estimated using a permutation-based method (10,000 permutations), in order to correct for multiple comparisons (22). As a result, the displayed figures show t-statistics for each association thresholded at a multiple-comparison corrected P value of 0.05. The skeletonized results were then thickened for better visibility (13). Significant results are shown in red-to-yellow colorings of voxels on the skeleton, with yellow representing higher t-values and color intensities standardized between all figures.

RESULTS

Mean age of the study population ($N = 832$) was 67.3 years and 419 (50.4%) participants were women. Mean volume percentage of global normal-appearing white matter was 34.4% (SD 3.7). Median volume percentage of white matter lesions was 0.3% (interquartile range 0.2-0.5%). A significant decrease in FA was seen in multiple regions on the white matter skeleton with increasing age (Fig. 2A), reflecting a loss of microstructural integrity of normal-appearing white matter. However, nearly all of these regional decreases in FA were explained by either white matter atrophy (Fig. 2B) or by white matter lesions (Fig. 2C). When adjusted for both white matter atrophy and white matter lesions, only few regions in the normal-appearing white matter still displayed changes with age (Fig. 2D), most notably a small region bilateral in the inferior longitudinal fasciculus (Fig. 3).

The white matter regions that showed FA changes associated with either white matter atrophy or white matter lesions differed clearly. White matter atrophy was related to loss of micro-



structural integrity in the body of the corpus callosum, the fornix and in the cingulate bundle along its complete course from anterior up to its posterior connection to the hippocampal region (Fig. 2B and Figs. 4 and 5). In contrast, a larger relative volume of white

Figure 1. Identification of voxels on the white matter skeleton originating in white matter lesions. Axial mean fractional anisotropy image with overprojection of the white matter skeleton (in red). Voxels that were segmented as white matter lesions in a single individual on structural MR images are depicted in brown. In green, the voxels on the white matter skeleton that originate in a white matter lesion are shown. These green voxels were then removed from the individual's skeleton in order to obtain a skeleton of the normal-appearing white matter.

matter lesions caused FA decreases in periventricular regions (Fig. 2C and Fig. 6). We did not find any increases in FA with age, white matter atrophy or white matter lesions.

When analyzing lobar white matter atrophy, we found that for each lobe, white matter atrophy in that region was associated with a similar pattern in FA decreases compared with global white matter atrophy (see Supplementary Figure). Also, there were no differences between left or right lobes in this respect (results not shown).

Similarly to FA changes, we found that changes in λ_{ax} and λ_{rad} that occurred with increasing age were almost fully explained by white matter atrophy or by white matter lesions, apart from the region bilateral in the inferior longitudinal fasciculus. Also corresponding to FA changes, we found regional differences in λ_{ax} and λ_{rad} between atrophy and lesions. White matter atrophy was associated with increases in both λ_{ax} and λ_{rad} in fornix and hippocampal regions, the same regions where FA showed decreases with atrophy (Fig. 7). λ_{ax} was increased with atrophy in posterior periventricular regions, without accompanying change in λ_{rad} (Fig. 7). In contrast, significant increases in λ_{rad} almost fully explained the previously described FA decreases in the corpus callosum and cingulate bundle (Fig. 7).

Regarding white matter lesions, we found with increasing lesion load significant increases in λ_{ax} lateral from the ventricles extending to the centrum semiovale and corona radiata, without an associated increase in λ_{rad} (Fig. 8) or change in FA. In contrast, λ_{rad} was mainly increased in posterior periventricular regions with increasing white matter lesion load (Fig. 8). We did not find any decreases in λ_{ax} or λ_{rad} with age, white matter atrophy or white matter lesions.

DISCUSSION

Using DTI, we found that independent of age, both white matter atrophy and white matter lesion burden are related to loss of integrity in multiple yet distinct regions of normal-appearing white matter.

Strengths of our study are the large sample of persons from a general elderly population in whom both structural MRI and DTI were performed, and our automated and validated techniques for quantification of white matter atrophy and white matter lesion volume. The voxel-wise analysis technique we used, TBSS (13), is an automated observer-independent method which has been shown to be more robust and accurate than other voxelwise analysis techniques (such as statistical-parametrical mapping) which are prone to residual misalignment and in which the amount of spatial smoothing greatly affects the results (23).

Our results have several major implications for the understanding of white matter changes in the aging brain. Firstly, they confirm that FA, and thus microstructural integrity, is reduced even in normal-appearing white matter, although no macroscopic alterations are visible on conventional MRI. Age-related changes in normal-appearing white matter microstructure have previously been described by studies measuring FA in manually placed regions-of-interest (24-26). Also, in small case-control studies, FA reductions in normal-appearing white matter were found to be more pronounced in persons with signs of ischemic brain disease (7, 27, 28) and in persons with Alzheimer's Disease or mild cognitive impairment (29, 30) in comparison with healthy controls. We now demonstrate in a large sample of the general population the predilection areas of age-related changes in the normal-appearing white matter, and we show that these changes are associated with both ischemic white matter lesions and with white matter atrophy.

Secondly, our data show that aging related loss of microstructural integrity of white matter is primarily explained by white matter atrophy and white matter lesion formation. White matter breakdown in aging and associated loss of "connectivity" is thought to be a major factor in cognitive decline (31). Our results may therefore provide a better understanding of the pathophysiologic processes underlying cognitive deterioration in aging.

Thirdly, our results indicate that white matter atrophy and white matter lesion formation, which are very common in the aging brain, are related to FA reductions and increases in directional diffusivities in distinct brain regions. The regions that showed loss of microstructural integrity associated with white matter atrophy, namely the fornix, cingulate bundle and hippocampal region, are those that are part of the limbic system which is the anatomic substrate for memory, emotion and learning, and which since long has been related to development of cognitive decline and Alzheimer's disease (32). The normal-appearing white matter regions that showed reduced FA in relation to a larger burden of white matter lesions, the periventricular regions, are specifically known to be vulnerable to ischemic events (33).

Furthermore, we found that the regions where changes in λ_{ax} and λ_{rad} occurred differed for white matter atrophy and white matter lesions, but also that increases in λ_{ax} and λ_{rad} did not always overlap. Several animal studies have shown that the nature of the underlying white matter pathology may be reflected in changes in λ_{ax} and λ_{rad} . Myelin degradation has been shown to primarily lead to increases in diffusivity perpendicular to the tracts (λ_{rad}), whilst acute axonal injury in animal models led to (transient) decreases in parallel diffusivity (λ_{ax}) (8, 10). In the present study, we did not find any decreases in diffusivity, but rather increases in λ_{ax} and λ_{rad} , in line with other reports in humans that studied aging (34-36) or trauma (37) or even preterm infants with diffuse white matter changes (38). It has been suggested that

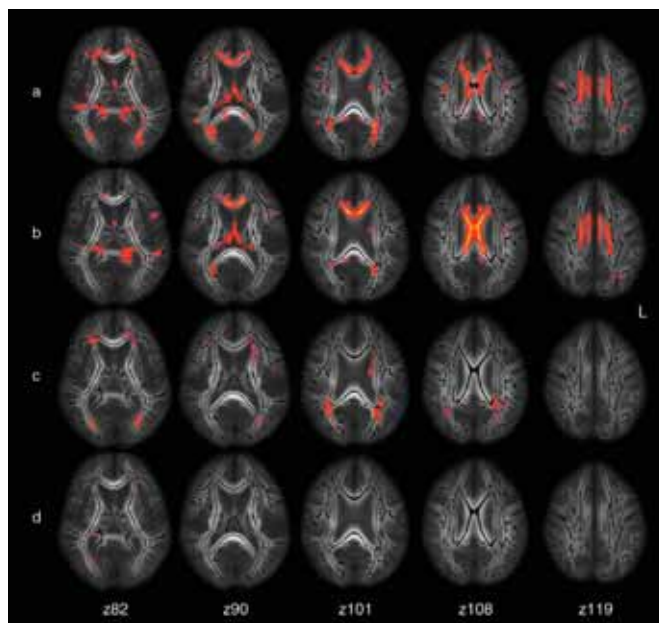


Figure 2. Effects of age, global white matter atrophy and white matter lesions on fractional anisotropy values of normal-appearing white matter. Images are shown in the Montreal Neurological Institute (MNI) stereotactic space, with MNI coordinates for axial levels (z) depicted for each column. The white matter skeleton (black) is projected onto the axial MR images. Yellow-to-red colors represent normal-appearing white matter regions with reduced fractional anisotropy (FA) in relation to (A) increasing age, adjusted for sex only, (B) global white matter atrophy, adjusted for age, sex and white matter lesions, (C) white matter lesions, adjusted for age, sex and white matter atrophy and (D) increasing age, adjusted for sex, white matter atrophy and white matter lesions. With increasing age, multiple regions show significant decreases in FA (A). However, after adjustment for white matter atrophy and white matter lesions, only few regions remain (D).

main (D). White matter atrophy (B) relates to decreases in FA in the hippocampal region (z82), fornix (z90), corpus callosum (z90 to z108) and along the cingulate bundle (z119). In contrast, white matter lesion burden (C) is associated with reduced periventricular FA (z82 to z108).

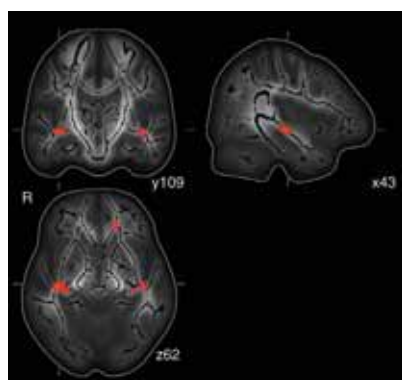


Figure 3. Aging and reduced fractional anisotropy in inferior longitudinal fasciculus. Coronal, sagittal and axial projections of mean fractional anisotropy (FA) MRI image on which the white matter skeleton (black) is projected. MNI coordinates are depicted for each projection. Yellow-to-red colors represent normal-appearing white matter regions with reduced FA in relation to increasing age. When adjusted for global white matter atrophy and white matter lesion volume, only very few regions in the normal-appearing white matter show reduced FA with age, most notably a small region bilateral in the inferior longitudinal fasciculus.

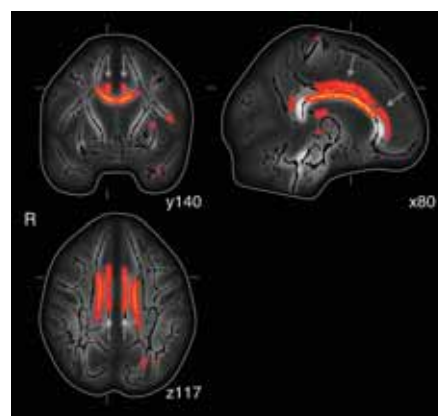


Figure 4. Global white matter atrophy and reduced fractional anisotropy in cingulate bundle. Coronal, sagittal and axial projections of mean fractional anisotropy (FA) MRI image on which the white matter skeleton (black) is projected. MNI coordinates are depicted for each projection. Yellow-to-red colors represent normal-appearing white matter regions with reduced FA in relation to white matter atrophy. Arrows indicate the cingulate bundle on both sides.

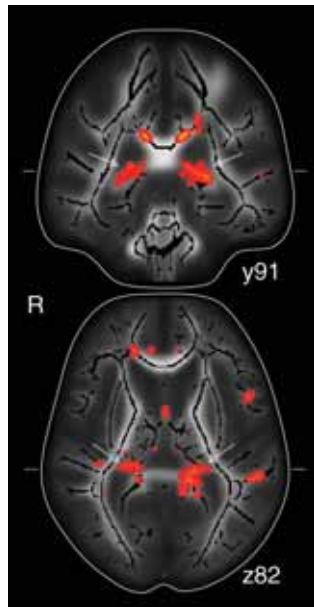


Figure 5. Global white matter atrophy and reduced fractional anisotropy in hippocampal region. Coronal and axial projection of mean fractional anisotropy (FA) MRI image on which the white matter skeleton (black) is projected. MNI coordinates are depicted for both projections. Yellow-to-red colors represent normal-appearing white matter regions with reduced FA in relation to white matter atrophy. Arrows indicate the hippocampal region on both sides.

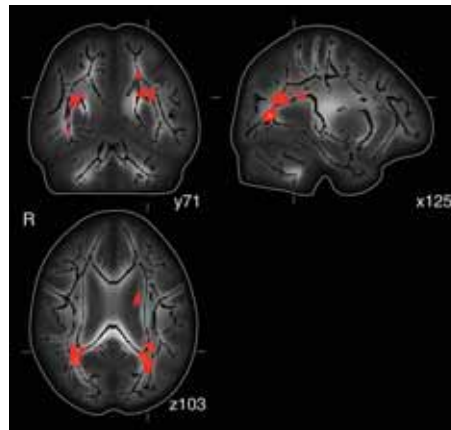


Figure 6. White matter lesions and reduced fractional anisotropy in periventricular regions. Coronal, sagittal and axial projections of mean fractional anisotropy (FA) MRI image on which the white matter skeleton (black) is projected. MNI coordinates are depicted for each projection. Normal-appearing white matter with reduced FA in relation to white matter lesions is visible in posterior periventricular regions (yellow-to-red colors).

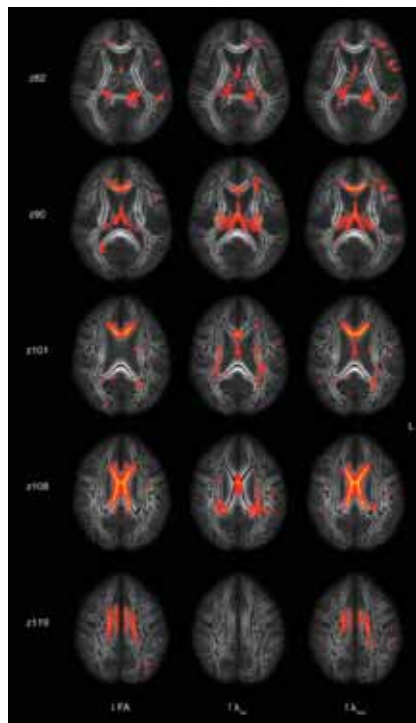


Figure 7. Global white matter atrophy and increased directional diffusivity. Axial projections of mean fractional anisotropy (FA) MRI images on which the white matter skeleton (black) is projected. Columns show regions where global white matter atrophy is associated with decreases in FA or increases in axial (λ_{ax}) and radial (λ_{rad}) diffusivity, respectively. Rows depict the same axial levels as Figure 2, in MNI coordinates (z). The first ($z= 82$) and second ($z= 90$) rows show decreases in FA in the hippocampal region and fornix associated with white matter atrophy, accompanied by increases of both λ_{ax} and λ_{rad} (yellow-to-red colors) in these regions. The third ($z= 101$) and fourth row ($z = 108$) show that reductions of FA in the corpus callosum and cingulate bundle are almost fully explained by increases in λ_{rad} in these regions, without accompanying changes in λ_{ax} . In contrast, λ_{ax} is increased in posterior periventricular regions ($z= 108$), without a marked change in λ_{rad} .

increases in both λ_{ax} and λ_{rad} reflect decreased packing within a voxel (36) or that apparent increases in λ_{ax} result from loss of fiber coherence in regions with fiber crossing (38).

In summary, the regional distinction in loss of integrity of the normal-appearing white matter in relation to atrophy or white matter lesion formation indicates that the two processes are not sequential events but are rather independent and thus pathophysiologically potentially different. As such, our study provides new insight into white matter changes in aging and a starting point for further research into preventive measures.

Acknowledgements

The authors would like to express their gratitude to Mr. Tobias A. Knoch and Mr. Anis Abuseiris from the Erasmus Grid Office and to Ms. Renske de Boer for their considerable support in performing the computationally intensive registrations for this manuscript.

REFERENCES

- O'Sullivan M, Jones DK, Summers PE, Morris RG, Williams SC, Markus HS. Evidence for cortical "disconnection" as a mechanism of age-related cognitive decline. *Neurology* 2001; 57:632-638.
- Meier-Ruge W, Ulrich J, Bruhlmann M, Meier E. Age-related white matter atrophy in the human brain. *Ann N Y Acad Sci* 1992; 673:260-269.
- de Leeuw FE, de Groot JC, Achten E, et al. Prevalence of cerebral white matter lesions in elderly people: a population based magnetic resonance imaging study. The Rotterdam Scan Study. *J Neurol Neurosurg Psychiatry* 2001; 70:9-14.
- Englund E, Brun A, Alling C. White matter changes in dementia of Alzheimer's type. Biochemical and neuropathological correlates. *Brain* 1988; 111:1425-1439.
- Ikram MA, Vrooman HA, Vernooij MW, et al. Brain tissue volumes in the general elderly population. The Rotterdam Scan Study. *Neurobiol Aging* 2008; 29:882-890.
- Basser PJ, Jones DK. Diffusion-tensor MRI: theory, experimental design and data analysis - a technical review. *NMR Biomed* 2002; 15:456-467.
- O'Sullivan M, Summers PE, Jones DK, Jarosz JM, Williams SC, Markus HS. Normal-appearing white matter in ischemic leukoaraiosis: a diffusion tensor MRI study. *Neurology* 2001; 57:2307-2310.
- Song SK, Sun SW, Ju WK, Lin SJ, Cross AH, Neufeld AH. Diffusion tensor imaging detects and differentiates axon and myelin degeneration in mouse optic nerve after retinal ischemia. *Neuroimage* 2003; 20:1714-1722.
- Song SK, Yoshino J, Le TQ, et al. Demyelination increases radial diffusivity in corpus callosum of mouse brain. *Neuroimage* 2005; 26:132-140.
- Sun SW, Liang HF, Trinkaus K, Cross AH, Armstrong RC, Song SK. Noninvasive detection of cuprizone induced axonal damage and demyelination in the mouse corpus callosum. *Magn Reson Med* 2006; 55:302-308.
- Salat DH, Tuch DS, Greve DN, et al. Age-related

- alterations in white matter microstructure measured by diffusion tensor imaging. *Neurobiol Aging* 2005; 26:1215-1227.
12. Bookstein FL. "Voxel-based morphometry" should not be used with imperfectly registered images. *Neuroimage* 2001; 14:1454-1462.
13. Smith SM, Jenkinson M, Johansen-Berg H, et al. Tract-based spatial statistics: voxelwise analysis of multi-subject diffusion data. *Neuroimage* 2006; 31:1487-1505.
14. Hofman A, Breteler MM, van Duijn CM, et al. The Rotterdam Study: objectives and design update. *Eur J Epidemiol* 2007; 22:819-829.
15. Vrooman HA, Cocosco CA, van der Lijn F, et al. Multi-spectral brain tissue segmentation using automatically trained k-Nearest-Neighbor classification. *Neuroimage* 2007; 37:71-81.
16. Anbeek P, Vincken KL, van Bochove GS, van Osch MJ, van der Grond J. Probabilistic segmentation of brain tissue in MR imaging. *Neuroimage* 2005; 27:795-804.
17. Rueckert D, Sonoda LI, Hayes C, Hill DL, Leach MO, Hawkes DJ. Nonrigid registration using free-form deformations: application to breast MR images. *IEEE Trans Med Imaging* 1999; 18:712-721.
18. Ikram MA, Vrooman HA, Vernooij MW, et al. Brain tissue volumes in relation to cognitive function and risk of dementia. *Neurobiol Aging* 2008; in press; doi:10.1016/j.neurobiolaging.2008.1004.1008.
19. Smith SM, Jenkinson M, Woolrich MW, et al. Advances in functional and structural MR image analysis and implementation as FSL. *Neuroimage* 2004; 23 Suppl 1:S208-219.
20. Smith SM. Fast robust automated brain extraction. *Hum Brain Mapp* 2002; 17:143-155.
21. Mazziotta J, Toga A, Evans A, et al. A probabilistic atlas and reference system for the human brain: International Consortium for Brain Mapping (ICBM). *Philos Trans R Soc Lond B Biol Sci* 2001; 356:1293-1322.
22. Nichols TE, Holmes AP. Nonparametric permutation tests for functional neuroimaging: a primer with examples. *Hum Brain Mapp* 2002; 15:1-25.
23. Jones DK, Symms MR, Cercignani M, Howard RJ. The effect of filter size on VBM analyses of DT-MRI data. *Neuroimage* 2005; 26:546-554.
24. Abe O, Aoki S, Hayashi N, et al. Normal aging in the central nervous system: quantitative MR diffusion-tensor analysis. *Neurobiol Aging* 2002; 23:433-441.
25. Bartzokis G, Sultzer D, Lu PH, Nuechterlein KH, Mintz J, Cummings JL. Heterogeneous age-related breakdown of white matter structural integrity: implications for cortical "disconnection" in aging and Alzheimer's disease. *Neurobiol Aging* 2004; 25:843-851.
26. Helenius J, Soinne L, Perkio J, et al. Diffusion-weighted MR imaging in normal human brains in various age groups. *AJNR Am J Neuroradiol* 2002; 23:194-199.
27. Jones DK, Lythgoe D, Horsfield MA, Simmons A, Williams SC, Markus HS. Characterization of white matter damage in ischemic leukoaraiosis with diffusion tensor MRI. *Stroke* 1999; 30:393-397.
28. Chabriat H, Pappata S, Poupon C, et al. Clinical severity in CADASIL related to ultrastructural damage in white matter: in vivo study with diffusion tensor MRI. *Stroke* 1999; 30:2637-2643.
29. Fellgiebel A, Muller MJ, Wille P, et al. Color-coded diffusion-tensor-imaging of posterior cingulate fiber tracts in mild cognitive impairment. *Neurobiol Aging* 2005; 26:1193-1198.
30. Kantarci K, Jack CR, Jr., Xu YC, et al. Mild

- cognitive impairment and Alzheimer disease: regional diffusivity of water. *Radiology* 2001; 219:101-107.
31. Fazekas F, Schmidt R, Scheltens P. Pathophysiologic mechanisms in the development of age-related white matter changes of the brain. *Dement Geriatr Cogn Disord* 1998; 9 (Suppl 1):2-5.
 32. Hopper MW, Vogel FS. The limbic system in Alzheimer's disease. A neuropathologic investigation. *Am J Pathol* 1976; 85:1-20.
 33. Chalela JA, Wolf RL, Maldjian JA, Kasner SE. MRI identification of early white matter injury in anoxic-ischemic encephalopathy. *Neurology* 2001; 56:481-485.
 34. Salat DH, Tuch DS, van der Kouwe AJ, et al. White matter pathology isolates the hippocampal formation in Alzheimer's disease. *Neurobiol Aging* 2008;in press; doi:10.1016/j.neurobiolaging.2008.1003.1013.
 35. Bastin ME, Clayden JD, Pattie A, Gerrish IF, Wardlaw JM, Deary IJ. Diffusion tensor and magnetization transfer MRI measurements of periventricular white matter hyperintensities in old age. *Neurobiol Aging* 2007;in press; doi:10.1016/j.neurobiolaging.2007.1005.1013.
 36. Sullivan EV, Rohlfing T, Pfefferbaum A. Quantitative fiber tracking of lateral and interhemispheric white matter systems in normal aging: Relations to timed performance. *Neurobiol Aging* 2008;in press; doi:10.1016/j.neurobiolaging.2008.1004.1007.
 37. Kraus MF, Susmaras T, Caughlin BP, Walker CJ, Sweeney JA, Little DM. White matter integrity and cognition in chronic traumatic brain injury: a diffusion tensor imaging study. *Brain* 2007; 130:2508-2519.
 38. Counsell SJ, Shen Y, Boardman JP, et al. Axial and radial diffusivity in preterm infants who have diffuse white matter changes on magnetic resonance imaging at term-equivalent age. *Pediatrics* 2006; 117:376-386.

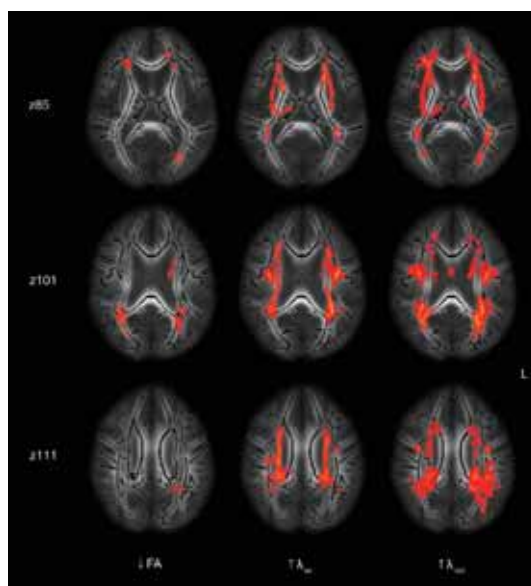
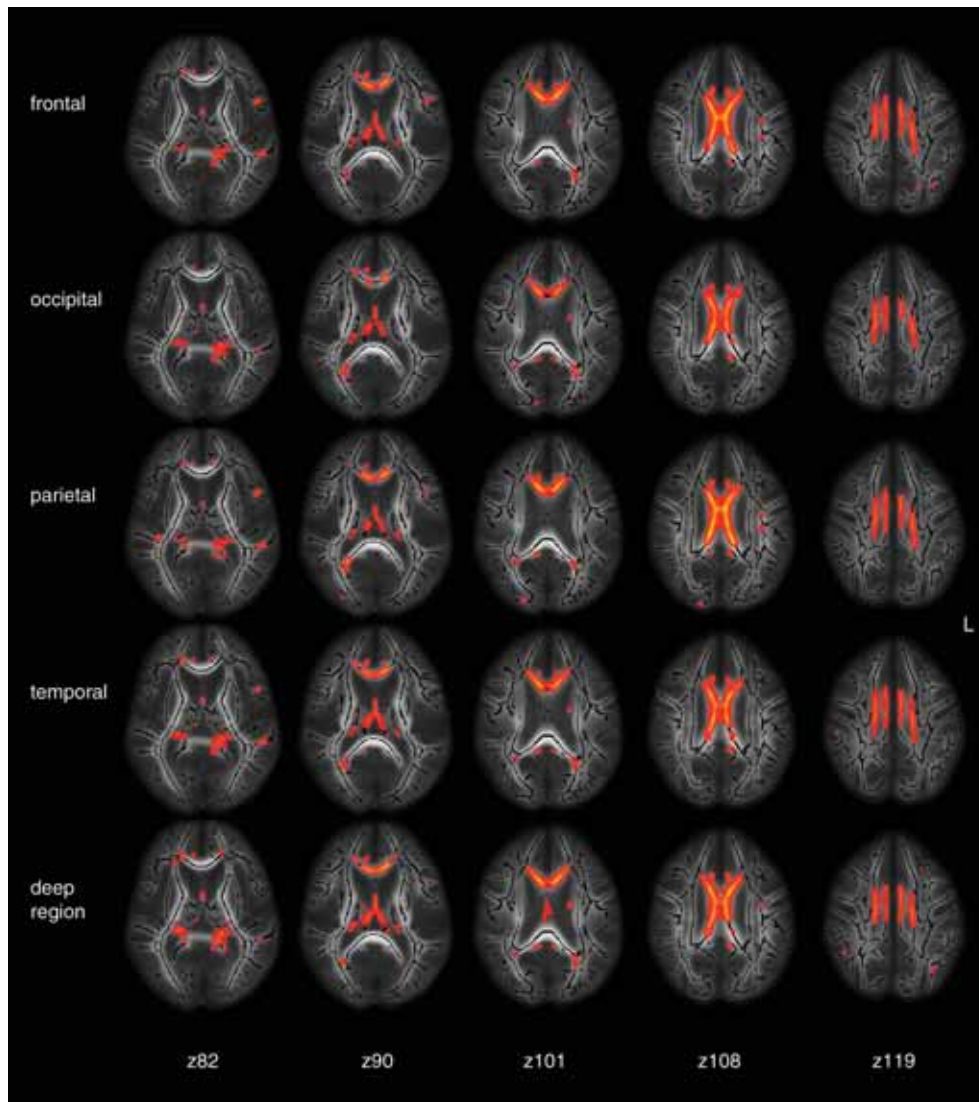


Figure 8. White matter lesions and increased directional diffusivity. Axial projections of mean fractional anisotropy (FA) MRI images on which the white matter skeleton (black) is projected. Columns show regions where relative white matter lesion volume is associated with decreases in FA or increases in axial (λ_{ax}) and radial (λ_{rad}) diffusivity, respectively. Rows depict axial levels in MNI coordinates (z). The first ($z=85$) and second ($z=101$) rows show in the anterior periventricular regions and bilateral in the extreme capsule increases in both λ_{ax} and λ_{rad} (yellow-to-red colors) associated with white matter lesions, but no change in FA. The second ($z=101$) and third row ($z=111$) show increases in λ_{ax} lateral from the ventricles extending to the centrum semiovale and corona radiata, without accompanying increases of λ_{rad} in these regions. In contrast, λ_{rad} shows marked increases in posterior periventricular regions.



Supplementary Figure. Lobar white matter atrophy and reductions in fractional anisotropy. Axial projections of mean fractional anisotropy (FA) MRI images on which the white matter skeleton (black) is projected. Images are shown in the Montreal Neurological Institute (MNI) stereotactic space, with MNI coordinates for axial levels (z) depicted for each column. Axial levels correspond to the levels depicted in Figure 2. Yellow-to-red colors represent normal-appearing white matter regions with reduced fractional anisotropy (FA) in relation to lobar white matter atrophy (represented in rows; respectively frontal, occipital, parietal and temporal lobes and the deep region), adjusted for age, sex and relative white matter lesion volume. The regions that show significant reductions in FA associated with lobar white matter atrophy do not differ between the lobes and are furthermore similar to the regions that show FA reductions with global white matter atrophy (see Figure 2).



6

GENERAL DISCUSSION

The objective of this thesis was to study with magnetic resonance imaging (MRI) age-related brain changes that may function as preclinical markers of neurodegenerative or cerebrovascular disease.

In the elderly, neurodegenerative and cerebrovascular diseases are very common and both entities often coexist. Despite their frequent occurrence, therapeutic opportunities after onset of disease are still scarce and therefore preventive measures are needed. Furthermore, evidence is accumulating that the joint occurrence of these diseases is based not merely on chance: They share many vascular risk factors (1); presentation and severity of both diseases may interact; and brains of persons diagnosed with late-onset dementia often show at autopsy a mixture of ischemic disease and typical Alzheimer's disease (AD) pathology (2). To unravel a potential shared etiology, and to better understand the pathophysiology of the separate entities, it is important to identify underlying pathology in an early, preclinical phase.

Over the past decades, MRI has shown to be a useful non-invasive imaging modality to detect and study biomarkers of brain disease. The Rotterdam Scan Study is a population-based imaging study that aims to investigate causes and consequences of age-related brain diseases using advanced MRI techniques (3). Imaging data from the general elderly population can help us distinguish normal from abnormal, understand pathophysiologic processes and identify persons at risk for disease. This thesis covers both the methodology of the Rotterdam Scan Study and several new imaging biomarkers that signal age-related brain changes and that may ultimately serve as markers of neurodegenerative or cerebrovascular disease.

In this chapter, I will first address methodological considerations related to our study design. I will then summarize our main findings and review their interpretation in the context of current knowledge. Although observational epidemiological studies are typically not designed to develop clinical guidelines, our work may have clinical implications that I will discuss. Finally, I will suggest directions for future research.

STUDY DESIGN CONSIDERATIONS

Magnetic resonance imaging protocol

There is a rapid growth in studies that use imaging to examine the aging brain in a population-based setting (4-10). Many of these are designed to acquire longitudinal imaging data and aim to use automated algorithms for the processing of large volumes of data. This calls for a standardized imaging protocol yielding high quality data that can answer specific research questions and that can be fed into automated pipelines for processing. Furthermore, a stable

performance of hardware and software over time is needed to allow robust follow-up of brain changes.

In this thesis, we discuss the imaging methodology and protocol considerations of the Rotterdam Scan Study. Given that elderly persons are scanned it is necessary to find a balance between costs, the inconvenience for the participants, the time spent in the confined space of the MRI scanner and the relevance and quality of the acquired data. We describe a 30-minute protocol that covers high-resolution macrostructural imaging, microstructural imaging and flow quantification on 1.5 T. We use relatively novel MRI techniques such as 3D high-resolution T2*-weighted imaging and diffusion tensor imaging (DTI), which are not yet commonly applied in clinical practice. The resulting protocol can be easily transferred to other manufacturer platforms without further modifications. Changes or updates in hardware or software configuration are avoided and regular quality checks performed, to secure validity of cross-subject and cross-scan comparisons. This protocol may serve as a guideline that can be implemented by others and may facilitate pooling of imaging data across studies.

Observer-dependent measurements

Although we strived for fully automated measurement of all image information, several studies described in this thesis were dependent on manual or visual assessment of image parameters. For example, cerebral microbleeds and infarcts were rated visually and cerebral blood flow was measured by manually placed regions-of-interest. Manual and visual measurements are time intensive, dependent on individual observers and may not be reproducible over long study periods in which raters change over time. Therefore, it would be preferable to use validated fully automated processing techniques, for example the techniques described in this thesis for brain tissue segmentation and for analysis of DTI data. Yet, the measurements for which automated analysis was not available were performed by two independent raters, and inter-rater reliabilities for these measurements were invariably very high. Future developments in image processing will likely render more possibilities for automated measurements.

Cross-sectional analyses

The studies described in this thesis were all performed in the context of the Rotterdam Scan Study, a longitudinal population-based cohort study. However, the data used to conduct our research were acquired cross-sectionally, thus limiting our abilities to distinguish cause and effect. As we had no information on the temporal relation between determinants and imaging biomarkers, we cannot state with certainty that determinants preceded the brain changes that we assessed on MRI. Longitudinal measurements within the Rotterdam Scan Study are needed to further elucidate associations between potential risk factors and these imaging biomarkers. Also, follow-up of our study participants will provide data on incident cases of

dementia and stroke, enabling us to relate the imaging biomarkers we studied to neurological outcomes.

REVIEW AND INTERPRETATION OF MAIN FINDINGS

Incidental brain findings

Performing brain MRI in volunteers may lead to the discovery of unexpected, asymptomatic brain abnormalities that are unrelated to the purpose of the imaging study. Despite the frequent use of volunteers in neuroimaging studies, data on the prevalence and management of such incidental brain findings were very scarce. In this thesis, we described the frequency of incidentally discovered brain abnormalities in 2,000 middle-aged and elderly Rotterdam Scan Study participants. We found that the prevalence of incidental brain findings in our study was much higher than was reported previously (11-14). Around 2% of participants had brain abnormalities that required further clinical investigation (15). This overall prevalence figure as well as the prevalence estimates for specific findings remained constant over a larger amount of acquired MRI scans (to date, over 3,500).

The majority of these incidental brain abnormalities were meningiomas and aneurysms, findings for which established protocols of clinical management in symptomatic patients exist. Yet, the natural course of these and many other abnormalities in asymptomatic persons is often not known and may differ greatly from prognosis in symptomatic patients. Some findings may not need further evaluation or treatment, so it can be questioned whether participants should be confronted with information that will unnecessarily cause psychological stress or lead to costly additional medical examinations with associated risk of complications (16).

Based on existing evidence and experts' opinions, we had a priori developed a protocol how to deal with incidental brain findings. After presenting our data, we have been criticized on the one side for being too reserved in referring participants with aneurysms (17), and on the other side for inducing unnecessary fear of asymptomatic insidious brain abnormalities among the general public (18). We are of the opinion that in the absence of information on the natural history of incidental findings, the optimal management should be based on the best available evidence (19). Regarding small unruptured aneurysms, the ISUIA study (20) currently provides in our view the best prospective data to guide management. In the ISUIA study, the rupture risk for aneurysms <7 mm in the anterior circulation was 0% (20) and in persons over 40 years the risks associated with treatment of these aneurysms were found to outweigh the benefits (21). Therefore, we decided not to refer these persons. In line with this,

referral of all persons with incidental meningiomas may possibly be unwarranted, but prospective data in support of this are not yet available.

A large-scale discussion on the topic of incidental brain findings is needed to create awareness among clinicians and researchers that standards need to be developed for adequate informed consent forms and for management of these findings. This discussion is by no means new (22-25), but previously lacked robust data on the scale of the problem, which are now provided by our study. We expect to acquire more information on the natural course of these brain findings from follow-up examinations, which will further contribute to this discussion and aid in protocol development and decision making.

Cerebral microbleeds

In patients admitted for stroke, cerebral microbleeds have become acknowledged as risk factors for stroke recurrence and hemorrhagic transformation of ischemic brain areas (26-28). Furthermore, the number of microbleeds was found to predict the future risk of symptomatic hemorrhage in survivors of primary lobar hemorrhage (29). Despite this potentially large clinical relevance, very little was known on risk factors for and prognosis of microbleeds in non-stroke patients. In this thesis, we have shown that an optimized, high-resolution T2*-weighted MRI sequence detected significantly more microbleeds compared with a conventional MRI sequence. The quality of spatial and contrast resolution of the MRI sequence used for microbleed detection may explain in part the large differences in microbleed prevalence that are present across studies (7, 30-32). Using this optimized MRI sequence, we found that microbleeds were present in nearly 1 in 5 persons over age of 60 and in over 1 in 3 in persons aged 80 years and older. This prevalence is much higher than was described previously (30, 31), making the issue of microbleed prognosis in non-stroke patients even more relevant.

We furthermore established that risk factors for microbleeds varied according to microbleed location in the brain. Cardiovascular risk factors and markers of ischemic small vessel disease were associated with deep or infratentorial microbleeds, while apolipoprotein (APOE) $\epsilon 4$ allele, a known risk factor for both cerebral amyloid angiopathy (CAA) and AD (33, 34), related to strictly lobar microbleeds. This is indirect support that deep or infratentorial microbleeds reflect arteriolosclerotic angiopathy, whereas strictly lobar microbleeds are caused by CAA and may even relate to risk of AD. These findings need yet to be confirmed in other studies, but do suggest that future studies should consider separate subgroup analyses according to microbleed location.

Our studies have contributed to the development of criteria for microbleed detection, definition and interpretation formulated by the Microbleed Study Group, an international con-

sortium on microbleed research (35). This group of experts has stressed the importance of MRI parameters for microbleed detection, supports the view that microbleed location may be reflective of underlying pathology, and favors evolution of a shared set of standards for microbleed detection that will allow fruitful cross-study comparisons and enable robust longitudinal data collection (35).

Whether use of antithrombotic or thrombolytic medication in persons with microbleeds may increase the risk of symptomatic intracerebral hemorrhage is heavily disputed in the scientific community (36-38), and needs to be further elucidated, particularly in light of the broadening indications for antithrombotic therapy. We showed that persons who had used or were using antithrombotic medication at time of MRI significantly more often had cerebral microbleeds. Though the interpretation of these analyses was restricted by their cross-sectional nature and by the possibility of confounding by indication, our results justify further longitudinal research into the relation between antithrombotic drugs and microbleeds. A specific case that we encountered within our cohort, though anecdotal, seems to support this view: A stroke-free neurologically asymptomatic person, using antiplatelet drugs, developed a symptomatic intracerebral hemorrhage precisely at the site of a small cerebral microbleed. This case illustrates a direct chronological and spatial relationship between microbleeds and symptomatic hemorrhage and advocates a thorough study of the potential risks associated with presence of microbleeds; not only in stroke patients, but also in the general population.

Cerebral blood flow

The brain is dependent on cerebral blood flow for adequate supply of oxygen and nutrients. Under normal conditions, cerebral autoregulation mechanisms maintain blood flow to the brain within tight limits, ensuring adequate brain tissue perfusion (39). However, certain disease states such as hypertension may impair autoregulation (40). It is thought that impaired cerebral perfusion is often present in cerebrovascular and neurodegenerative disease. This association may either be causal, for example that reduced flow induces ischemia or atrophy (41-44), or it may be that abnormal perfusion actually reflects brain disease (44), for example because cerebral arterioles narrow due to vascular amyloid deposition (45).

Cerebral perfusion on a population level has very little been investigated, as most techniques that measure perfusion are too invasive, time-consuming or expensive to apply in large populations (46). Using a non-invasive, fast and robust phase contrast MRI technique (47), we measured total cerebral blood flow (tCBF), which we reasoned to be an indirect measure of brain perfusion, in persons aged 60 years and older. In contrast to other studies, we furthermore tried to minimize confounding by brain atrophy by calculating total brain perfusion (tCBF per 100 ml brain volume). We found that determinants of tCBF and total brain perfu-

sion differed largely, because of the large influence of brain volume on tCBF values. Persons with low total brain perfusion had significantly more white matter lesions compared to those with high total brain perfusion. Although cross-sectionally, this suggests that tissue hypoperfusion may contribute to white matter lesion pathogenesis, a notion which has also been reported by others (48, 49).

Cerebral hypoperfusion has also been associated with worse cognitive function (50). We found that lower tCBF was associated with worse information-processing speed, executive function, and global cognition. However, for total brain perfusion, in which brain size is taken into account, these associations disappeared. The association between tCBF and cognition may thus be mediated or confounded by brain atrophy. This indicates that future studies measuring cerebral blood flow should take into account brain atrophy.

White matter microstructural integrity

The importance of the cerebral white matter for intact brain functioning is increasingly being recognized. Conventional MRI enables the non-invasive visualization and quantification of macrostructural changes of the white matter, including white matter lesions and atrophy (51, 52). However, these changes have a variable expression with regard to cognition and functional ability, and can often be detected to some degree in cognitively intact people (53).

In the past decade, DTI has evolved as a method to sensitively measure the microstructural integrity of white matter (54). We investigated whether DTI has added value over macrostructural white matter changes in the study of white matter and cognitive function. In the largest population studied with DTI to date (860 persons), we found that microstructural integrity in white matter and in white matter lesions relates to cognitive function, regardless of concurrent macrostructural changes. This indicates that the deleterious effect of white matter changes on cognition not only depends on lesion burden or amount of atrophy, but also on characteristics that are not easily evaluated by conventional MRI. Thus, measuring white matter microstructural integrity may be helpful to distinguish white matter changes that have a large effect on cognitive functioning from those that affect cognition to a lesser extent.

There is abundant evidence from small studies in populations with large age-differences that white matter microstructure loses its integrity with aging (55, 56). However, most of these reports applied region-of-interest measurements in selected brain regions. Using a voxel-wise analysis method specifically designed for DTI data (57), we demonstrated in which brain locations age-related changes in the normal-appearing white matter primarily occur. More importantly, we showed that these changes are primarily explained by white matter atrophy and white matter lesion formation and not by the aging process in itself. This challenges the

notion of ‘aging’ as a pathological process. Furthermore, our results indicate that white matter atrophy and white matter lesion formation are related to loss of integrity in distinct brain regions, indicating that the two processes are not sequential events but are rather independent and thus pathophysiologically potentially different. These results provide new insight into white matter changes in aging.

CLINICAL IMPLICATIONS OF FINDINGS FROM THIS WORK

By the time persons are diagnosed with cognitive impairment due to dementia, they already have irreversible brain pathology (58). Furthermore, only 13% of persons with first stroke will ever have received a warning (59). The focus in brain research is therefore gradually shifting from diagnosis and treatment of disease to possible prevention and early detection of pathologic changes. Population-based studies like ours can identify preclinical markers of disease to act upon to modify risk or prevent progression of disease. Though longitudinal examination is needed to assess whether certain imaging biomarkers indeed indicate an early disease state, the studies described in this thesis have identified MRI findings that can serve as the basis for further research.

Our finding that cerebral microbleeds are highly prevalent in the general population is important in the context of ongoing clinical studies questioning whether presence of microbleeds in stroke patients should affect treatment decisions (37, 38, 60), but also regarding preventive treatment in the general population. Depending on results of future studies on the risk of antithrombotic or thrombolysis-related hemorrhage associated with microbleed presence, screening of patients before administration of therapy may be needed. Furthermore, as our studies have identified microbleeds as potential imaging biomarkers of arteriolosclerotic angiopathy or CAA, this may have future clinical implications in diagnosis of patients.

Regarding microstructural white matter integrity, we showed that each standard deviation increase in mean diffusivity of normal-appearing white matter had the same effect on cognitive performance as being nearly 3 years older, regardless of concurrent white matter atrophy or high white matter lesion load. This indicates that DTI may reveal important changes in white matter that appears normal on conventional MRI, and thus that measurement of microstructural white matter integrity may become an important clinical tool to sensitively assess early white matter damage or to provide surrogate markers to monitor treatment effect.

Quantification of an individual's risk of neurodegenerative or cerebrovascular disease becomes more and more important. Though several imaging biomarkers have previously been shown promising to aid in diagnosing AD, for example hippocampal atrophy (61), these cannot yet be used to reliably discriminate within a group of asymptomatic persons those who will develop disease from those who will not. Also, the imaging biomarkers described in this thesis will not directly translate into risk estimates of disease. The likely value of imaging to predict an individual's risk of disease will be in combining neuroimaging studies with other data on genetic risk and biochemical biomarkers (for example, cerebrospinal fluid and serum). This might increase diagnostic sensitivity and specificity, as well as the predictive value of the information and may ultimately be used to screen individuals at high risk for developing dementia, for example those carrying the APOE ϵ 4 allele (62). Of note is, however, that the true impact of a discriminating test will depend on the effectiveness and availability of preventive treatment for the disease.

SUGGESTIONS FOR FUTURE RESEARCH

The work described in this thesis has put forward several MRI findings as potential relevant biomarkers of age-related brain disease. However, our findings need to be replicated and further evaluated in longitudinal investigations. Also, our work has generated several new questions that merit consideration in future research. In the following paragraphs, I will discuss directions for future research into the imaging biomarkers described in this thesis. Also, I will briefly address important progress in image processing and will highlight the benefits of collaborations with other cohort studies. Finally, I will point out future MRI strategies for research into age-related brain disease.

Cerebral microbleeds

The potential link between cerebral microbleeds, CAA and AD is interesting to further explore. We have shown that strictly lobar microbleeds may indicate presence of CAA, a disease that is highly frequent among persons with AD (63). Both CAA and AD are characterized by amyloid β -protein deposition, either in leptomeningeal vessel walls (CAA) or in brain parenchyma (AD). Familial forms of CAA and AD are both linked to mutations in amyloid precursor protein and presenilin genes (64), providing more support for the link between both diseases. Our findings may be taken further by hypothesizing that presence of lobar microbleeds in elderly may relate not only to CAA but also to (risk of) AD. Though evidence is scarce, there are suggestions that cerebral microbleeds may indeed relate to worse cognitive function (65, 66). Also, microbleeds were shown to be highly prevalent among persons attending a memory clinic (67). Follow-up of participants of the Rotterdam Scan Study over

time for occurrence of new microbleeds, decrease of cognitive function or onset of dementia may further elucidate this presumed association. Genome wide analysis (68) of persons with (lobar) microbleeds versus those without may reveal genes that relate to microbleed presence, and possibly further support the presumed link with CAA and AD.

Furthermore, the possibility that microbleeds indicate an increased risk of future symptomatic brain hemorrhage, especially in relation to antithrombotic or thrombolytic treatment, has large potential clinical relevance and should be further evaluated. Evidence in favor or against microbleed-associated bleeding risk is not yet conclusive (37, 38, 60), but the high prevalence of microbleeds in the general population we assessed in combination with broadening indications for antithrombotic therapy, calls for thorough longitudinal investigation. In doing so, it will be important to use optimized MRI sequences for microbleed detection to avoid misclassification of subjects. Also, analyzing microbleeds according to their spatial distribution is strongly recommended to take into account different underlying vascular pathologies. The few prospective studies to date on presence of microbleeds and risk of thrombolysis-related hemorrhage (38) likely suffered from underrating of microbleeds due to use of low-resolution MRI sequences and non-standard protocols across research centers (69). Furthermore, they did not classify or analyze microbleeds according to their location (69). It may well be that antithrombotic- and thrombolysis-related hemorrhage risk differs according to microbleed location, and is especially pronounced for lobar microbleeds. To solve this issue, trials investigating the beneficial effects of antithrombotic treatment or thrombolysis for cerebrovascular or cardiovascular disease should assess the presence of cerebral microbleeds prior to start of therapy, using optimized T2*-weighted MRI sequences and standardized rating methods. The analysis of drug-related intracerebral hemorrhage in these studies should take spatial distribution of microbleeds into account. International collaboration of trials on this topic will increase the power to reveal whether the risk-benefit ratio of antithrombotic or thrombolytic medication is less favorable for subgroups of patients with (lobar) microbleeds.

Cerebral blood flow

Evidence is accumulating that late-onset dementia is a heterogeneous disorder in which not only deposition of plaques and tangles, but also vascular risk factors and cerebrovascular disease may be involved (1). In this respect, cerebral blood flow may prove an interesting biomarker for further studies. Cardiac factors and vascular changes in aortic or common carotid vessels may lead to reductions of cerebral blood flow upstream in internal carotids and basilar arteries, whilst downstream damage to cerebral small vessels or capillary occlusion (e.g. due to amyloid deposits in CAA (70)) may also cause abnormal cerebral blood flow. It will be difficult to disentangle these effects cross-sectionally, but longitudinal assessment of brain changes and alterations in cerebral blood flow may elucidate this issue.

An important drawback of the phase contrast method we used to measure tCBF, is that it does not provide information on regional blood flow nor on perfusion of gray versus white matter. Methods to apply phase contrast MRI to the circle of Willis can enable a more regional assessment of cerebral blood flow (71), but still do not provide very detailed information. A much larger value for cohort studies is to be expected from arterial spin labeling (ASL), a more advanced MRI technique that can quantify regional cerebral perfusion without administration of intravenous contrast agents or use of radiation (72). Recently, several groups have shown that pulsed or continuous ASL methods can be relatively easily and reliably applied in populations of elderly subjects for regional blood flow measurement (73-75). Though acquisition times of ASL sequences are still rather long (in the order of 5 to 8 minutes due to a high number of repeats for signal averaging) for use in a population-based setting, the fact that ASL can yield quantitative voxel-based measurements of cerebral blood flow is very valuable, for example in combining these data with quantitative voxel measurements of tissue microstructural integrity (with DTI). Therefore, if time allows, application of ASL within our study protocol in the near future would be a valuable addition.

White matter microstructural integrity

In the near future, it will be important to develop methodologies that make use of the entire dimensionality of DTI data. For example, most studies only measure fractional anisotropy (FA) and mean diffusivity (MD), whilst separate components of FA, i.e. axial and radial diffusivity, are thought to provide additional information on underlying white matter pathology. In animal models, axial diffusivity was shown to relate to axonal degeneration, whilst radial diffusivity reflects myelin degradation (76). In humans, relations between directional diffusivities and white matter pathology needs to be explored further, as well as whether additional information can be derived from the full tensor model. Furthermore, studies of non-myelinated axons of squids and garfish have shown that myelination of white matter is not a requirement for the presence of anisotropic diffusion, but rather that axonal membranes play a major role (77, 78). In humans however, much less is known on the different contribution of axons and myelin to values of anisotropy and diffusion. Limited available radiologic-pathologic correlation studies suggest that FA and MD correlate directly with the amount of myelin in the white matter, and to a lesser extent also to axonal count (79), but further evaluation, for example by postmortem examination, is needed to fully understand what type of pathology is reflected by changes in DTI parameters.

Visualization of white matter tracts (DTI tractography) and performing tract-based statistics are promising methods for quantification of structural integrity of white matter tracts across individuals (57, 80, 81). DTI tractography can also help explore structural connectivity between brain regions, increasing our understanding of anatomy and how pathology in

one region may affect structural integrity within the other, connected, region (82, 83). DTI tractography, however, still suffers from several limitations that will need to be addressed before implementation in population studies or even in clinical practice can be reliably done. Coarsely sampled, noisy data or artifacts may interfere with reliable fiber tracking, whilst the crossing or branching of fibers cannot be adequately resolved. Newer DTI acquisition methods, such as Q-ball imaging (49) or high angular resolution diffusion imaging (HARDI) (49) have the potential to yield more robust measures of fiber tractography, but at the price of more complex and time-consuming data acquisition. Besides alterations in acquisition schemes, Behrens et al. (84) described an elegant method of probabilistic mapping that can be used to explore and quantify connectivity, taking into account the uncertainty in fiber direction caused by data limitations.

The limits imposed by time and study design on quality of DTI data within population-based imaging will be especially challenging to circumvent. Efficient sequence designs balancing the spatial resolution, number of acquisitions and gradient sampling scheme can maximize the amount of information acquired within a set time. However, there are (yet) no clear set of criteria defining the minimum requirements for DTI data that need to be met in order to perform reliable global, regional or tract-specific measurements. Some guidelines can be followed (85), but researchers need to explore the limitations of their data to understand which analysis methods can reliably be applied. For large studies, one of the first areas to act upon should be the quality check of raw DTI data, as DTI is inherently susceptible to artifacts of motion and field distortions. The large amount of data acquired in each DTI acquisition will require automated procedures to verify data quality in cohort studies. Also, tract-specific DTI parameters (e.g. fiber density, fiber length, tract volume, tract curvature etc.) need to be evaluated for their robustness and the amount of information on pathologic change they provide. Furthermore, to date, longitudinal studies on DTI in aging have not been published, and it will be of great interest to analyze serial DTI scans for developing white matter pathology within individuals and on a group-level.

Automated image analysis

Besides ever-increasing advances in MRI hardware, software and sequence design, major advances in MRI brain research are to be expected from automated image analysis. Computer processing of MRI images will enable to make fully use of all information contained within the image. For example, volumetric measurements of brain structures will allow for more robust and powerful comparisons between subjects (86). Determination of shape differences within structures (e.g. the hippocampus) based on high parametric deformation algorithms may reveal changes related to disease (87). Deformation field morphometry, in which a brain is transformed to a template and information is obtained from the degree of deformation

needed to perform this, may be applied to individual patients to assess regional changes that relate to disease (88). Cortical thickness measurement can identify regions where grey matter decrease is most prominent in relation to cognitive decline (89).

Apart from the fact that image processing may introduce new imaging biomarkers, the vast amount of imaging data that are acquired in population-based studies like ours renders visual assessment or manual measurements virtually impossible, introducing the need for (fully) automated methods of data extraction and analysis.

Collaboration with other cohort studies

There are currently many population-based studies that examine the aging brain using MRI (4-10). Many of these use comparable study designs and MRI protocols. Replication of data from one study in another is crucial, to establish consistency of findings across studies. In addition, the use of complementary MRI protocols in separate studies would be an efficient way to explore additional research questions that are generated by other studies. Furthermore, in order to make the most use of all acquired data and to increase the power to detect subtle changes, it would be highly effective for different studies to compile their data and perform joint analyses. International collaboration is thus crucial to advance the field of population-based brain MRI research.

Future magnetic resonance imaging strategies

Of all available imaging modalities to study age-related brain disease, MRI has the advantages that it is non-invasive, relatively widely available and that it offers superior structural information. Major progress in structural MR imaging is to be expected in the short run from scanning at increasing field strength (3.0-7.0 T or even beyond), which will yield large increases in spatial resolution, signal-to-noise ratio or scanning speed. Yet, whether high field MRI will be readily available for population-based imaging will depend on financial and practical issues.

MRI techniques that go beyond traditional macrostructural volumetric methods will likely further progress to provide information about white matter tissue integrity and organization at the microstructural level. DTI has already been discussed extensively. Magnetization transfer imaging (MTI) (90), T2 relaxography (91) and magnetic resonance spectroscopy (MRS) (92) are also able to show subtle neuropathological changes in vivo before they are manifested on conventional MRI. To what extent these methods measure different pathology and thus may be complementary still needs further evaluation. Most of these techniques are relatively time consuming, prohibiting their parallel use in cohort studies. However, there may be an important role for collaborative studies to examine this, for example by applying a complementary study design, or alternatively, one could directly compare some of these techniques within a well defined subset of participants from respective populations.

Besides structural imaging, assessment of brain function with MRI is very promising, using functional MRI (fMRI). fMRI non-invasively measures the haemodynamic response related to neural activity in the brain. This technique is hypothesized to demonstrate functional changes that precede actual structural damage. The neural activity visualized by fMRI can be task-related (e.g. finger-tapping or a memory-related task) or can be measured in a resting-state, showing functional connectivity of intrinsic brain activity in the “default-mode” network (93). Resting-state fMRI is especially interesting for application in an elderly population, as it does not require active participation or extensive instructions to the participant, whilst it reflects activity in brain regions that are involved in cognitive function (93).

The emphasis in the studies described in this thesis was on the use of MRI to study potential new biomarkers of brain disease in a population-based setting. Of course, there are many other imaging modalities, some of which are also readily applicable in population-based studies, that were not discussed, but that are of use to investigate age-related brain changes. It should further be noted that the role of imaging in searching preclinical markers for disease should always be put in the context of other imaging and non-imaging approaches. It is likely that a combination of biomarkers derived from imaging methods and other technologies (94) (e.g. genetics (33), proteomics (95), or cerebrospinal fluid analysis (96)) will ultimately be most fruitful in defining and predicting disease.

REFERENCES

1. Breteler MM. Vascular risk factors for Alzheimer's disease: an epidemiologic perspective. *Neurobiol Aging* 2000; 21:153-160.
2. Leys D, Henon H, Mackowiak-Cordoliani MA, Pasquier F. Poststroke dementia. *Lancet Neurol* 2005; 4:752-759.
3. Hofman A, Breteler MM, van Duijn CM, et al. The Rotterdam Study: objectives and design update. *Eur J Epidemiol* 2007; 22:819-829.
4. Bryan RN, Cai J, Burke G, et al. Prevalence and anatomic characteristics of infarct-like lesions on MR images of middle-aged adults: the atherosclerosis risk in communities study. *AJNR* 1999; 20:1273-1280.
5. Schmidt R, Lechner H, Fazekas F, et al. Assessment of cerebrovascular risk profiles in healthy persons: definition of research goals and the Austrian Stroke Prevention Study (ASPS). *Neuroepidemiology* 1994; 13:308-313.
6. Resnick SM, Goldszal AF, Davatzikos C, et al. One-year age changes in MRI brain volumes in older adults. *Cereb Cortex* 2000; 10:464-472.
7. Sveinbjornsdottir S, Sigurdsson S, Aspelund T, et al. Cerebral microbleeds in the population based AGES Reykjavik study: Prevalence and location. *J Neurol Neurosurg Psychiatry* 2008; 79:1002-1006.
8. DeCarli C, Massaro J, Harvey D, et al. Measures of brain morphology and infarction in the framingham heart study: establishing what is

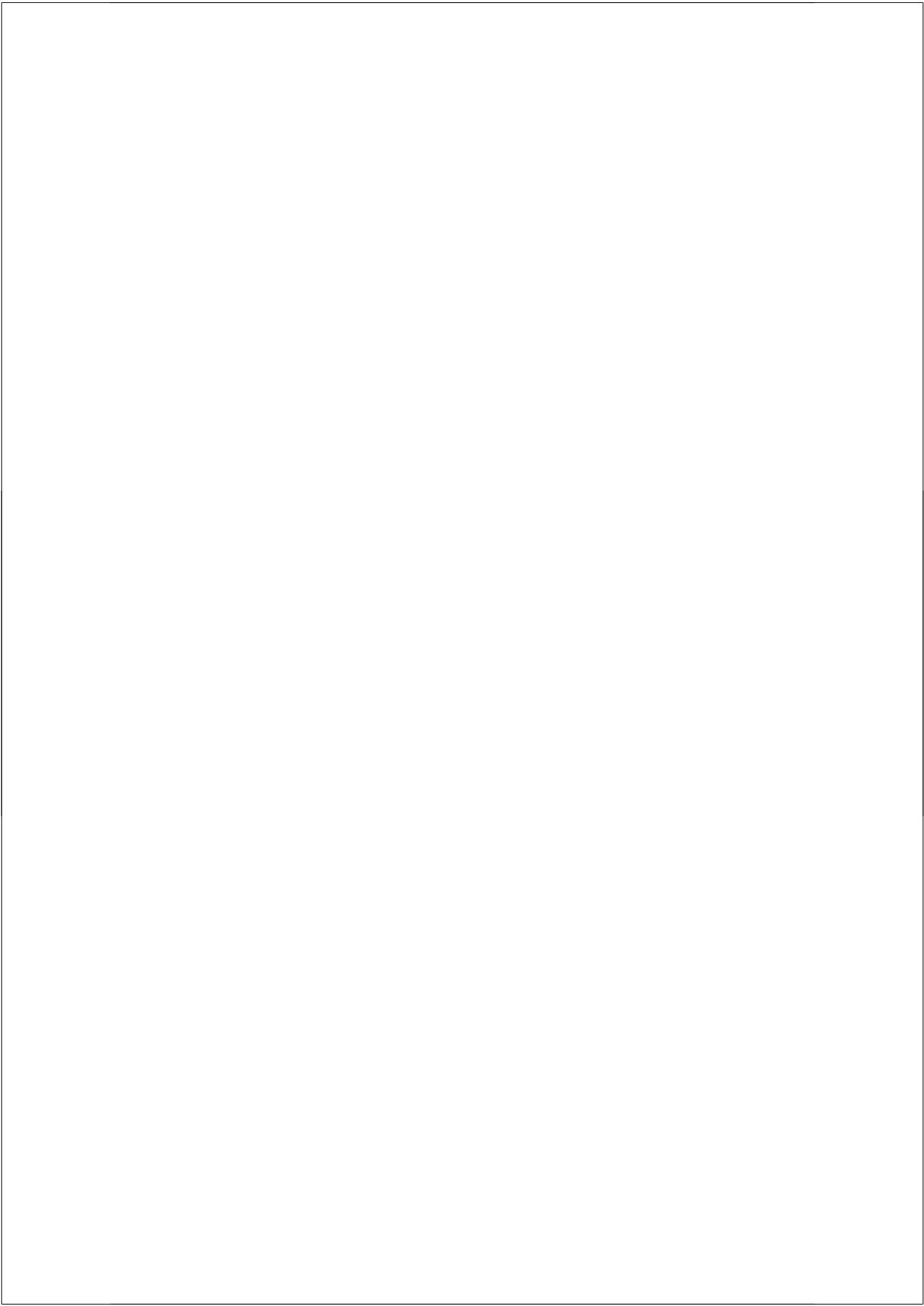
- normal. *Neurobiol Aging* 2005; 26:491-510.
9. Longstreth WT, Jr., Manolio TA, Arnold A, et al. Clinical correlates of white matter findings on cranial magnetic resonance imaging of 3301 elderly people. The Cardiovascular Health Study. *Stroke* 1996; 27:1274-1282.
 10. Dufouil C, de Kersaint-Gilly A, Besancon V, et al. Longitudinal study of blood pressure and white matter hyperintensities: the EVA MRI Cohort. *Neurology* 2001; 56:921-926.
 11. Katzman GL, Dagher AP, Patronas NJ. Incidental findings on brain magnetic resonance imaging from 1000 asymptomatic volunteers. *Jama* 1999; 282:36-39.
 12. Tsushima Y, Taketomi-Takahashi A, Endo K. Prevalence of abnormal findings on brain magnetic resonance (MR) examinations in adult participants of brain docking. *BMC Neurol* 2005; 5:18.
 13. Weber F, Knopf H. Incidental findings in magnetic resonance imaging of the brains of healthy young men. *J Neurol Sci* 2006; 240:81-84.
 14. Yue NC, Longstreth WT, Jr., Elster AD, Jungreis CA, O'Leary DH, Poirier VC. Clinically serious abnormalities found incidentally at MR imaging of the brain: data from the Cardiovascular Health Study. *Radiology* 1997; 202:41-46.
 15. Vernooij MW, Ikram MA, Tanghe HL, et al. Incidental findings on brain MRI in the general population. *N Engl J Med* 2007; 357:1821-1828.
 16. Illes J, Desmond JE, Huang LF, Raffin TA, Atlas SW. Ethical and practical considerations in managing incidental findings in functional magnetic resonance imaging. *Brain Cogn* 2002; 50:358-365.
 17. Rocque BG, Baskaya MK, Kuo JS. Incidental findings on brain MRI. *N Engl J Med* 2008; 358:853; author reply 854-855.
 18. Illes J. Brain screening and incidental findings: flocking to folly? *Lancet Neurol* 2008; 7:23-24.
 19. Vernooij MW, van der Lugt A, Breteler MMB. Incidental findings on brain MRI. *N Engl J Med* 2008; 358:author reply 854-855.
 20. Wiebers DO, Whisnant JP, Huston J, 3rd, et al. Unruptured intracranial aneurysms: natural history, clinical outcome, and risks of surgical and endovascular treatment. *Lancet* 2003; 362:103-110.
 21. Takao H, Nojo T. Treatment of unruptured intracranial aneurysms: decision and cost-effectiveness analysis. *Radiology* 2007; 244:755-766.
 22. Pickard JD, Gillard JH. Guidelines reduce the risk of brain-scan shock. *Nature* 2005; 435:17.
 23. How volunteering for an MRI scan changed my life. *Nature* 2005; 434:17.
 24. Olson S. Neuroimaging. An image of disease. *Science* 2005; 307:1550.
 25. Check E. Brain-scan ethics come under the spotlight. *Nature* 2005; 433:185.
 26. Nighoghossian N, Hermier M, Adeleine P, et al. Old microbleeds are a potential risk factor for cerebral bleeding after ischemic stroke: a gradient-echo T2*-weighted brain MRI study. *Stroke* 2002; 33:735-742.
 27. Kato H, Izumiyama M, Izumiyama K, Takahashi A, Itoyama Y. Silent cerebral microbleeds on T2*-weighted MRI: correlation with stroke subtype, stroke recurrence, and leukoaraiosis. *Stroke* 2002; 33:1536-1540.
 28. Fan YH, Zhang L, Lam WW, Mok VC, Wong KS. Cerebral microbleeds as a risk factor for subsequent intracerebral hemorrhages among patients with acute ischemic stroke. *Stroke* 2003; 34:2459-2462.
 29. Greenberg SM, Eng JA, Ning M, Smith EE,

- Rosand J. Hemorrhage burden predicts recurrent intracerebral hemorrhage after lobar hemorrhage. *Stroke* 2004; 35:1415-1420.
30. Jeerakathil T, Wolf PA, Beiser A, et al. Cerebral microbleeds: prevalence and associations with cardiovascular risk factors in the Framingham Study. *Stroke* 2004; 35:1831-1835.
31. Roob G, Schmidt R, Kapeller P, Lechner A, Hartung HP, Fazekas F. MRI evidence of past cerebral microbleeds in a healthy elderly population. *Neurology* 1999; 52:991-994.
32. Tsushima Y, Tanizaki Y, Aoki J, Endo K. MR detection of microhemorrhages in neurologically healthy adults. *Neuroradiology* 2002; 44:31-36.
33. Henderson AS, Eastel S, Jorm AF, et al. Apolipoprotein E allele epsilon 4, dementia, and cognitive decline in a population sample. *Lancet* 1995; 346:1387-1390.
34. McCarron MO, Nicoll JA. Apolipoprotein E genotype and cerebral amyloid angiopathy-related hemorrhage. *Ann N Y Acad Sci* 2000; 903:176-179.
35. Greenberg SM, van Buchem MA, Vernooij MW, et al. Cerebral Microbleeds: A Field Guide. *Lancet Neurology*; in press.
36. Derex L, Nighoghossian N. Intracerebral Haemorrhage after Thrombolysis for Acute Ischemic Stroke. An update. *J Neurol Neurosurg Psychiatry* 2008.
37. Kidwell CS, Saver JL, Villablanca JP, et al. Magnetic resonance imaging detection of microbleeds before thrombolysis: an emerging application. *Stroke* 2002; 33:95-98.
38. Fiehler J, Albers GW, Boulanger JM, et al. Bleeding risk analysis in stroke imaging before thrombolysis (BRASIL): pooled analysis of T2*-weighted magnetic resonance imaging data from 570 patients. *Stroke* 2007; 38:2738-2744.
39. Paulson OB, Strandgaard S, Edvinsson L. Cerebral autoregulation. *Cerebrovasc Brain Metab Rev* 1990; 2:161-192.
40. Paulson OB, Waldemar G, Schmidt JF, Strandgaard S. Cerebral circulation under normal and pathologic conditions. *Am J Cardiol* 1989; 63:2C-5C.
41. Kobayashi S, Okada K, Yamashita K. Incidence of silent lacunar lesion in normal adults and its relation to cerebral blood flow and risk factors. *Stroke* 1991; 22:1379-1383.
42. Meguro K, Hatazawa J, Itoh M, Miyazawa H, Matsuzawa T, Yamadori A. Cerebral blood flow correlated with carotid blood flow in neurologically normal elderly with severe white matter lesions. *Eur J Neurol* 1998; 5:143-149.
43. Suter OC, Sunthorn T, Kraftsik R, et al. Cerebral hypoperfusion generates cortical watershed microinfarcts in Alzheimer disease. *Stroke* 2002; 33:1986-1992.
44. Rogers RL, Meyer JS, Mortel KF, Mahurin RK, Judd BW. Decreased cerebral blood flow precedes multi-infarct dementia, but follows senile dementia of Alzheimer type. *Neurology* 1986; 36:1-6.
45. Kalback W, Esh C, Castano EM, et al. Atherosclerosis, vascular amyloidosis and brain hypoperfusion in the pathogenesis of sporadic Alzheimer's disease. *Neurol Res* 2004; 26:525-539.
46. Kirkness CJ. Cerebral blood flow monitoring in clinical practice. *AACN Clin Issues* 2005; 16:476-487.
47. Spilt A, Box FM, van der Geest RJ, et al. Reproducibility of total cerebral blood flow measurements using phase contrast magnetic resonance imaging. *J Magn Reson Imaging* 2002; 16:1-5.

48. ten Dam VH, van den Heuvel DM, de Craen AJ, et al. Decline in total cerebral blood flow is linked with increase in periventricular but not deep white matter hyperintensities. *Radiology* 2007; 243:198-203.
49. Bisschops RH, van der Graaf Y, Mali WP, van der Grond J. High total cerebral blood flow is associated with a decrease of white matter lesions. *J Neurol* 2004; 251:1481-1485.
50. Meyer JS, Rogers RL, Judd BW, Mortel KF, Sims P. Cognition and cerebral blood flow fluctuate together in multi-infarct dementia. *Stroke* 1988; 19:163-169.
51. de Groot JC, de Leeuw FE, Oudkerk M, et al. Cerebral white matter lesions and cognitive function: the Rotterdam Scan Study. *Ann Neurol* 2000; 47:145-151.
52. Ikram MA, Vrooman HA, Vernooij MW, et al. Brain tissue volumes in relation to cognitive function and risk of dementia. *Neurobiol Aging*; in press.
53. Gootjes L, Teipel SJ, Zebuhr Y, et al. Regional distribution of white matter hyperintensities in vascular dementia, Alzheimer's disease and healthy aging. *Dement Geriatr Cogn Disord* 2004; 18:180-188.
54. Le Bihan D, Mangin JF, Poupon C, et al. Diffusion tensor imaging: concepts and applications. *J Magn Reson Imaging* 2001; 13:534-546.
55. Engelter ST, Provenzale JM, Petrella JR, DeLong DM, MacFall JR. The effect of aging on the apparent diffusion coefficient of normal-appearing white matter. *AJR Am J Roentgenol* 2000; 175:425-430.
56. Bhagat YA, Beaulieu C. Diffusion anisotropy in subcortical white matter and cortical gray matter: changes with aging and the role of CSF-suppression. *J Magn Reson Imaging* 2004; 20:216-227.
57. Smith SM, Jenkinson M, Johansen-Berg H, et al. Tract-based spatial statistics: voxelwise analysis of multi-subject diffusion data. *Neuroimage* 2006; 31:1487-1505.
58. Ikonomic MD, Mufson EJ, Wu J, Cochran EJ, Bennett DA, DeKosky ST. Cholinergic plasticity in hippocampus of individuals with mild cognitive impairment: correlation with Alzheimer's neuropathology. *J Alzheimers Dis* 2003; 5:39-48.
59. Hachinski V. Vascular cognitive impairment and Alzheimer's disease: Time for a concerted approach. *International Psychogeriatrics* 2007; 19, suppl 1:3-16.
60. Derex L, Nighoghossian N, Hermier M, et al. Thrombolysis for ischemic stroke in patients with old microbleeds on pretreatment MRI. *Cerebrovasc Dis* 2004; 17:238-241.
61. Almkvist O, Winblad B. Early diagnosis of Alzheimer dementia based on clinical and biological factors. *Eur Arch Psychiatry Clin Neurosci* 1999; 249 Suppl 3:3-9.
62. Small GW. Use of neuroimaging to detect early brain changes in people at genetic risk for Alzheimer's disease. *Adv Drug Deliv Rev* 2002; 54:1561-1566.
63. Thal DR, Griffin WS, de Vos RA, Ghebremedhin E. Cerebral amyloid angiopathy and its relationship to Alzheimer's disease. *Acta Neuropathol* 2008; 115:599-609.
64. Revesz T, Ghiso J, Lashley T, et al. Cerebral amyloid angiopathies: a pathologic, biochemical, and genetic view. *J Neuropathol Exp Neurol* 2003; 62:885-898.
65. Yakushiji Y, Nishiyama M, Yakushiji S, et al. Brain Microbleeds and Global Cognitive Function in Adults Without Neurological Disorder. *Stroke* 2008.
66. Werring DJ, Frazer DW, Coward LJ, et al. Cognitive

- dysfunction in patients with cerebral microbleeds on T2*-weighted gradient-echo MRI. *Brain* 2004; 127:2265-2275.
67. Cordonnier C, van der Flier WM, Sluimer JD, Leys D, Barkhof F, Scheltens P. Prevalence and severity of microbleeds in a memory clinic setting. *Neurology* 2006; 66:1356-1360.
 68. Brown PO, Botstein D. Exploring the new world of the genome with DNA microarrays. *Nat Genet* 1999; 21:33-37.
 69. Vernooij MW, van der Lugt A, Breteler MM. Risk of thrombolysis-related hemorrhage associated with microbleed presence. *Stroke* 2008; 39:e115; author reply e116.
 70. Roher AE, Lowenson JD, Clarke S, et al. beta-Amyloid-(1-42) is a major component of cerebrovascular amyloid deposits: implications for the pathology of Alzheimer disease. *Proc Natl Acad Sci U S A* 1993; 90:10836-10840.
 71. Zhao M, Amin-Hanjani S, Ruland S, Curcio AP, Ostergren L, Charbel FT. Regional cerebral blood flow using quantitative MR angiography. *AJNR Am J Neuroradiol* 2007; 28:1470-1473.
 72. Petersen ET, Lim T, Golay X. Model-free arterial spin labeling quantification approach for perfusion MRI. *Magn Reson Med* 2006; 55:219-232.
 73. Dai W, Lopez OL, Carmichael OT, Becker JT, Kuller LH, Gach HM. Abnormal regional cerebral blood flow in cognitively normal elderly subjects with hypertension. *Stroke* 2008; 39:349-354.
 74. van Laar PJ, van der Graaf Y, Mali WP, van der Grond J, Hendrikse J. Effect of cerebrovascular risk factors on regional cerebral blood flow. *Radiology* 2008; 246:198-204.
 75. Bastos-Leite AJ, Kuijter JP, Rombouts SA, et al. Cerebral blood flow by using pulsed arterial spin-labeling in elderly subjects with white matter hyperintensities. *AJNR Am J Neuroradiol* 2008; 29:1296-1301.
 76. Song SK, Sun SW, Ju WK, Lin SJ, Cross AH, Neufeld AH. Diffusion tensor imaging detects and differentiates axon and myelin degeneration in mouse optic nerve after retinal ischemia. *Neuroimage* 2003; 20:1714-1722.
 77. Beaulieu C, Allen PS. Water diffusion in the giant axon of the squid: implications for diffusion-weighted MRI of the nervous system. *Magn Reson Med* 1994; 32:579-583.
 78. Beaulieu C. The basis of anisotropic water diffusion in the nervous system - a technical review. *NMR Biomed* 2002; 15:435-455.
 79. Schmierer K, Wheeler-Kingshott CA, Boulby PA, et al. Diffusion tensor imaging of post mortem multiple sclerosis brain. *Neuroimage* 2007; 35:467-477.
 80. Mori S, van Zijl PC. Fiber tracking: principles and strategies - a technical review. *NMR Biomed* 2002; 15:468-480.
 81. Sullivan EV, Rohlfing T, Pfefferbaum A. Quantitative fiber tracking of lateral and interhemispheric white matter systems in normal aging: Relations to timed performance. *Neurobiol Aging* 2008; in press; doi:10.1016/j.neurobiolaging.2008.1004.1007.
 82. Sonty SP, Mesulam MM, Weintraub S, Johnson NA, Parrish TB, Gitelman DR. Altered effective connectivity within the language network in primary progressive aphasia. *J Neurosci* 2007; 27:1334-1345.
 83. Mesulam M. Imaging connectivity in the human cerebral cortex: the next frontier? *Ann Neurol* 2005; 57:5-7.
 84. Behrens TE, Johansen-Berg H, Woolrich MW, et al. Non-invasive mapping of connections between human thalamus and cortex using diffusion imaging. *Nat Neurosci* 2003; 6:750-757.

85. Jones DK, Horsfield MA, Simmons A. Optimal strategies for measuring diffusion in anisotropic systems by magnetic resonance imaging. *Magn Reson Med* 1999; 42:515-525.
86. Ikram MA, Vrooman HA, Vernooij MW, et al. Brain tissue volumes in the general elderly population. The Rotterdam Scan Study. *Neurobiol Aging* 2008; 29:882-890.
87. Scher AI, Xu Y, Korf ES, et al. Hippocampal shape analysis in Alzheimer's disease: a population-based study. *Neuroimage* 2007; 36:8-18.
88. Pieperhoff P, Homke L, Schneider F, et al. Deformation field morphometry reveals age-related structural differences between the brains of adults up to 51 years. *J Neurosci* 2008; 28:828-842.
89. Lerch JP, Pruessner J, Zijdenbos AP, et al. Automated cortical thickness measurements from MRI can accurately separate Alzheimer's patients from normal elderly controls. *Neurobiol Aging* 2008; 29:23-30.
90. Wolff SD, Balaban RS. Magnetization transfer imaging: practical aspects and clinical applications. *Radiology* 1994; 192:593-599.
91. Townsend TN, Bernasconi N, Pike GB, Bernasconi A. Quantitative analysis of temporal lobe white matter T2 relaxation time in temporal lobe epilepsy. *Neuroimage* 2004; 23:318-324.
92. Valenzuela MJ, Sachdev PS, Wen W, Shnier R, Brodaty H, Gillies D. Dual voxel proton magnetic resonance spectroscopy in the healthy elderly: subcortical-frontal axonal N-acetylaspartate levels are correlated with fluid cognitive abilities independent of structural brain changes. *Neuroimage* 2000; 12:747-756.
93. Damoiseaux JS, Beckmann CF, Arigita EJ, et al. Reduced resting-state brain activity in the "default network" in normal aging. *Cereb Cortex* 2008; 18:1856-1864.
94. Hampel H, Burger K, Teipel SJ, Bokde AL, Zetterberg H, Blennow K. Core candidate neurochemical and imaging biomarkers of Alzheimer's disease. *Alzheimers Dement* 2008; 4:38-48.
95. Butterfield DA, Boyd-Kimball D. Proteomics analysis in Alzheimer's disease: new insights into mechanisms of neurodegeneration. *Int Rev Neurobiol* 2004; 61:159-188.
96. de Leon MJ, Mosconi L, Blennow K, et al. Imaging and CSF studies in the preclinical diagnosis of Alzheimer's disease. *Ann N Y Acad Sci* 2007; 1097:114-145.



7

SUMMARY

Neurodegenerative and cerebrovascular disease are common disorders in the elderly that exert a large influence on brain functioning. Therapeutic options after onset of disease are scarce whilst causative factors are still largely unknown. Identifying underlying pathology in a preclinical state may help to recognize persons at risk, assess determinants of disease and develop preventive measures. Therefore, the objective of the studies described in this thesis was to investigate with MRI brain changes that may function as preclinical imaging markers for neurodegenerative and cerebrovascular disease. For this goal, advanced MRI techniques were applied in the Rotterdam Scan Study, a large population-based brain imaging study among middle-aged and elderly persons. We studied the prevalence and distribution of age-related brain changes on MRI, investigated associated risk factors and related these brain changes to cognitive functioning.

METHODOLOGY

First, we designed a 30-minute brain imaging protocol that balances the restrictions of time, costs and inconvenience for the participants with the relevance and quality of the acquired imaging data (**chapter 2.1**). Performing brain MRI in volunteers may lead to the discovery of unexpected, asymptomatic brain abnormalities that are unrelated to the purpose of the research study but may have clinical relevance. We studied the frequency of such incidentally discovered brain abnormalities in 2,000 middle-aged and elderly study participants (**chapter 2.2**). We found that the prevalence of incidental brain findings was much higher than was reported previously. The most frequent findings were asymptomatic brain infarcts (7.2%), followed by aneurysms (1.8 %) and benign primary tumors (1.6%). An exceptionally rare finding that we discovered was an intravestibular lipoma (**chapter 2.3**), an abnormality for which adequate clinical management depends on a correct imaging diagnosis.

CEREBRAL MICROBLEEDS

One of the relatively new sequences we applied in the Rotterdam Scan Study MRI protocol was an optimized high-resolution T2*-weighted MRI sequence for detection of cerebral microbleeds. In a study of 200 elderly participants, we showed that this optimized sequence detected microbleeds in 36% of persons compared with only 21% on a conventional MRI sequence (**chapter 3.1**). Next, using this high-resolution T2*-weighted sequence, we studied the prevalence of microbleeds in a population of 1,062 elderly. We found that cerebral microbleeds were present in 1 in 5 persons over age of 60 and in over 1 in 3 in persons aged 80 years and older (**chapter 3.2**). This prevalence is much higher than reported previously,

which in part may be explained by the use of a more sensitive MRI sequence. Furthermore, we showed that risk factors for microbleeds varied according to the location of microbleeds in the brain. Cardiovascular risk factors and markers of ischemic small vessel disease were related to deep or infratentorial microbleeds, whilst Apolipoprotein E genotype related to strictly lobar microbleeds. This is indirect evidence that deep or infratentorial microbleeds result from arteriolosclerotic angiopathy, whereas strictly lobar microbleeds are caused by cerebral amyloid angiopathy.

The high prevalence of cerebral microbleeds and their potential link with bleeding-prone microangiopathy raised our interest in how these relate to antithrombotic drug use. We investigated the relation between use of antithrombotic drugs and cerebral microbleeds in the Rotterdam Scan Study and found that persons who had used or were using antithrombotic medication significantly more often had cerebral microbleeds (**chapter 3.3**). Furthermore, the antiplatelet drugs aspirin and carbasalate calcium seemed to differentially relate to presence of strictly lobar microbleeds: persons using aspirin had significantly more often lobar microbleeds compared with those using carbasalate calcium. It would be especially interesting to know whether persons with microbleeds are more prone to develop symptomatic intracerebral hemorrhage when using antithrombotic drugs. Though longitudinal data are needed to investigate this, we discovered within the Rotterdam Scan Study the case of a stroke-free person, using antiplatelet drugs, who developed a symptomatic intracerebral hemorrhage precisely at the site of a small cerebral microbleed (**chapter 3.4**). This is the first case that illustrates a direct chronological and spatial relationship between microbleeds and symptomatic hemorrhage in a neurologically asymptomatic person.

We also described the occurrence of superficial siderosis, deposition of blood-breakdown products on the brain surface, in our study population and we investigated its relation with microbleed presence (**chapter 3.5**). Among 1,062 persons, superficial siderosis was seen in seven participants. All of these seven persons also had lobar microbleeds, which supports the presumed link between superficial siderosis and cerebral amyloid angiopathy.

Finally, we pathologically verified that a small focus of signal loss on T2*-weighted MRI indeed correlated with a deposit of hemosiderin in microscopic analysis (**chapter 3.6**).

CEREBRAL BLOOD FLOW

We measured total cerebral blood flow (tCBF) and total brain perfusion (tCBF per 100 ml brain tissue) using a fast and non-invasive phase-contrast MRI technique (**chapter 4**). Study-

ing determinants of tCBF and total brain perfusion in 892 persons aged 60 years and older, we found that determinants of tCBF and total brain perfusion differed largely, due to the large influence of brain volume on tCBF values (**chapter 4.1**). Higher pulse pressure, higher BMI, and current smoking were all associated with higher total brain perfusion. Furthermore, persons with low total brain perfusion had significantly more white matter lesions compared to those with high total brain perfusion. This suggests that tissue hypoperfusion may contribute to white matter lesion pathogenesis.

Cerebral hypoperfusion has also been associated with worse cognitive function. In our study population, we found that lower tCBF was indeed associated with worse information-processing speed, executive function, and global cognition (**chapter 4.2**). However, these associations disappeared for total brain perfusion, which takes into account brain volume. The association between tCBF and cognition may thus be mediated or confounded by brain atrophy.

WHITE MATTER MICROSTRUCTURAL INTEGRITY

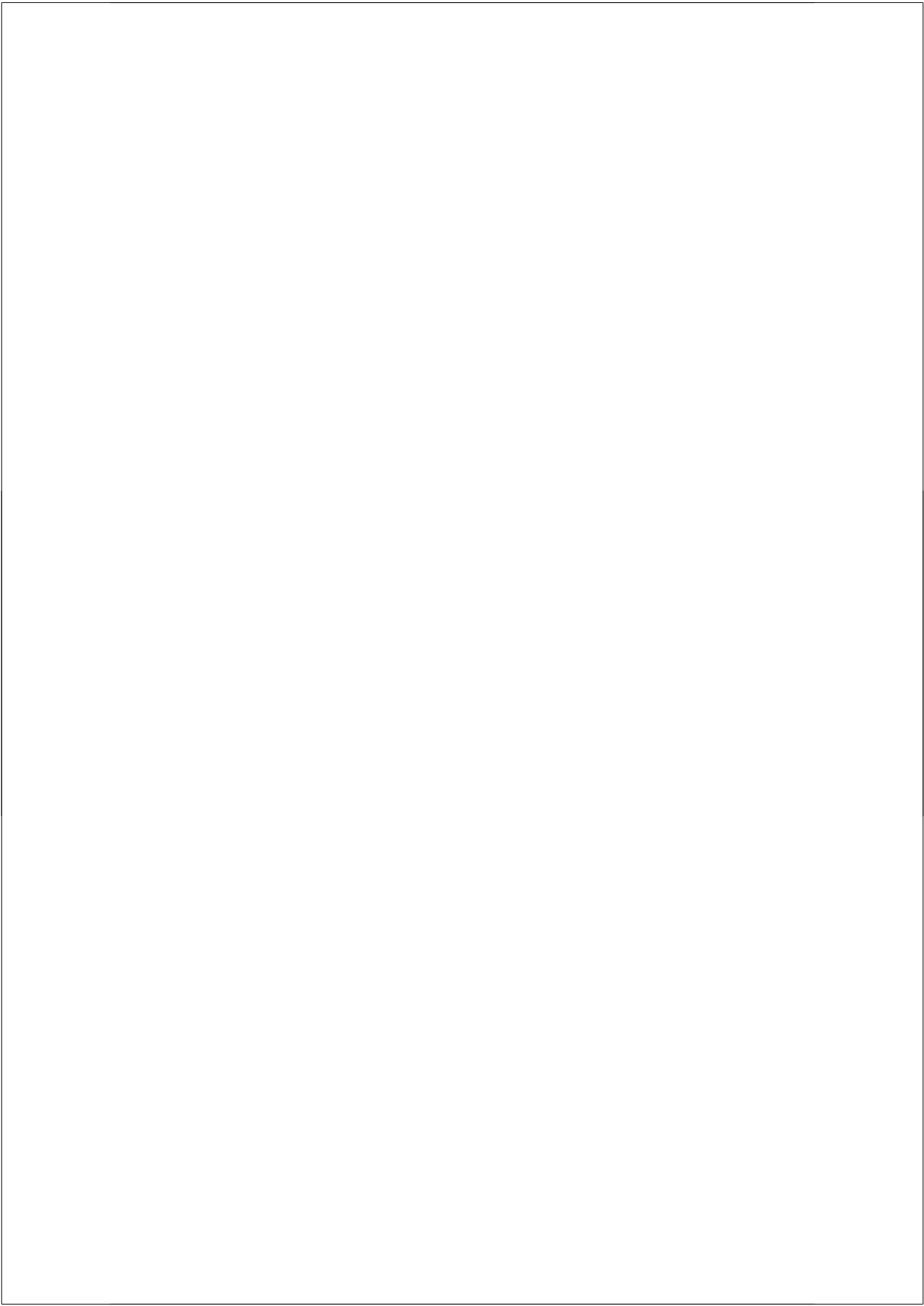
We used diffusion tensor imaging (DTI) to sensitively measure the microstructural integrity of white matter (**chapter 5**). DTI parameters within white matter lesions or normal-appearing white matter were associated with cognitive function, even when taking into account volume of white matter lesions and white matter atrophy (**chapter 5.1**). This indicates that the deleterious effect of white matter changes on cognition not only depends on lesion burden or amount of atrophy, but also on characteristics that are not easily evaluated by conventional MRI.

Next, we studied in which brain locations age-related changes in the normal-appearing white matter occur (**chapter 5.2**). We demonstrated that these changes are primarily explained by white matter atrophy and white matter lesion formation and not by the aging process in itself. Furthermore, we found that white matter atrophy and white matter lesion formation related to loss of integrity in distinct brain regions, indicating that the two processes are not sequential events but are rather independent and thus pathophysiologically potentially different.

FUTURE RESEARCH

The studies described in this thesis have identified several age-related brain changes that have potential to serve as imaging markers for neurodegenerative or cerebrovascular disease. Our findings are, of course, not the end; they're merely the beginning. Future research (**chapter**

6) on cerebral microbleeds should primarily focus on their prognosis in relation to neurodegenerative and cerebrovascular disease, taking into account that their spatial distribution likely reflects differences in underlying etiology. Measuring cerebral blood flow is promising to provide important information on the etiology of brain pathology, and advances should be made in assessment of regional perfusion on a population-level, for example by using arterial spin labeling MRI. Regarding DTI, we are only starting to grasp its full use and meaning and exciting new applications such as DTI tractography are waiting to be further explored. Automated image processing techniques will likely introduce yet new imaging markers, whilst at the same time they will facilitate analysis of large volumes of data. Major advances in studying pathology and predicting disease risk are furthermore to be expected from combining MRI data with information from other imaging modalities (PET, SPECT) and non-imaging biomarkers (e.g. genetics, proteomics).



SAMENVATTING

Dementie (een neurodegeneratieve ziekte) en beroerte (een cerebrovasculaire ziekte) zijn aandoeningen die frequent voorkomen in ouderen en een grote invloed op de hersenfuncties hebben. Er is nog relatief weinig bekend over de oorzaken, en de behandelmogelijkheden zijn op dit moment nog beperkt. Het vaststellen van onderliggende hersenafwijkingen in een fase wanneer er nog geen klachten zijn, kan helpen om risicofactoren voor deze ziektes op te sporen en om preventieve maatregelen te ontwikkelen. Dit heeft als doel om personen die risico lopen op het ontstaan van deze ziektes vroegtijdig op te sporen en te behandelen.

Het doel van het onderzoek beschreven in dit proefschrift was om met behulp van magnetic resonance imaging, beter bekend als MRI, die hersenveranderingen te onderzoeken die mogelijk als vroege markers voor neurodegeneratieve en cerebrovasculaire ziekte kunnen dienen. Hiervoor hebben we geavanceerde MRI technieken gebruikt binnen de Rotterdam Scan Studie, een grote bevolkingsstudie uitgevoerd onder personen van middelbare en oudere leeftijd. We bestudeerden hoe vaak aan veroudering gerelateerde hersenveranderingen op MRI voorkomen, onderzochten risicofactoren die hiermee samenhangen en relateerden de hersenveranderingen aan het cognitief functioneren van de deelnemers.

METHODOLOGIE

Allereerst ontwikkelden we een 30-minuten durend MRI protocol om de hersenen af te beelden; in dit protocol werd een balans gezocht tussen de maximale tijdsduur die het onderzoek in mocht nemen, de kosten van het onderzoek en de mate van belasting voor de studiedeelnemers (**hoofdstuk 2.1**). Als MRI onderzoek van de hersenen in vrijwilligers wordt uitgevoerd, kan dit leiden tot de ontdekking van tot dan toe niet bij de deelnemer bekende hersenafwijkingen, die geen verband hebben met het onderzoeksdoel, maar mogelijk wel klinische betekenis hebben. Wij bestudeerden de prevalentie (frequentie van voorkomen) van dergelijke 'toevalsbevindingen' op MRI van de hersenen in 2000 personen van middelbare en oudere leeftijd (**hoofdstuk 2.2**). We constateerden dat de frequentie waarmee dergelijke bevindingen voorkwamen veel hoger was dan totnogtoe bekend. De meest frequente bevindingen waren asymptomatische herseninfarcten (in 7.2% van de personen), aneurysmata (uitstulpingen in de wand van bloedvaten) (1.8%) en goedaardige hersentumoren (1.6%). Een erg zeldzame toevalsbevinding die we ontdekten betrof een intravestibulair lipoom (een goedaardig gezwel van vetcellen in het binnenoor) (**hoofdstuk 2.3**), een afwijking waarvoor adequaat klinisch beleid afhangt van een juiste radiologische diagnose.

CEREBRALE MICROBLOEDINGEN

De kwaliteit van MRI-afbeeldingen is niet alleen afhankelijk van de technische specificaties van de scanner, maar ook van de instellingen waarmee beelden gemaakt worden, ofwel de sequentie. Een van de relatief nieuwe MRI sequenties die we toepasten in de Rotterdam Scan Studie was een zogenaamde driedimensionale hoge-resolutie T2*-gewogen sequentie voor het opsporen van cerebrale microbloedingen. In een onderzoek onder 200 oudere deelnemers werden met behulp van deze MRI techniek microbloedingen gedetecteerd in 36% van de deelnemers, vergeleken met slechts 21% bij het gebruik van een standaard MRI sequentie (**hoofdstuk 3.1**).

Vervolgens bestudeerden wij met behulp van deze hoge-resolutie T2*-gewogen sequentie de prevalentie van microbloedingen in een populatie van 1062 ouderen. Wij vonden cerebrale microbloedingen bij 1 op de 5 personen ouder dan 60 jaar. Bij personen ouder dan 80 jaar lag de prevalentie zelfs boven de 1 op de 3 (**hoofdstuk 3.2**). Hiermee toonden we aan dat de frequentie van cerebrale microbloedingen veel hoger ligt dan eerder is gerapporteerd, wat waarschijnlijk ten dele verklaard kan worden door het feit dat wij een gevoeliger MRI sequentie gebruikten. Verder lieten wij zien dat de risicofactoren voor microbloedingen verschilden naar gelang de locatie waar de bloedingen zich in de hersenen bevonden. Risicofactoren voor hart-en vaatziekten en tekenen van zuurstofgebrek in de hersenen (infarcten en witte stofafwijkingen) waren gerelateerd aan microbloedingen diep in het brein of infratentorieel (in de kleine hersenen). Dit is een indirect bewijs dat diepe of infratentoriële microbloedingen waarschijnlijk het gevolg zijn van vaatschade door hoge bloeddruk en verstijving van de wand van de kleine slagaders. Daarnaast hebben wij een associatie aangetoond tussen het apolipoproteïne E gen en lobaire microbloedingen (in de kwabben van de grote hersenen). Dit suggereert dat lobaire microbloedingen mogelijk veroorzaakt worden door cerebrale amyloid angiopathie, een aandoening waarbij de kleine hersenvaten door stapeling van amyloid-eiwit broos worden en daardoor gemakkelijk bloeden.

De hoge prevalentie van cerebrale microbloedingen en hun mogelijke link met broze hersenvaten, wekte onze interesse in de relatie tussen het gebruik van anti-thrombotische medicijnen (bloedverdunners) en microbloedingen. Wij onderzochten deze relatie in de Rotterdam Scan Studie en vonden dat personen die anti-thrombotische medicijnen gebruikten aantoonbaar vaker cerebrale microbloedingen hadden dan personen die niet dit soort medicijnen gebruikten (**hoofdstuk 3.3**). Ook constateerden wij dat er een verschil leek te bestaan tussen aspirine en carbasalaat calcium, twee soorten bloedverdunners, en het hebben van microbloedingen: mensen die aspirine gebruikten hadden vaker lobaire microbloedingen dan degenen die carbasalaat calcium gebruikten. Het zou met name interessant zijn om te weten of personen met

microbloedingen meer risico lopen om een grote bloeding in de hersenen te krijgen wanneer zij anti-thrombotische medicijnen gebruiken. Om deze vraag te beantwoorden is het nodig om de onderzoeksdeelnemers langduriger in de tijd te vervolgen. Wel ontdekten wij binnen de Rotterdam Scan Studie dat een van onze onderzoeksdeelnemers, die geen neurologische voorgeschiedenis of klachten had maar wel bloedverdunners gebruikte, een hersenbloeding kreeg precies op de plek waar wij eerder een kleine microbloeding hadden vastgesteld (**hoofdstuk 3.4**). Dit is de eerste keer dat een direct verband in de tijd en in de hersen-lokatie beschreven is tussen een microbloeding en een symptomatische hersenbloeding in een persoon zonder verdere neurologische klachten.

In dit proefschrift beschrijf ik verder het voorkomen van superficiële siderose, de afzetting van afbraakprodukten van oud bloed op het hersenoppervlak, in onze studiepopulatie, en de relatie van deze siderose met de aanwezigheid van microbloedingen (**hoofdstuk 3.5**). In een groep van 1062 personen constateerden wij superficiële siderose in zeven deelnemers. Al deze zeven personen hadden tegelijkertijd ook lobaire microbloedingen, hetgeen de veronderstelling dat superficiële siderose en cerebrale amyloid angiopathie met elkaar verbonden zijn verder ondersteunt.

Tenslotte hebben we een microbloeding die we op hoge-resolutie T2*-gewogen MRI beelden zagen in de hersenen van een overleden persoon, microscopisch onderzocht om te kunnen bevestigen dat de MRI afwijking inderdaad een oude kleine bloeding betrof (**hoofdstuk 3.6**).

DOORBLOEDING VAN DE HERSENEN

Om een eventuele relatie tussen de aanwezigheid van wittestofafwijkingen en doorbloeding van de hersenen te onderzoeken hebben we door middel van een snelle en niet-invasieve fase-contrast MRI methode (**hoofdstuk 4**) de totale doorbloeding van de hersenen gemeten en deze resultaten afgezet tegen de hoeveelheid wittestofafwijkingen. Omdat de bloedtoevoer naar de hersenen sterk afhankelijk bleek van het totale hersenvolume, berekenden we ook de doorbloeding per 100 ml hersenvolume. Factoren die de cerebrale doorbloeding bepalen bleken te verschillen afhankelijk van het wel of niet corrigeren voor het hersenvolume (**hoofdstuk 4.1**). Hoge bloeddruk, hogere body mass index (de verhouding tussen gewicht en lengte), en roken waren gerelateerd aan een hogere doorbloeding (ml/min) per 100 ml hersenweefsel. Personen met een lage hersendoorbloeding hadden meer wittestofafwijkingen in vergelijking met personen met een hoge doorbloeding. Dit kan betekenen dat lage weefsel-doorbloeding mogelijk bijdraagt aan het ontstaan van wittestofafwijkingen.

Een lage cerebrale doorbloeding is in eerder onderzoek ook in verband gebracht met slechter cognitief functioneren. In onze studiepopulatie vonden we dat een lage totale doorbloeding, niet gecorrigeerd voor het hersenvolume, inderdaad gerelateerd was aan slechtere prestaties op diverse cognitieve gebieden (snelheid van informatie verwerking, uitvoerende functies en globale cognitie) (**hoofdstuk 4.2**). Echter, wanneer we rekening hielden met het totale hersenvolume in de berekening van de hersendoorbloeding, dan verdwenen deze associaties. Het verband tussen hersendoorbloeding en cognitie wordt dus mogelijk vertroebeld of gedreven door atrofie (verlies) van hersenweefsel.

MICROSTRUCTURELE INTEGRITEIT VAN DE WITTE STOF

Het is bekend dat witte stof atrofie en wittestofafwijkingen een negatief effect hebben op het cognitief functioneren en gepaard kunnen gaan met een hoger risico op dementie. Deze macrostructurele hersenveranderingen worden echter beschouwd als late tekenen van hersenschade; het opsporen van subtielere witte stof veranderingen zou mogelijk meer inzicht in de rol van witte stof in cognitieve achteruitgang kunnen geven. Diffusion tensor imaging (DTI) is een speciale MRI techniek waarmee de microstructurele integriteit, ofwel de kwaliteit, van de witte stof op gevoelige wijze gemeten kan worden. Wij vonden dat de DTI waardes van de witte stof en van wittestofafwijkingen gerelateerd waren aan de cognitieve functie, zelfs wanneer we corrigeerden voor de atrofie van witte stof of voor het de hoeveelheid wittestofafwijkingen (**hoofdstuk 5.1**). Dit geeft aan dat het nadelige effect van witte stof veranderingen op cognitie niet alleen afhangt van afwijkingen die duidelijk op MRI zichtbaar zijn, zoals verlies van witte stof of wittestofafwijkingen, maar ook van meer subtielere veranderingen zoals de microstructurele kwaliteit van de witte stof.

Vervolgens onderzochten we in welke hersengebieden de aan veroudering gerelateerde microstructurele veranderingen in de witte stof met name optraden (**hoofdstuk 5.2**). We lieten zien dat deze veranderingen met name verklaard kunnen worden door de gelijktijdige aanwezigheid van atrofie en wittestofafwijkingen, en niet zozeer veroorzaakt worden door het 'ouder worden' op zich. Verder constateerden we ook dat microstructurele veranderingen in de witte stof die gerelateerd waren aan atrofie, in andere hersengebieden optraden dan wanneer deze samenhangen met wittestofafwijkingen. Dit suggereert dat deze twee processen, witte stof atrofie en vorming van wittestofafwijkingen, waarschijnlijk onafhankelijk van elkaar zijn en mogelijk dus een andere onderliggende pathologie hebben.

TOEKOMSTIG ONDERZOEK

Het in dit proefschrift beschreven onderzoek heeft geleid tot de vaststelling van meerdere verouderings-gerelateerde hersenveranderingen die potentieel gebruikt kunnen worden als radiologische markers voor neurodegeneratieve of cerebrovasculaire ziekte. Onze resultaten zijn natuurlijk niet het einde van dit onderzoek; ze vormen slechts het begin. Toekomstig onderzoek (**hoofdstuk 6**) naar cerebrale microbloedingen zou primair gericht moeten zijn op de prognose van microbloedingen in relatie tot dementie en beroerte, waarbij rekening gehouden moet worden met het feit dat de lokatie van de microbloedingen waarschijnlijk een reflectie is van de onderliggende pathologie. Het meten van hersendoorbloeding kan waarschijnlijk belangrijke informatie verschaffen over de oorzaken van hersenafwijkingen, en vooruitgang kan geboekt worden in het bepalen van de doorbloeding van de verschillende hersengebieden op populatieniveau, bijvoorbeeld door de arterial spin labeling MRI techniek hiervoor te gebruiken.

Wat betreft DTI beginnen we juist nu pas het scala aan mogelijkheden te ontdekken en veelbelovende toepassingen zoals DTI tractografie (het afbeelden van de zenuwbanen) wachten op verdere verkenning. Geautomatiseerde beeldbewerkingstechnieken zullen waarschijnlijk leiden tot de ontdekking van nieuwe radiologische markers, en tegelijkertijd de analyse van grote hoeveelheden data vergemakkelijken. Belangrijke vooruitgang in de bestudering van hersenpathologie en het voorspellen van het risico op ziekte zijn te verwachten van de combinatie van MRI data met informatie uit andere bronnen, zowel beeldvorming als bijvoorbeeld genetische analyses en eiwitonderzoek.

DANKWOORD

Wat vond ik het spannend om in 2005 de klinische omgeving waar ik mij zo thuis voelde te verlaten om aan dit promotie-onderzoek te beginnen. Nu ik 3,5 jaar later dezelfde switch maak, maar dan andersom, komt datzelfde gevoel weer terug. Want het is een geweldige researchtijd geweest, niet in de laatste plaats omdat ik het geluk heb gehad dat het een prachtig project is geworden, maar vooral ook door de vele mensen van wie ik heb mogen leren, met wie ik prettig heb samengewerkt of van wie ik belangrijke ondersteuning heb gekregen. Allen wil ik op deze plaats bedanken en een aantal van hen wil ik in het bijzonder noemen.

Allereerst mijn beide promotoren, professor Monique Breteler en professor Gabriel Krestin. Beste Monique, wat heb je met de Rotterdam Scan Studie een prachtige studie opgezet, wereldwijd bekend en geroemd. Het voelt als een groot voorrecht dat ik hier deel van uit heb kunnen maken. Ik heb onzettend veel geleerd van jouw scherpe analytische geest en je kernachtige en heldere aanpak en ben je daar heel dankbaar voor. Professor Krestin, ik zou me geen betere opleider kunnen wensen. U bent betrokken, spoort mij aan het maximale te halen uit alles wat ik doe en heeft bovenal het vertrouwen in mij gehouden toen ik ervoor koos een andere weg in te slaan dan u verstandig achtte. Dank voor alle mogelijkheden die u mij biedt die zowel mijn opleiding als mijn onderzoekstijd zo waardevol maken.

Dr. Aad van der Lugt, mijn co-promotor; beste Aad, wat een geluk dat hevige sneeuwval in maart 2005 alle vliegtuigen aan de grond hield en wij daardoor in Wenen aan de praat raakten over dit onderzoeksproject. Jouw energie en enthousiasme werkten direct aanstekelijk en zijn nog steeds tekenend voor je dagelijkse begeleiding – bedankt!

Mijn hartelijke dank gaat verder uit naar de promotie commissie, in het bijzonder de leden van de leescommissie; Professor Hunink, beste Myriam, je warme persoonlijkheid en je oprechte interesse in mij en mijn onderzoeksproject, tezamen met je grote expertise op zowel het radiologische als besliskunde vlak maken je tot het gedroomde commissielid. Professor van Buchem, beste Mark, ik vond het een plezier om via de Microbleed Study Group kennis met je te maken en te ontdekken hoezeer onze onderzoeksgebieden overlappen. Professor Greenberg, dear Steve, it has been a great pleasure to work with you on the microbleed review paper, and I am honoured and thankful that you have undertaken the long journey to Rotterdam!

Al die MRI scans waren er niet gekomen zonder de enorme inzet van het team ERGO-laboranten. Lydia Buist en Pauli van Eldik, jullie zijn werkelijk onvervangbaar. Met groot enthousiasme en verantwoordelijkheidsgevoel namen jullie mij steeds meer werk uit handen en loopt alles rondom het scannen inmiddels als een geoliede machine; ik verlaat jullie met

een gerust hart maar ga de gezelligheid zeker missen! Charlotte, Hilda, Marja en Karin, jullie vormden in de loop der jaren een zeer waardevolle aanvulling op het team, waarvoor dank.

Onmisbare ondersteuning heb ik mogen ontvangen van het team automatisering van de afdeling epidemiologie, de heren van het PACS-beheer van de afdeling radiologie, de MRI technici radiologie en de ziekenhuisadministratie (voor die duizenden ergomri-nummers). In het bijzonder wil ik Frank van Rooij bedanken voor zijn zeer consciëntieuze management van alle MRI logistiek, van het maken van wekelijkse scan-roosters tot het uiterst accuraat bijhouden van de databases.

Alle medewerkers van het ERGO-centrum wil ik bedanken voor hun gedrevenheid in het verzamelen van alle onderzoeksdata en de goede sfeer op het onderzoekscentrum. Anneke Korving, onder jouw bezielende leiding kon ik erop vertrouwen dat alle praktische zaken rondom de MRI afspraken in orde kwamen, bedankt. Dick Slof, wat fijn dat jij altijd bereid was om ons uit de brand te helpen met allerlei logistieke problemen. Jolande Verkroost, nog voordat ik mijn vraag gesteld had zat jouw antwoord vaak al in mijn inbox.

De ERGO-deelnemers en huisartsen uit de wijk Ommoord zijn van onschatbare waarde voor al het onderzoek binnen de Rotterdam Studie en verdienen veel dank. Professor Hofman, beste Bert, bedankt dat je mij in 1998 voor het research master traject aannam, en mij jaren later weer even enthousiast op je afdeling verwelkomde!

MRI issues were often made easier - though sometimes more complex - by the non-Dutchies in our department of Radiology. Piotr Wielopolski, thank you for designing the MRI protocol and for always answering my questions so promptly. Gavin Houston, you have never let us down regarding solving artifact issues, resuscitating the scanner or providing us with flow measurement tools – thanks!

Uiterst belangrijke ondersteuning op gebied van hardware, software en *problem solving* ontvingen wij verder van GE Healthcare. Arjan van der Weele, jij bent een fantastisch visitekaartje voor je bedrijf – wat een service verleende je ons (zelfs 's avonds en in het weekend) – dank!

De deelnemers aan het expertpanel toevalsbevindingen wil ik danken voor hun tijdsinvestering en het delen van hun expertise om tot een goed en werkbaar protocol te komen. Medisch specialisten Arnaud Vincent, Richard Feelders, Fop van Kooten en Peter Koudstaal ben ik zeer erkentelijk voor hun bereidwilligheid om ERGO deelnemers op korte termijn op hun spreekuur te ontvangen. Jan Heeringa, dank voor het vormen van een brug tussen onderzoek en huisartsenpraktijk, wanneer dat nodig was. Hervé Tanghe, fijn dat je als 'achtervanger' fungeerde voor de lastigste MRI scans.

De secretariaten epidemiologie en radiologie en het Research Office radiologie, dank voor het oplossen van allerhande administratieve problemen. Ton Everaers: bedankt voor je inzet en harde werk om dit proefschrift deze mooie vorm te geven!

Collega-onderzoekers uit de neuro-epidemiologie groep: bedankt voor de inspiratie en gezelligheid gedurende de afgelopen jaren – niet alleen op de werkvloer maar vooral ook tijdens de jaarlijkse avontuurlijke uitjes. Roomie Mendel, ik ben heel trots dat je de eindstreep vorige maand gehaald hebt – laat nu vooral je grote creatieve talent weer de vrije loop en geniet! Jory en Mariëlle, ik ben blij met jullie als opvolgers in het project en kijk er naar uit om met jullie verder samen te werken. Alle overige epi-promovendi: dank voor de geslaagde borrels en etentjes die zo trouw werden georganiseerd. Mark Sie, wat leuk om jou als oud klas- en studiegenoot weer als collega bij de epidemiologie te treffen – en wat een eer dat ik jouw paranimf mocht zijn. Alle andere collega's van de afdeling epidemiologie, teveel om bij naam te noemen, dank voor de goede werksfeer.

De Biomedical Imaging Group Rotterdam was niet alleen van onschatbare waarde voor dit project maar bracht mij bovenal een nieuwe groep vrienden. Professor Niessen, beste Wiro, jij mag met recht trots zijn op de geweldige groep mensen die je om je heen hebt verzameld. Henri, met jouw “ik los dat probleem wel even op mei(s)ke” verdiende je bij mij de heldenstatus! Brainiacs Fedde, Renske en Marius, ik kon me geen gezelliger (en spitsvondiger) mensen in jullie plaats indenken. Marius, het was een feest om samen met jou en je tomeloze enthousiasme het TBSS paper te schrijven. Ik hoop met jullie en de vatentrekkers, Coert, Michiel, Reinhard, Stefan en Rashindra, nog veel te zullen DE-en, feesten en reizen!

Collega's van de afdeling radiologie, bedankt dat jullie mij al die jaren zijn blijven beschouwen als één van jullie, en dat ik na mijn terugkeer weer enthousiast werd ontvangen.

Ladies van de ladies night: Marion, Indra en -later- Renske: onderzoek vloeide naadloos over in bijzonder leuke avondjes uit die mij steeds weer veel energie gaven – dank jullie wel. Marion, een van de mooiste ‘bijzaken’ van mijn promotietraject vind ik onze hierdoor ontstane vriendschap – allebei rasneuroot en superambitieuze, wat een feest van herkenning!

Mijn paranimfen, Ylian Liem en Arfan Ikram, ik ben heel blij dat jullie me op 11 maart terzijde staan. Lieve Yl, het is dat je al een tweelingzus hebt, want wat begrijp je mij goed! Dat je vanuit Denemarken bent gekomen om hier vandaag te zijn is tekenend voor de ongelooflijk lieve vriendin die je bent. Arfan, mijn onderzoeksmaatje vanaf dag één. Ik dacht dat ik niet het samenwerkende-type was, maar had er niet op gerekend dat ik iemand tegen zou komen

die zo slim, collegiaal en humorvol is als jij. Zonder jou was het lang zo leuk niet geweest en ik ben dan ook heel blij dat je straks weer mijn collega wordt!

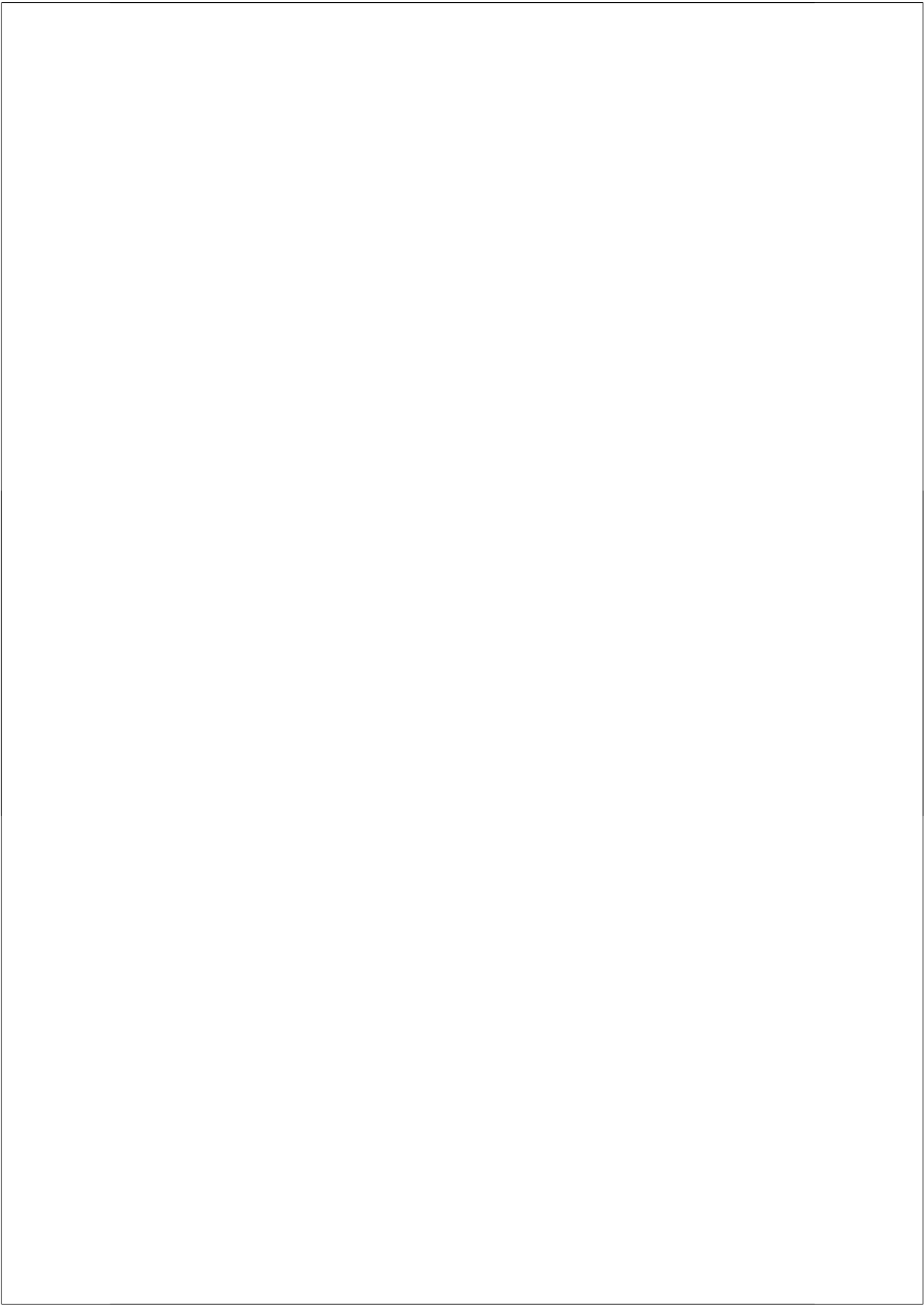
Familie en vrienden, bedankt voor jullie niet aflatende interesse in mijn werk en voor alle ontspanning en afleiding. Dirk en Nel Westerhuis en die twee andere Daltons, Rob en Dolf, bij jullie voel ik me altijd thuis. Vriend(inn)en uit Rotterdam, Utrecht, Leiden en (iets) verder: bedankt voor jullie betrokkenheid en vriendschap, nu is het tijd voor een feestje! Friends who travelled from abroad: I am so happy and grateful that you are present today.

Gelukkig wordt niet alles bepaald door het lot. Twaalf en een half jaar na dato besef ik meer dan ooit hoe groot de invloed op mijn loopbaan is geweest van de durf en inzet van het toenmalige College van Bestuur van de Erasmus Universiteit Rotterdam en in het bijzonder van professor Anton Grootegoed. Mijn dank hiervoor is groot.

Mijn ouders, Kees en Faustine, verdienen veel meer dan de paar zinnen die deze ruimte mij biedt. Jullie onvoorwaardelijke steun, liefde en aandacht hebben me gebracht waar ik nu ben. Dat jullie altijd zo trots op me zijn maakt me gelukkiger dan welke prestatie ook. Femke, mijn lieve grote zus, bedankt voor al die leuke USA trips, maar wat fijn dat je nu weer wat dichterbij woont! Joe, thank you for taking up the challenge of moving overseas and reuniting our family – I hope you and Fem will be very happy here.

En Geert. De omslag van dit proefschrift staat voor alles wat jij me geeft: een leven vol avontuur waar geen impactfactor aan kan tippen!

Meike



PHD PORTFOLIO

PHD PORTFOLIO - *Summary of PhD training and teaching activities*

	YEAR
<i>Research skills</i>	
MSc in Health Services Research, Nihes, Rotterdam, NL	1998-2000
Biomedical English Writing and Communication	2000
<i>In-depth courses</i>	
NWO Talent day 2008, workshops Negotiating and Mediatraining, Utrecht, NL	2008
MRI physics course, Philips Medical Systems, Hilvarenbeek, NL	2007
Good Clinical Practice Course, Rotterdam, NL	2007
FSL & Freesurfer Course (FMRIB), Cardiff, UK	2007
Conceptual Foundation of Epidemiologic Study Design, Nihes, Rotterdam, NL	2006
Bayesian Statistics, Nihes, Rotterdam, NL	2006
Spatial Epidemiology, Nihes, Rotterdam, NL	2006
MRI Quality Assurance Training, MagNET, Imperial College London, UK	2006
Principles of Epidemiologic Data Analysis, Nihes, Rotterdam, NL	2006
<i>Invited lectures and seminars</i>	
1st Cerebral Microbleed Consortium Meeting, Chicago, USA; seminars 'Comparison of 3D T2*GRE imaging and 2D T2*GRE imaging for the detection of cerebral microbleeds' and 'Cerebral microbleeds: prevalence and risk factors in a general population.'	2008
6th Dutch Endo-Neuro-Psycho Meeting, Doorwerth, NL; seminar 'Cerebral microbleeds: prevalence, risk factors and clinical correlates.'	2007
Research Institute for Diseases in the Elderly (RIDE), Amsterdam, NL; lecture 'New MRI sequences for the detection of structural and functional brain changes.'	2007
Research Institute for Diseases in the Elderly (RIDE), Rotterdam, NL; lecture 'The Rotterdam Scan Study – preliminary findings and results.'	2006
MRI Users Day, General Electric Healthcare, Utrecht, NL; seminar 'Brain imaging in the Rotterdam Scan Study.'	2005
Junior image interpretation session at European Congress of Radiology (ECR), Vienna, Austria; invited panel member for case interpretation.	2005
<i>International conference presentations</i>	
Radiological Society of North America, 94th scientific meeting, Chicago, USA; oral presentation 'White Matter Microstructural Integrity and Cognitive Function: a Diffusion Tensor Imaging Study.'	2008

YEAR

Radiological Society of North America, 93rd scientific meeting, Chicago, USA; oral presentation 'Comparison of 3D T2* GRE imaging and 2D T2* GRE imaging for the detection of cerebral microbleeds'.	2007
International Society for Vascular Behavioral and Cognitive Disorders Meeting (VasCog), San Antonio, USA; oral presentation 'Cerebral blood flow, white matter lesion volume and cognitive function'.	2007
International Society for Magnetic Resonance in Medicine, 15th scientific meeting, Berlin, Germany; oral presentations 'Incidental findings on brain MRI in the general middle-aged and elderly population', 'Cerebral microbleeds on brain MRI in the general elderly population: prevalence and relation to small vessel disease', and 'Structural asymmetry of the white matter language pathway in relation to functional hemispheric language lateralization in both left- and right-handed subjects'.	2007
Radiological Society of North America, 92nd scientific meeting, Chicago, USA; oral presentations 'Cerebral microbleeds in a healthy aging population: detection by 3D T2* GRE MRI' and 'Incidental findings on brain MRI in elderly persons'.	2006
International Society for Magnetic Resonance in Medicine, 14th scientific meeting, Seattle, USA; oral presentation 'Combining functional MRI and Diffusion Tensor Imaging in the pre-operative assessment of the hand and foot fibers within the corticospinal tract'.	2006
International Conference on Alzheimer's Disease and Related Disorders (ICAD), Madrid, Spain; oral presentation 'Prevalence and risk factors of cerebral microbleeds in the Rotterdam Scan Study'.	2006
Organization for Human Brain Mapping, Florence, Italy; poster presentations 'Combining functional MRI and Diffusion Tensor Imaging to visualize the Corticospinal Tract: tracking the homunculus' and 'Using Diffusion Tensor Imaging to assess language hemispheric dominance in the pre-operative assessment of brain tumor patients'.	2006
Teaching	
Supervising and teaching MSc and PhD students, Department of Epidemiology, Erasmus MC, Rotterdam, NL	2007-current
Teaching practicals in epidemiology at Nihes and Faculty of Medicine, Erasmus MC, Rotterdam, NL	2006-2008
Other	
Referee activities for various international scientific journals (Neurology, Stroke, Brain)	2006-current
Organisation and program coordination research seminars, Department of Epidemiology, Erasmus MC, Rotterdam, NL	2007-2008



LIST OF PUBLICATIONS

PUBLICATIONS

Vernooij MW, Ikram MA, Tanghe HL, Vincent AJPE, Hofman A, Krestin GP, Niessen WJ, Breteler MMB, Van der Lugt A. Incidental findings on brain MRI in the general population. *The New England Journal of Medicine* 2007; 357:1821-1828.

Vernooij MW, Ikram MA, Vrooman HA, Wielopolski PA, Krestin GP, Hofman A, Niessen WJ, Van der Lugt A, Breteler MMB. White matter microstructural integrity and cognitive function in a general elderly population. *Archives of General Psychiatry*; in press.

Vernooij MW, Van der Lugt A, Ikram MA, Wielopolski PA, Niessen WJ, Hofman A, Krestin GP, Breteler MMB. Prevalence and risk factors of cerebral microbleeds. The Rotterdam Scan Study. *Neurology* 2008; 70:1208-1214.

Vernooij MW, Heeringa J, De Jong GJ, Van der Lugt A, Breteler MMB. Cerebral microbleed preceding symptomatic hemorrhage in a stroke-free person. *Neurology*; in press.

Vernooij MW*, Haag MDM*, Van der Lugt A, Hofman A, Krestin GP, Stricker BH, Breteler MMB. *joint principal authorship. Use of antithrombotic drugs and presence of cerebral microbleeds. The Rotterdam Scan Study. *Archives of Neurology*; in press.

Vernooij MW, Ikram MA, Wielopolski PA, Krestin GP, Breteler MMB, Van der Lugt A. Cerebral microbleeds: accelerated 3D T2*-weighted GRE MR imaging versus conventional 2D T2*-weighted GRE MR imaging for detection. *Radiology* 2008; 248:272-277.

Vernooij MW*, De Groot M*, Van der Lugt A, Ikram MA, Krestin GP, Hofman A, Niessen WJ, Breteler MMB. *joint principal authorship. White matter atrophy and lesion formation explain the loss of structural integrity of white matter in aging. *NeuroImage* 2008; 43:470-477.

Vernooij MW*, Smits M*, Wielopolski PA, Houston GC, Krestin GP, Van der Lugt A. *joint principal authorship. Fiber density asymmetry of the arcuate fasciculus in relation to functional hemispheric language lateralization in both right- and left-handed healthy subjects: A combined fMRI and DTI study. *NeuroImage* 2007; 35:1064-1076.

Vernooij MW, Van der Lugt A, Ikram MA, Wielopolski PA, Vrooman HA, Hofman A, Krestin GP, Breteler MMB. Total cerebral blood flow and total brain perfusion in the general population. The Rotterdam Scan Study. *Journal of Cerebral Blood Flow & Metabolism*, 2008; 28:412-419.

Vernooij MW, Ikram MA, Vincent AJPE, Breteler MMB, Van der Lugt A. Intravestibular lipoma – An important imaging diagnosis. *Archives of Otolaryngology – Head & Neck Surgery* 2008; 134:1225-1228.

Smits M*, **Vernooij MW***, Wielopolski PA, Vincent AJPE, Houston GC, Van der Lugt A. *joint principal authorship. Incorporating functional MR imaging into diffusion tensor tractography in the preoperative assessment of the corticospinal tract in patients with brain tumors. *American Journal of Neuroradiology* 2007; 28:1354-1361.

Greenberg SM, **Vernooij MW**, Cordonnier C, Al-Shahi Salman R, Viswanathan A, Launer LJ, Van Buchem MA, Breteler MMB. Cerebral microbleeds: A field guide to their detection and interpretation. *The Lancet Neurology*; in press.

Ikram MA, **Vernooij MW**, Hofman A, Niessen WJ, Van der Lugt A, Breteler MMB. Kidney function is related to cerebral small vessel disease. The Rotterdam Scan Study. *Stroke* 2008; 39:55-61.

Ikram MA, **Vernooij MW**, Vrooman HA, Hofman A, Breteler MMB. Brain tissue volumes and small vessel disease in relation to the risk of mortality. *Neurobiology of Aging*; in press.

De Jong FJ, **Vernooij MW**, Ikram MK, Ikram MA, Hofman A, Krestin GP, Van der Lugt A, De Jong PT, Breteler MMB. Arteriolar oxygen saturation, cerebral blood flow, and retinal vessel diameters. The Rotterdam Study. *Ophthalmology* 2008;115:887-892.

Ikram MA, Vrooman HA, **Vernooij MW**, Den Heijer TD, Hofman A, Niessen WJ, Van der Lugt A, Koudstaal PJ, Breteler MMB. Brain tissue volumes in relation to cognitive function and risk of dementia. *Neurobiology of Aging*; in press.

Ikram MA, Vrooman HA, **Vernooij MW**, Van der Lijn F, Hofman A, Van der Lugt A, Niessen WJ, Breteler MMB. Brain tissue volumes in the general elderly population. The Rotterdam Scan Study. *Neurobiology of Aging* 2008; 29:882–890.

Poels MME, Ikram MA, **Vernooij MW**, Krestin GP, Hofman A, Niessen WJ, Van der Lugt A, Breteler MMB. Total cerebral blood flow in relation to cognitive function. The Rotterdam Scan Study. *Journal of Cerebral Blood Flow & Metabolism* 2008; 28:1652-1655.

Van der Sluis IM, Boot AM, **Vernooij MW**, Meradji M, Kroon AA. Idiopathic infantile arterial calcification: clinical presentation, therapy and long-term follow-up. *European Journal of Pediatrics* 2006; 165:590-593.

Vrooman HA, Cocosco CA, Van der Lijn F, Stokking R, Ikram MA, **Vernooij MW**, Breteler MMB, Niessen WJ. Multi-spectral brain tissue segmentation using automatically trained k-Nearest-Neighbor classification. *NeuroImage* 2007; 37:71-81.

LETTERS AND SHORT COMMUNICATIONS

Vernooij MW, Breteler MMB, Van der Lugt A. Letter in reply: Incidental findings on brain MRI in the general population. *The New England Journal of Medicine* 2008; 358:854-855.

Vernooij MW, Van der Lugt A, Breteler MMB. Risk of thrombolysis-related hemorrhage associated with microbleed presence. *Stroke* 2008; 39:115.

Vernooij MW, Van der Lugt A, Breteler MMB. Microbleeds and risk of hemorrhagic transformation after ischemic stroke. *Journal of Neurology, Neurosurgery & Psychiatry* 2008; e-pub.

Vernooij MW, Van der Lugt A, Breteler MMB. MRI studie van het verouderend brein. *Gamma professional* 2008; 58:12-16.

PUBLISHED ABSTRACTS

(Co)author of over 25 abstracts presented at various international conferences.

ABOUT THE AUTHOR

ABOUT THE AUTHOR

Meike Vernooij was born on December 12, 1978 in Maassluis, The Netherlands. She attended grammar school at the Stedelijk Gymnasium in Schiedam, from which she graduated in 1996. That same year, she moved to Rotterdam for her medical studies. In 2000, she obtained her master degree in Medicine cum laude (Erasmus University Rotterdam) as well as a master degree in Health Services Research from the Netherlands Institute for Health Sciences (Nihs; funded by a scholarship from Erasmus University). As part of her research training, she attended a summer school in Clinical Epidemiology at the Harvard School of Public Health (Boston, USA). In 2002, she received her medical degree cum laude from Erasmus University, for which the Batavian Society for Experimental Philosophy awarded her its yearly prize for best graduate student in Medicine. Her graduate research project was on socio-economic and ethnic differences in health problems among children presenting at a pediatric outpatient clinic, conducted at the Department of Pediatrics, Sophia Children's Hospital (principal investigator, Prof. Dr. Henriëtte Moll).

During her medical training, Meike took elective clerkships in Radiology in 2001 and 2002 at the Departments of Radiology of Maasstad Ziekenhuis (former MCRZ), location Clara, Rotterdam (head, Dr. Dammis Vroegindeweyj) and St. Michael's Hospital, Toronto, Canada (undergraduate program director, Dr. Timothy Dowdell). In December 2002, she started her residency in Radiology at Erasmus MC University Medical Center (head, Prof. Dr. Gabriel Krestin), during which she spent in 2004 three months as a visiting resident at Stanford University Medical Center, Palo Alto, USA (head, Prof. Dr. Gary Glazer) and at Massachusetts General Hospital, Boston, USA (head, Prof. Dr. James Thrall).

From June 2005 onwards, she conducted the work described in this thesis at the Department of Epidemiology of Erasmus MC University Medical Center (head, Prof. Dr. Albert Hofman), under the supervision of Prof. Dr. Monique Breteler (Department of Epidemiology) and Prof. Dr. Gabriel Krestin (Department of Radiology).

In 2006, she won the first prize in the 'Brains at Work' Competition in Advanced Brain Imaging organized by General Electric Healthcare. Her paper on incidental brain findings on MRI was rated among the top 10 medical articles of 2007 (Amedeo). In 2008, she was awarded the Lourens Penning Prize for her work on imaging of age-related brain changes by the University Medical Center Groningen research fund and the Neuroradiology section of the Radiological Society of the Netherlands.

As of December 2008, Meike is continuing her residency in Radiology at Erasmus MC University Medical Center.

